Timing of rifting in the southern Gulf of California and its conjugate margins: Insights from the plutonic record

Jose Duque-Trujillo[1], Luca Ferrari[1,†], Teresa Orozco-Esquivel[1], Margarita López-Martínez[2], Peter Lonsdale[3], Scott E. Bryan[4], Jared Kluesner[3,§], Doris Piñero-Lajas[2,#], and Luigi Solari[1]

[1]*Centro de Geociencias, Universidad Nacional Autónoma de México, Campus Juriquilla, Querétaro, 76230 Querétaro, México*

[2]*Departamento de Geología, Centro de Investigación Científica y de Educación Superior de Ensenada (CICESE), Carretera Ensenada-Tijuana No. 3918, 22860 Ensenada, Baja California, México*

[3]*Scripps Institution of Oceanography, University of California at San Diego, La Jolla, California 92093, USA*

[4]*School of Earth, Environmental and Biological Sciences, Queensland University of Technology, Brisbane, Queensland 4001, Australia*

ABSTRACT

The Gulf of California is a young example of crustal stretching and transtensional shearing leading to the birth of a new oceanic basin at a formerly convergent margin. Previous studies focused along the southwestern rifted margin in Baja California indicated rifting was initiated after subduction and related magmatism ceased at ca. 14–12.5 Ma. However, the geologic record on the Mexico mainland (Sinaloa and Nayarit States) indicates crustal stretching in the region began as early as late Oligocene. The timing of cooling and exhumation of pre- and synrift plutonic rocks can provide constraints on the timing and rate of rifting. Here, we present results of a regional study on intrusive rocks in the southern Gulf of California sampled along the conjugate Baja California and Nayarit-Sinaloa rift margins, as well as plutonic rocks now exposed on submerged rifted blocks inside the gulf. Forty-one samples were dated via U/Pb zircon and ^{40}Ar/^{39}Ar mineral ages, providing emplacement age and thermochronological constraints on timing and rate of cooling. We found an extensive suite of early and middle Miocene plutons emplaced at shallow depths within the basement Cretaceous–Paleocene Peninsular Range and Sinaloa-Jalisco Batholiths. Early Miocene granitoids occur in an elongated WNW-ESE belt crossing the entire southern gulf from southern Baja California to Nayarit and Sinaloa. Most have an intermediate composition (<67 SiO_2 wt%), but a distinctive group of high-silica granites (>75 SiO_2 wt%) was emplaced 20.1–18.3 Ma, near the end of the early Miocene. Age span and chemical composition of the early Miocene silicic plutons essentially overlap ignimbrites and domes exposed in the southern Sierra Madre Occidental and in southern Baja California, suggesting that eruptive sources for the early Miocene ignimbrite flare-up may also have been located within the southern Gulf of California. Early Miocene plutons cooled below the ^{40}Ar-^{39}Ar biotite closure temperature (350–400 °C) in less than 2.5 m.y., which we interpret as evidence of a regional extensional event leading to the opening of the Gulf of California. A less widely distributed suite of intermediate-composition, middle Miocene granitoids (15–13 Ma) was sampled from the central-western part of the gulf, west of the Pescadero Basin, and these correspond to an episode of scarce volcanism recorded by the middle and upper members of the onshore Comondú Group in Baja California. Our widely spaced sampling of the generally sediment-covered igneous crust suggests that middle Miocene primary volcanic rocks are much less abundant than implied by previous models in which the gulf was the site of a robust Comondú arc. Thermobarometry data also indicate a very shallow depth (<5 km) of emplacement for the middle Miocene plutonic rocks. Some of these rocks also show a distinctive inequigranular texture indicative of at least two crystallization stages at different pressure. Early and middle Miocene granitoids away from the gulf axis yielded ^{40}Ar-^{39}Ar cooling ages very close to U-Pb zircon ages, demonstrating rapid cooling to <350 °C, which we attribute to their shallow emplacement and, possibly, to exhumation soon after intrusion. Since Comondú-age and middle Miocene magmatism in the gulf region coincided with rapid cooling of young plutons that predate the end of subduction, we suggest that intense crustal stretching controlled the pattern and timing of Comondú-age magmatism, rather than the middle Miocene magmatism controlling the locus of <12 Ma extension.

INTRODUCTION

The geologic record shows that, in continental extensional systems, the process of complete lithosphere rupture can take from 25 to 80 m.y. before the onset of seafloor spreading (Bohannon et al., 1989; Menzies et al., 1997; Abbate et al., 2001; Ziegler and Cloetingh, 2004; Omar and Steckler, 1995; Pik et al., 2008; Corti, 2009). The main factors controlling the time scale of continental breakup are crustal thickness, lithospheric rheology, thermal structure, and the magnitude and rate of forces applied to the lithosphere (e.g., Ziegler and Cloetingh, 2004; Nagel and Buck, 2007). In this context, the Gulf of California has been considered an anomalously fast rift, in which rupture of the continental lithosphere is thought to have been accomplished in only 6–10 m.y. (see review in Umhoefer, 2011). Despite early studies recognizing that Basin and Range extension may have affected the eastern margin of the future gulf well before the end of subduction (e.g., Henry, 1989), virtually all literature over the past two decades has reinforced the view that rifting in the gulf area only began once subduction of

†luca@unam.mx.

§Present address: Department of Earth and Planetary Sciences, University of California, Santa Cruz, California 95064, USA.

#Present address: Departamento de Oceanografía Física, Centro de Investigación Científica y de Educación Superior de Ensenada (CICESE), Carretera Ensenada-Tijuana No. 3918, 22860 Ensenada, Baja California, México.

GSA Bulletin; May/June 2015; v. 127; no. 5/6; p. 702–736; doi: 10.1130/B31008.1; 13 figures; 3 tables; Data Repository item 2015022; published online 4 December 2014.

the last remnants of the Farallon plate finished at ca. 14–12.5 Ma and the Baja California peninsula started to move with the Pacific plate (Stock and Hodges, 1989; Henry and Aranda-Gomez, 2000; Umhoefer et al., 2002; Fletcher et al., 2007; Lizarralde et al., 2007; Sutherland et al., 2012). To explain this apparently rapid rifting, three main factors have been invoked (Umhoefer, 2011, and references therein): (1) focusing of rifting along an inherited long, narrow belt of hot, weak crust generated by the preceding arc volcanism, (2) relatively rapid plate motions and high strain rates, and (3) a dominant role of strike-slip faulting and highly oblique-divergent setting.

A precise estimation of the timing of rift initiation is crucial to confirm if the Gulf of California is an anomaly among continental rifts. Restoration of the ~300 km of dextral offset estimated in the northern gulf since ca. 6.5 Ma (Oskin and Stock, 2003; Oskin et al., 2001) still leaves 250 km of orthogonal separation between the western (Baja California) and eastern (Mexico mainland) borders of the rift in the southern Gulf of California (Fig. 1; see fig. 2 of Stock and Hodges, 1989) that has to be accommodated in just ~6 m.y. at a high rate of 41 mm/yr. The alternative kinematic model for gulf opening of Fletcher et al. (2007) requires ~460 km of combined transtensional shear within the southern gulf since 12.3 Ma, which translates to a slightly lower rate of separation of ~37 mm/yr. Both values approximate the present-day, postrift rate of opening in the southern gulf (45.1 ± 0.8–51.1 ± 2.5 mm/yr; DeMets, 1995), but they are otherwise uncommon for continental rifts, where geodetically measured rates of opening are typically <10 mm/yr (Calais et al., 1998; Fernandes et al., 2004; Bendick et al., 2006).

It can be misleading to use the subaerial part of just one of the conjugate margins to estimate the timing of rifting and pattern of magmatism. For the Gulf of California, a late Miocene onset of rifting is supported by structural and thermochronology studies, mostly along the narrow onshore part of the Baja California margin and Tiburón Island in the northern Gulf of California (e.g., Stock and Hodges, 1989; Martín-Barajas et al., 1995; Fletcher et al., 2000; Oskin et al., 2001; Umhoefer et al., 2002; Oskin and Stock, 2003; Seiler et al., 2011; Mark et al., 2014). In contrast, studies along the much broader eastern margin side of the Gulf Extensional Province have shown that extension began as early as the late Oligocene (Gans, 1997; McDowell et al., 1997; Wong et al., 2010; Murray et al., 2013) in a wide region and that by ca. 18 Ma, extension had focused toward the present Gulf of California (Ferrari et al., 2013; Bryan et al., 2014).

Insights on the timing of rifting can be obtained by studying plutonic rocks emplaced in the gulf region and their exhumation driven by extensional and transtensional tectonics. In particular, the timing of exhumation, and also the relative timing of emplacement to exhumation, can provide more direct constraints on the onset of rifting in the Gulf of California. In this paper, we present the first integrated geologic, geochronologic, and geochemical study targeted at intrusive rocks exposed on both the subaerial and submarine continental margins of the two sides of the southern Gulf of California rift. Samples from continental blocks submerged in the southern Gulf of California were collected during the DANA (2004), ROCA (2008), and BEKL (2009) cruises. A principal result of our study is that significant amounts of early Miocene and, to a lesser extent, middle Miocene intrusive rocks, initially emplaced in the upper continental crust, are now exposed on the floor of the Gulf of California and along the subaerial margins. Petrographic and geochronologic characteristics of these rocks support an exhumation and crustal thinning phase between ca. 18 and 12 Ma. Our study rekindles early interpretations (e.g., Henry, 1989) that Oligocene to middle Miocene volcanism (Sierra Madre Occidental and Comondú Group) within the southern gulf region, despite being concurrent with the closing phases of subduction off Baja California, was essentially related to continental rifting that led to the opening of the Gulf of California.

MAGMATISM AND TECTONICS OF THE GULF REGION

Western Mexico consists of a series of magmatic and tectonic provinces recording a prolonged history of subduction and extensional tectonics that have affected this segment of the western North American margin since the Cretaceous. Continental magmatism prior to the cessation of subduction off Baja California at ca. 12.5 Ma consisted of three main igneous episodes: (1) the Late Cretaceous–Paleogene, when the Peninsular Range Batholith, which outcrops in Baja California and in adjacent parts of mainland Mexico, was constructed; (2) the late Eocene–early Miocene, when the silicic to bimodal Sierra Madre Occidental silicic large igneous province was emplaced; and (3) the middle Miocene, when volumetrically subordinate intermediate volcanism (the Comondú Group) developed principally along eastern Baja California. These igneous episodes are summarized next, followed by a brief synthesis of the tectonic setting of the Gulf of California.

Peninsular Range and Western Mexico Cretaceous–Paleogene Batholiths

The Peninsular Range Batholith is a N-NW–trending and almost continuous series of batholith-sized intrusive complexes, which form the backbone of Baja California peninsula. The batholith is well exposed for over ~800 km along strike in northern Baja California, it continues beneath the Cenozoic cover in southern Baja California, and it is exposed again south of La Paz in the Los Cabos block (Gastil, 1975) (Fig. 1). Intrusion ages and compositions have formed the basis for correlating the Peninsular Range Batholith with batholiths exposed in mainland Mexico in the states of Sinaloa and Jalisco (Fig. 1; Gastil, 1975; Schaaf et al., 2000; Ortega-Rivera, 2003; Henry et al., 2003), making a 150–200-km-wide igneous belt of Cretaceous to Paleogene age.

The Peninsular Range Batholith has been divided into western and eastern zones on the basis of pluton composition, depth of emplacement, age, host rock geology, and magnetic and gravimetric signatures (Gastil, 1975; Gastil et al., 1990; Silver and Chappell, 1988; Langenheim et al., 2014). Western intrusions have an island-arc geochemical affinity, range in composition between gabbro and monzogranite, and were intruded between ca. 140 and 105 Ma (Gastil, 1975). This part of the batholith is interpreted as the plutonic underpinnings of a Jurassic to Early Cretaceous fringing volcanic arc developed on older oceanic crust that was accreted to the North American plate in Albian times (Silver and Chappell, 1988; Gastil, 1993; Todd et al., 1988, Busby et al., 1998; Busby, 2004). The eastern part of the batholith is composed of nested tonalites and low-K granodiorites plus other smaller, isolated intrusions. This part of the batholith is dominated by La Posta–type tonalite-granodiorite intrusions (Silver and Chappell, 1988; Walawender et al., 1990) with U/Pb zircon ages indicating a short interval of intrusion (ca. 99–92 Ma). Rocks partly overlapping in age with the Peninsular Range Batholith are extensively exposed in Sinaloa (Henry at al., 2003), and in southern Nayarit (Fig. 1). Published ages for the composite and long-lived Sinaloa Batholith span between 101 and 45 Ma, with compositions from gabbro to granite, although granodiorite is the most common rock type (Henry et al., 2003). Intrusive rocks in southern Nayarit are part of the Puerto Vallarta Batholith, which yielded intrusion ages between ca. 92 and 65 Ma (Gastil et al., 1979; Köhler et al., 1988; Zimmermann et al., 1988; Schaaf et al., 1995). On the basis of geochemical and isotopic data, the Puerto Vallarta Batholith is considered equivalent to the Peninsular Range Batholith exposed in the Los Cabos block (Schaaf et al., 2000).

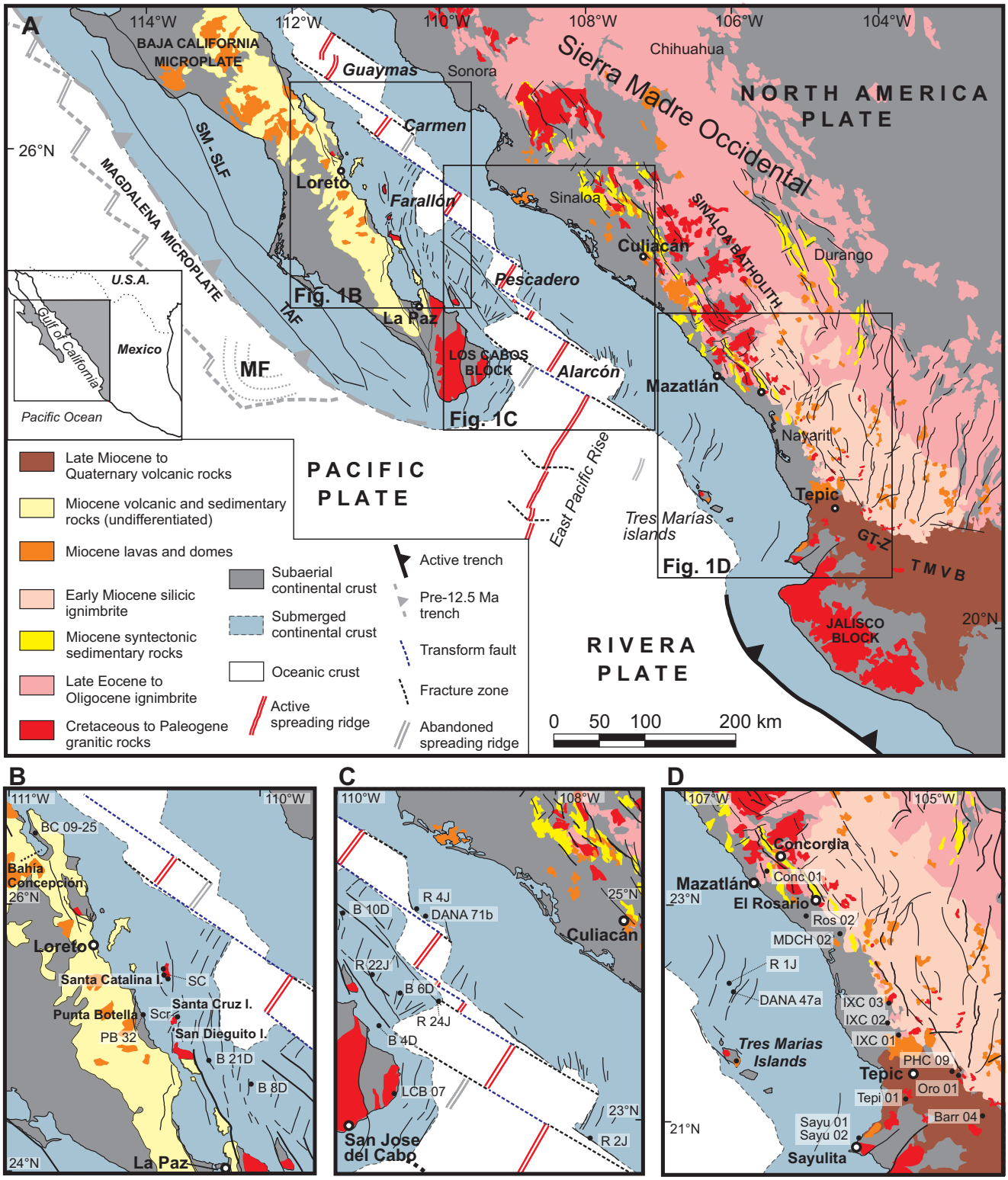

Figure 1. (A) Regional geology and tectonic map of the southern Gulf of California and adjacent margins showing the distribution of submerged continental crust (blue) from Ferrari et al., (2013). Geology is compiled from Ferrari et al. (2007, 2013). Location of the ocean-continent boundary is taken from Lonsdale and Kluesner (2010). (B–D) Detailed areas and location of sampling sites, with samples listed in Tables 1, 2, and 3. Remotely operated vehicle (ROV) dives are indicated with the letter R (sample prefix ROCA), and *Jason* dive number (e.g., R 4J); BEKL dredges are indicated with letter B and dredge number (e.g., B 21D); SC includes all samples from Santa Catalina Island; SCr includes all samples from Santa Cruz Island. GT-Z—Graben Tepic-Zacoalco; MF—Magdalena Fan; SM-SLF—Santa Margarita–San Lorenzo fault; TAF—Tosco-Abreojos fault; TMVB—Trans-Mexican volcanic belt.

Sierra Madre Occidental

The Sierra Madre Occidental preserves the record of continental magmatism preceding the opening of the Gulf of California (Ferrari et al., 2007; Bryan et al., 2014). The province extends from the United States–Mexico border to the Trans-Mexican volcanic belt and constitutes a 1200-km-long and 200–400-km-wide, elongated high plateau with average elevations over 2000 m above sea level (asl; Ferrari et al., 2007). Underlying the Sierra Madre Occidental succession, there are latest Cretaceous to early Eocene intermediate volcanic rocks partly coeval with the Peninsular Range Batholith and traditionally called the Lower Volcanic Complex (McDowell and Clabaugh, 1979; McDowell et al., 1997). However, recent studies indicate that some mafic-intermediate volcanic rocks previously ascribed to the Lower Volcanic Complex are actually interbedded within the Sierra Madre Occidental succession and are thus much younger in age (Murray et al., 2013). The widespread Upper Volcanic Supergroup (McDowell and Keizer, 1977), which defines the Sierra Madre Occidental succession, is mainly composed of voluminous silicic ignimbrites (85%–90% of the total erupted volume) and lesser rhyolitic domes and basaltic lavas. The Upper Volcanic Supergroup makes the Sierra Madre Occidental one of the largest silicic igneous provinces in North America and the most recent of such an event on Earth (Bryan, 2007; Ferrari et al., 2007; Bryan and Ferrari, 2013). Two main "ignimbrite flare-ups" were identified at ca. 34–28 Ma and ca. 24–18 Ma (Ferrari et al., 2007). The Oligocene pulse covers an ~400,000 km^2, NW-trending area and is responsible for at least three quarters (300,000 km^3) of the total erupted volume. The early Miocene ignimbrite flare-up (ca. 24–18 Ma) is essentially concentrated in the southern Sierra Madre Occidental, with a tendency to migrate to the southwest in time (Ferrari et al., 2002, 2007; Bryan et al., 2008).

Geochronologic studies in different areas of the Sierra Madre Occidental have revealed that the emplacement of the ignimbrite successions, locally reaching over 1000 m of thickness, occurred in 1 m.y. or less, hinting at notable high rates of generation of silicic magma (McDowell and Keizer, 1977; Ferrari et al., 2002, 2007; Bryan et al., 2008). Generally, basaltic to basaltic-andesitic lavas are intercalated with or cap the youngest ignimbrite units and have previously been referred to as the Southern Cordillera basaltic andesite suite (SCORBA) in Chihuahua and northern Sinaloa, where they show a transitional to alkaline geochemical signature, more akin to an intraplate environment than to a magmatic arc (Cameron et al., 1989; Luhr et al., 2001).

The Sierra Madre Occidental has been affected by several episodes of extensional deformation since the late Eocene (Henry and Aranda-Gomez, 1992, 2000; Aranda-Gómez and McDowell, 1998; Ferrari et al., 2007, 2013). The central core of the Sierra Madre Occidental, however, is flat-lying and unextended, and it has been used to define the limit between the so-called "Mexican Basin and Range" to the east and the Gulf Extensional Province to the west (Henry and Aranda-Gomez, 2000; Ferrari et al., 2007). The Gulf Extensional Province is widely thought to encapsulate all extension related to the opening of the Gulf of California, which has long been considered to have initiated at ca. 14–13 Ma, when subduction waned and eventually ceased off Baja California (Stock and Hodges, 1989; Henry and Aranda-Gomez, 2000; Umhoefer et al., 2001; Fletcher et al., 2007; Umhoefer, 2011). However, new field and geochronologic studies have shown that the onset of extension in the southern and central part of the Gulf Extensional Province dates back to the late Oligocene and occurred over a broad region up to 350 km from the plate boundary (Ferrari et al., 2013; Bryan and Ferrari, 2013; Bryan et al., 2014). A similar age of extension has been recognized in the northern Sierra Madre Occidental (e.g., Gans, 1997; McDowell et al., 1997; Wong et al., 2010; Murray et al., 2013).

Comondú Group

The Comondú Group consists of volcanic and volcano-sedimentary rocks of latest Oligocene to middle Miocene age, deposited on the northwestern margin of Mexico before the separation of Baja California (Hausback, 1984; Sawlan and Smith, 1984; Sawlan, 1991; Umhoefer et al., 2001). At present, the group is mainly exposed on the eastern side of Baja California, where it has been divided into three members (Umhoefer et al., 2001). The lower Comondú member is a clastic succession of fluvial, eolian, and resedimented tuffaceous sandstones and conglomerates interbedded with silicic ignimbrites. In the Loreto area (Fig. 1), detrital zircon U/Pb data on eolian sandstones indicate a maximum depositional age of ca. 25 Ma (Godinez et al., 2010), and tuffs intercalated in the unit yielded ^{40}Ar-^{39}Ar ages of 22.2–20.2 Ma (Umhoefer et al., 2001). Hausback (1984) reported similar ages (ca. 24–18 Ma) for ignimbrites exposed along the coast north of La Paz. The middle member of the Comondú Group is composed of massive sedimentary breccias and minor andesite-dacite lavas and domes with ages mainly between ca. 19 and 15 Ma. Breccia units are interpreted to thicken to the east and have locally been found to interfinger with the lower member (Hausback, 1984; McLean, 1988). An eastward coarsening is inferred to reflect increasing proximity to arc volcanoes or stratocones now submerged within the gulf. The upper member is dominated by lavas and massive volcanic breccias with a few reported ages between ca. 15 and 12 Ma (Hausback, 1984; Umhoefer et al., 2001; Godinez et al., 2010). The middle and upper Comondú members have a composite thickness exceeding 1 km (Umhoefer et al., 2001). Some shallow intermediate plutons and andesitic porphyry intrusions are associated with the Comondú Group. McFall (1968) reported a 20 ± 0.2 Ma K/Ar age for a tonalitic intrusion in Bahía Concepción. An andesite porphyry at Las Parras, west of Loreto, yielded a U/Pb intrusion age of 19.9 ± 0.7 Ma (Godinez et al., 2010) and a K/Ar (hornblende) age of 19.4 ± 0.9 Ma (McLean, 1988). Godinez et al. (2010) also described a pluton along the Loreto–La Purisima road that yielded several Cretaceous zircon xenocrysts and an intrusion age of 16.3 ± 0.5 Ma. Hypabyssal porphyritic intrusions in the Bahía Concepción and Loreto and east of La Paz (Pichilingüe) have been interpreted to represent core facies of an andesitic arc that, for the most part, extended to the east of the peninsula, within the present gulf (Hausback, 1984).

The ages and lithology of the lower member of the Comondú Group indicate that it represents the distal deposits of the last (early Miocene) ignimbrite flare-up of the Sierra Madre Occidental and therefore can be ascribed to the Sierra Madre Occidental magmatic episode (Umhoefer et al., 2001; Ferrari et al., 2007). By contrast, the middle and upper members of the Comondú Group represent a distinct igneous episode of early to middle Miocene age, characterized by a dominantly effusive style of volcanism (domes, lava flows, and related dikes and subvolcanic intrusion), more intermediate magma compositions, and extensive volcaniclastic and epiclastic deposits.

Southern Gulf of California

The present Gulf of California is an ~1500-km-long, active oblique rift separating mainland Mexico (North American plate) from the Baja California peninsula (Lonsdale, 1989). The rift contains oceanic basins with short NE-striking spreading axes linked by long NW-striking transform faults, which, in many places, bound actively shearing continental margins (Figs. 1 and 2A). Recent geologic and geodetic studies show that Baja California is not completely attached to the Pacific plate, as ~10% of the total Pacific–North America motion is accommodated along its western margin; therefore, the peninsula is defined as a microplate

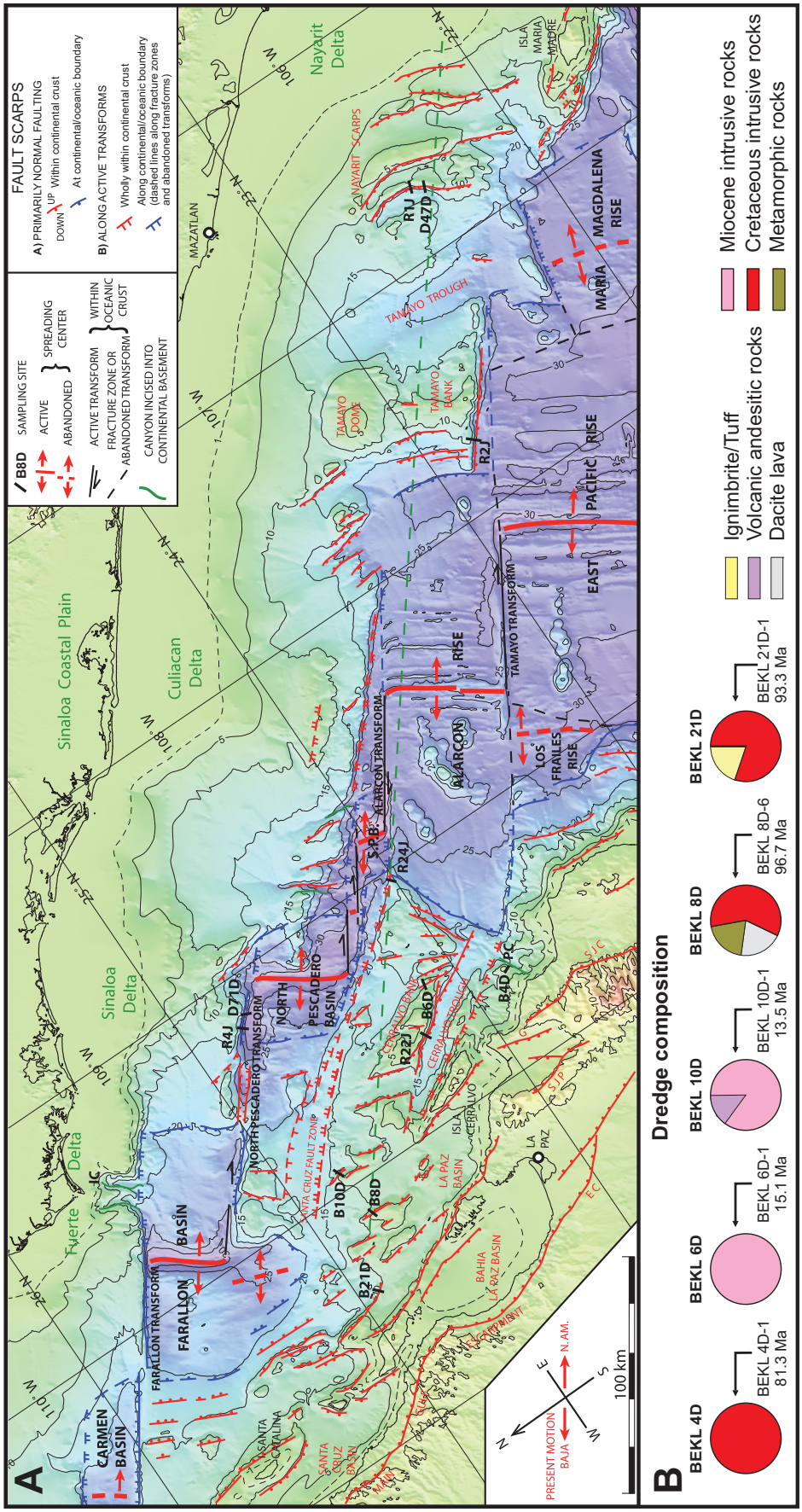

Figure 2. (A) Topographic map of southern Gulf of California, oriented parallel to present geodetically determined motion of the Baja California microplate with respect to the North American plate (Plattner et al., 2007), showing location of DANA dredges (D), BEKL dredges (B), and ROCA dives (R). Bathymetry is from multibeam survey, supplemented in shallow water by contour interpolation of archival soundings; subaerial relief is from satellite altimetry. The green dashed line from northwest to southeast near the middle of the map locates the seismic profile of Sutherland et al. (2012). SJP—San Juan de los Planes fault; SJC—San Jose del Cabo fault; G—La Gata fault; EC—El Carrizal fault; SPB—southern Pescadero Basin; IC—Ignacio Canyon; PC—Pescadero Canyon. (B) Relative abundance of different rock types in BEKL dredges 4D, 6D, 10D, 8D, and 21D, shown in pie charts, together with the ages of intrusive rocks reported in this work.

(Fletcher and Munguía, 2000; Plattner et al., 2007; Fletcher et al., 2007).

The extent and composition of the continental crust in the southern Gulf of California (Figs. 1 and 2A) have been only indirectly inferred by interpretation of structures and wide-angle, multichannel seismic (MCS), and seismic-refraction profiles collected during the National Science Foundation (NSF) MARGINS program in the past decade (Lizarralde et al., 2007; Páramo et al., 2008; Lonsdale and Kluesner, 2010; Kluesner, 2011; Sutherland et al., 2012). Based on seismic velocities, these studies have roughly defined the limits of newly accreted oceanic crust in the Farallón, Pescadero, and Alarcón Basins, as well as southeast of the Los Cabos block (Fig. 2A). The Farallón and Pescadero spreading centers have produced much less oceanic crust than the Alarcón Rise, where the formation of new oceanic crust began between ca. 3.7 and 3.5 Ma (south to north; Lonsdale, 1989, 1995). In all MCS profiles, the prerift basement displays seismic velocities typical of crystalline rocks, which are interpreted to be intrusive rocks of the Peninsular Range Batholith (Páramo et al., 2008; Sutherland et al., 2012). On the conjugate margins of the Alarcón Basin, Sutherland et al. (2012) also recognized a distinctive, reflective "ropey layer," which they interpreted as a volcanic or volcaniclastic succession of the Comondú Group that predated basin formation. Direct information about prerift continental crustal rocks in the mouth of the Gulf of California comes from exposures in the Tres Marías islands, located ~100 km west of Nayarit coast. Mid-Jurassic (163–170 Ma) migmatites and orthogneisses define the crystalline basement of the island, which is cut by Cretaceous intrusions (80.8–83.4 Ma) of tonalitic to granitic composition that are in turn overlain by ignimbrites, volcanic breccias, and lavas of Cretaceous (71.6–80.6 Ma) and Eocene (55.4 Ma) age (Pompa-Mera et al., 2013). Undeformed or slightly deformed sediments that postdate the main rift phase are also recognized in all basins along the gulf, with thicknesses typically increasing toward the center of the gulf. Significant subsidence and marine sedimentation are well documented as early as ca. 8 Ma at Isla Tiburón (Oskin and Stock, 2003), Tres Marías Islands (McCloy et al., 1988), and Isla San José (Carreño, 1992; Fletcher et al., 2000; McTeague, 2006).

METHODS

Introduction

In this work, we sampled the two conjugate rift margins both onshore and offshore to examine the evolving geographic distribution of magmatism and exhumation across the entire southern Gulf of California. Whenever possible, intrusive rocks were dated by both U-Pb (on zircon) and Ar-Ar (hornblende, biotite, or feldspar) methods to provide insight into the rate at which they were exhumed. The samples were analyzed for major and trace elements for correlative purposes relative to onshore intrusive and volcanic suites. Mineral chemistry was also determined on selected samples suitable to apply hornblende geothermobarometry. A brief description of the methodological procedures followed during the present study is presented here. Further details on laboratory procedures are summarized in supplemental file 1 (GSA Data Repository).[1]

Onshore and Submarine Sampling

Subaerial samples used in this work were selected to be representative of the Cretaceous and Miocene intrusive bodies exposed (1) on the southeastern Baja California peninsula and two of its offshore islands (Santa Catalina and Santa Cruz), and (2) on the mainland side of the margin, along the coastal plain and the Sierra Madre Occidental foothills of Nayarit and Sinaloa (Fig. 1). Sampling was guided by the 1:250,000 and 1:50,000 geological maps published by the Mexican Geological Survey (Servicio Geológico Mexicano [SGM]) and by our own mapping (Piñero-Lajas, 2008; Ferrari et al., 2013).

Submarine rock sampling first required locating and mapping patches of rock and talus slopes that crop out through the muddy sediment that covers >90% of the submerged continental crust of the southern gulf, thwarting several earlier sampling attempts. This was accomplished by a multibeam bathymetry and reflectivity survey during the 2004 DANA cruise of R/V *Revelle* (Lonsdale, chief scientist). Steep, highly reflective slopes likely to be good sampling targets included the sides of subaerially incised, now submerged canyons, the steep scarps of sheared continental margins, especially the walls of transtensional rifts along active transform faults, and extensional fault scarps, as well as some steep volcanic slopes. An exploratory DANA dredging campaign immediately after the multibeam survey included 18 successful sampling sites on the submerged continental crust of the Sinaloa-Nayarit margin, six of them yielding granitic intrusive rocks. The 2008 ROCA cruise of R/V *Atlantis* (Lonsdale, chief scientist), with the remote operated vehicle (ROV) *Jason* as its rock-sampling tool, made 11 dives on the mainland continental margin of the southern gulf (including ROCA 1J, 2J, and 4J; Figs. 2 and 3), and three dives on the Baja California margin (including ROCA 22J and ROCA24J; Figs. 2 and 3). The 2009 BEKL cruise of R/V *New Horizon* (Kluesner, chief scientist) dredge-sampled the continental borderland of the southwestern side of the gulf, much of which was geologically unexplored, except for its islands, despite having less obscuring sediment cover than the northeastern margin. Only around the tip of Baja California, south of our study area, was the offshore continental geology relatively well known from interpretations of many previous dredge hauls (Shepard, 1964; Normark and Curray, 1968). We collected granitic rocks from the steep side of Pescadero Canyon and between Pescadero Canyon and Isla Santa Catalina (Fig. 2). Specific objectives were to test how well submarine basement geology could be extrapolated from the adjacent peninsula and its offshore islands, with special attention to testing hypotheses about the geologic history and significance of the Comondú Group.

The steps used for dredging during the DANA and BEKL cruises were (1) to maintain the ship's position as the dredge was lowered to the seafloor, (2) to slowly move the ship 400–600 m directly upslope across rocky terrain while keeping the dredge stationary, and (3) to stop the ship while winching in the dredge until it left the seafloor, 150–200 m shallower than where it landed. With this method, the depth and location are precisely known for the beginning of the dredge track, but less well determined for the end. In addition, the precise depth and location at which individual stones were collected along the 400–600 m dredging track are unknown.

During the ROCA cruise, the ROV *Jason* was operated in a somewhat similar fashion, as a "smart dredge." It was slowly driven, in tandem with its support ship, for 0.5–4.5 km along straight-uphill dive tracks selected using the multibeam imagery while maintaining visual (video) contact with the seafloor. On some dives (e.g., ROCA 1J and 2J; Fig. 3), we conducted two or three uphill profiles spaced along the same fault scarp, separated by "midwater" transits out of sight of the seafloor. Ultrashort-baseline transponder navigation continuously recorded ROV position (±10 m) with respect to the global positioning system (GPS)–positioned ship, and the vehicle's precision depth gauge and echo-sounder recorded its depth and altitude. When ROV video, transmitted in real time to the ship, showed suitable sites, the vehicle was stopped and rocks were grabbed by a manipulator, photographed, and placed in

[1]GSA Data Repository item 2015022, Details on the methodology, thermobarometry, and geochronology, is available at http://www.geosociety.org/pubs/ft2015.htm or by request to editing@geosociety.org.

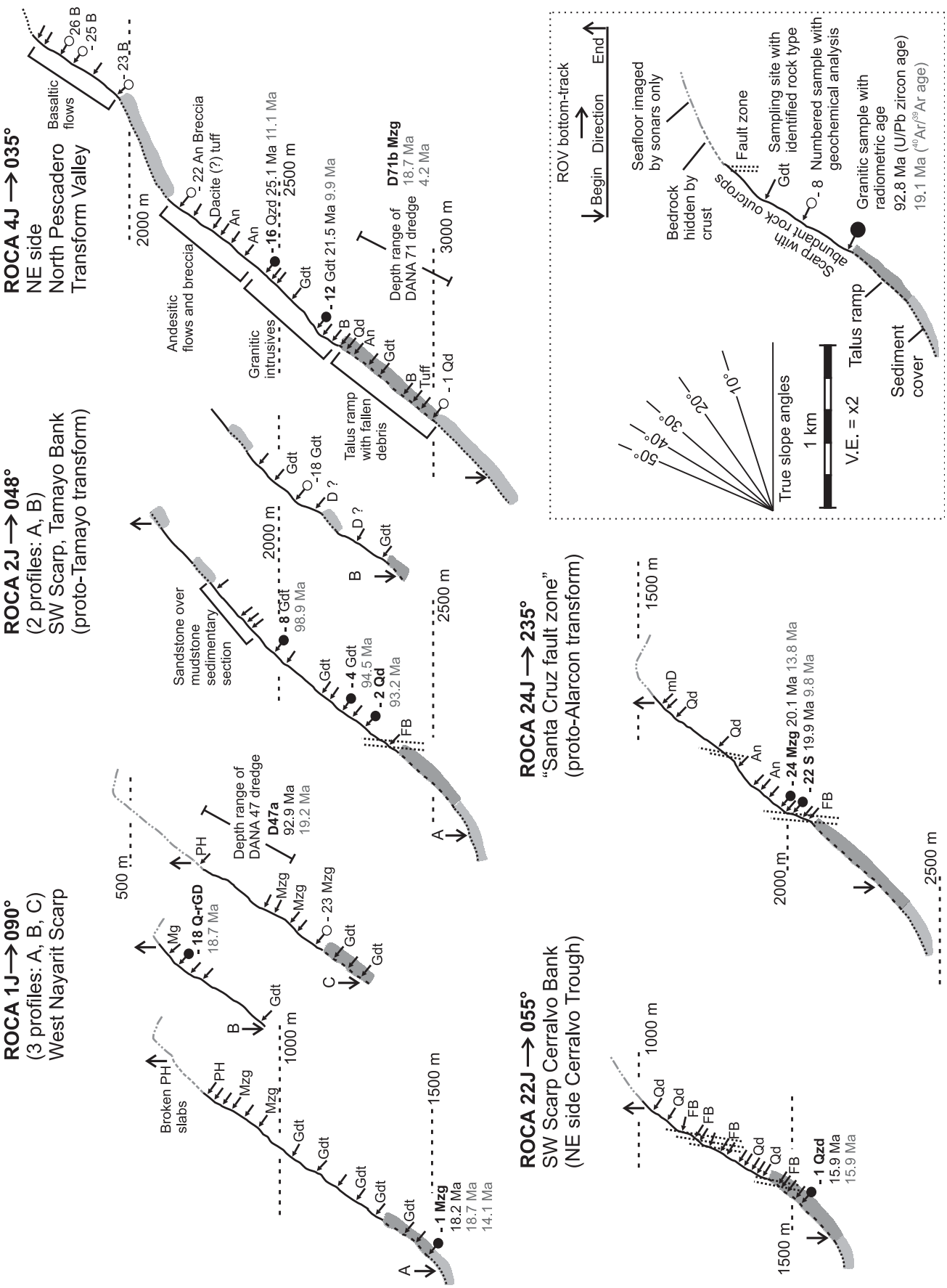

Figure 3. Altimetry profiles from ROCA dive sites from which selected samples were dated. Geomorphologic characteristics and lithologies observed during remotely operated vehicle (ROV) *Jason* dive, and sites of sample collection are shown at each profile.

numbered compartments of a collecting basket so that each one (15–35 per dive) could be identified when brought aboard ship.

Although ROV rock sampling has many advantages over dredge sampling, allowing recovery of selected specimens from visually well-characterized sites at precisely known depths and locations, it does have its limitations. The manipulators are not strong enough to break samples off sound outcrops of intrusive rock, especially if they are cemented with ferromanganese crusts. Along several of our dive tracks, especially along tectonically active plate-boundary fault zones (e.g., ROCA 4J), superficial rocks are pervasively fractured, and fresh fracture-bounded slabs could easily be taken from outcrops. Where samples could not be plucked from true outcrops, we collected rock fragments that appeared to be locally derived, e.g., from narrow ledges within steep outcrops, but a few of these samples may have fallen from outcrops further upslope. On several dives, samples were deliberately collected from scarp-foot talus ramps where loose rocks were clearly not in situ, but very easy to gather; this happened mostly where our initial landing site proved to be at or below a steep talus ramp (e.g., ROCA 4J and 22J), where we grabbed a few stones just to ensure that we brought some samples back even if technical problems curtailed the dive. Stones recovered from the upper surface of active talus ramps, having recently been shaken off upslope outcrops, proved to be among the least altered specimens we collected. Thick ferromanganese oxide encrustation did not prove to be a major problem in the gulf, where bottom waters are lower in dissolved oxygen than in the open ocean, but the shallowest parts of the ROCA 1J profiles were encased in impenetrable phosphorite crusts.

Petrography and Geochemistry

The modal composition and textural features of collected samples were determined in thin sections under the microscope, and results are reported in Table 1. Twenty-nine of the freshest samples were analyzed for major and trace elements and provide a representative characterization of the compositional variability of intrusive rocks in the southern Gulf of California. Onshore samples were collected as far as possible from deformation and alteration zones. Offshore samples were selected among those without strong oxidization and mineral alteration. Major elements were analyzed by X-ray fluorescence (XRF) using a Siemens SRS3000 instrument at Instituto de Geología, Universidad Nacional Autónoma de Mexico (UNAM), according to the procedures outlined in Bernal and Lozano-Santacruz (2005). Sample preparation for trace-element analysis was carried out at Centro de Geociencias (CGEO), UNAM, Campus Juriquilla, Queretaro, Mexico, in a clean laboratory, following the procedures outlined by Mori et al. (2007), incorporating two additional digestion steps in Parr® vessels in order to achieve complete dissolution of refractory minerals (e.g., zircon). Samples were analyzed with a Thermo X Series II quadrupole inductively coupled plasma–mass spectrometer (ICP-MS) at Laboratorio de Estudios Isotópicos, at CGEO, UNAM. Major- and trace-element analyses of DANA and ROCA samples were performed at GeoAnalytical Laboratory, Washington State University. A detailed description of the procedure is presented in supplemental File 1 (see footnote 1). Results of major- and trace-element analyses are presented in Table 2.

Mineral Chemistry

Amphibole and plagioclase analysis for thermobarometric calculations were obtained at Dipartimento di Scienze della Terra, Università degli Studi di Milano, with a JEOL JXA 8200 Superprobe equipped with five wavelength-dispersive spectrometers (WDS), using a 1 μm beam at 15 kV, and 15 nA beam current. Natural and synthetic minerals used as calibration standards were: omphacite and albite (Na), olivine (Mg), anorthite (Al), wollastonite (Ca, Si), apatite (P), K-feldspar (K), ilmenite (Ti), chromite (Cr), rodonite (Mn), and fayalite (Fe). Mineral compositions are listed in supplemental file 2 (see footnote 1).

Geochronology

Forty-one samples (39 plutonic rocks and two dikes) were dated, generating a total of 72 mineral ages using the U/Pb method (laser ablation [LA] ICP-MS) for zircon, and ^{40}Ar-^{39}Ar step-heating method on different materials (hornblende, biotite, muscovite, K-feldspar, and groundmass). Dating using both U/Pb and ^{40}Ar-^{39}Ar techniques was performed when possible, especially for the youngest samples, which required a confirmation of the middle Miocene intrusion age. Twenty samples were dated by both methods, and more than one mineral was analyzed by ^{40}Ar-^{39}Ar on 11 samples (Table 3).

U/Pb geochronological zircon analyses were carried out at Laboratorio de Estudios Isotópicos, Centro de Geociencias, UNAM. Details on the methodology can be found in supplemental file 1 (see footnote 1), and U/Pb analytical data are presented in supplemental file 3 (see footnote 1).

The ^{40}Ar-^{39}Ar analyses were carried out at Laboratorio de Geocronología, Departamento de Geología, Centro de Investigación Científica y de Educación Superior de Ensenada (CICESE), Baja California, Mexico. Information on the ^{40}Ar-^{39}Ar dating process is presented in supplemental file 1 (see footnote 1). Tables with relevant ^{40}Ar-^{39}Ar data for all analyzed samples, as well as a discussion of each age are presented in supplemental file 4 (see footnote 1).

In plutonic rocks, U/Pb zircon ages are usually considered to reflect the age of intrusion, because the closure temperature of the U/Pb systematics in zircon (>900 °C) is comparable with the initial crystallization temperatures of a differentiated magma (Cherniak and Watson, 2001). On the other hand, the ^{40}Ar-^{39}Ar ages are used to constrain the cooling of the sample through different temperatures, which can be interpreted to reflect tectonic and/or erosional exhumation. The most used ^{40}Ar-^{39}Ar closure temperatures are as follows: hornblende (400–600 °C), biotite (350–400 °C), muscovite (300–350 °C), and K-feldspar (150–350 °C) (Reiners et al., 2005, and references therein).

FIELD CONTEXT OF SOUTHERN GULF PLUTONS

The intrusive rocks analyzed in this study were sampled both onshore and offshore on the two rifted margins of the southern Gulf of California. Subaerial sampling sites include: (1) Bahía Concepción, Punta Botella, and some islands off the eastern coast of Baja California and (2) the western Mexico margin in the states of Sinaloa, Nayarit, and Jalisco (Figs. 1 and 2). Submarine sampling was concentrated on rifted continental crust on the northwest and southeast flanks of the Alarcón Basin (Fig. 2A). This basin has accreted a 190–160-km-wide strip of oceanic lithosphere in the past 3.7 m.y. (Castillo et al., 2010), and it is flanked by broad zones of extended continental crust (Lizarralde et al., 2007; Páramo et al., 2008; Sutherland et al., 2012). We also report analyses of intrusive rocks sampled from sites in the deep North Pescadero transform valley, which exposes part of the southeast rifted flank of Farallón Basin (Fig. 2A).

Western Rifted Margin in Eastern Baja California and Adjacent Islands

In the Baja California peninsula, intrusive rocks are exposed to the east of the Main Gulf Escarpment, a morphologic feature formed by a series of E-dipping, high-angle normal faults that mark the western boundary of the Gulf Extensional Province, and extend from Bahía Concepción in the north to La Paz in the south. Bahía Concepción, a bay apparently formed by the displacement of the Main Gulf Escarpment,

TABLE 1. PETROGRAPHIC DATA OF INTRUSIVE ROCKS FROM THE SOUTHERN GULF OF CALIFORNIA AND ITS ADJACENT MARGINS

	Location	QAP	Q′-ANOR	General texture	Pl	Afs	Qz	Amp	Bt	Ms	Px	Ap	Zrn	Ttn	Op
Cretaceous															
PB 32	Punta Botella, Baja California Sur	Qzd	D	E, C-g	63	18	7	4	8			<1	<1	<1	1
SC 17	Santa Catalina Island	Gdt	Gdt	E, M-g	49	15	23	7	6			<1	<1	<1	1
SCr 09-21	Santa Cruz Island	Qd		E, C-g (def)	65	5	5	15	10			<1	<1	<1	<1
SCr 09-20	Santa Cruz Island	T		E, C-g	48.5	4	25	7.5	15			<1	<1	<1	<1
SCr 27	Santa Cruz Island	Mzg	Gdt	E, M-g	18	16	46	15	5				<1		<1
BEKL 21D-1	San Jose scarp	Qzd		I, C-g (def)	63	11	18	2	6			<1	<1		<1
BEKL 8D-6	East of Partida bank	Mzg	Mzg	E, M-g	36	22	28	6	8			<1	<1	<1	1
BEKL 4D-1	Pescadero Canyon	Mzg	Mzg	I, M-g	35	30	22		13			<1	<1		<1
BEKL 4D-2	Pescadero Canyon	Mzg	Gdt	I, C-g	38	27	23		12			<1	<1		<1
ROCA 2J-2	Tamayo fracture zone	Qd		E, C-g (def)	60	3	6	20	11			<1	<1	1	<1
ROCA 2J-4	Tamayo fracture zone	Gdt	Qzd	E, C-g (def)	50	8	16	20	6			<1	<1	1	<1
ROCA 2J-8	Tamayo fracture zone	Gdt	Mzg	E, M-g	47	20	21	12				<1	<1	<1	<1
DANA 47D-1	West Nayarit Ridge fault scarp	Mzg	Mzg	I, M-g	35	19	37.5		8.5			<1	<1	<1	<1
Conc 01	Concordia, Sinaloa	Mzg	Gdt	E, M-g	25	32.5	25	4	13.5			<1	<1	<1	<1
MDCH 02	Mineral de Cucharas, Nayarit	Gdt		E, M-g	45	10	33	5	7			<1	<1		<1
Tepi 01	Tepic, Nayarit	Gdt	Mzg	I, M-g	46	22.5	21.5	1	9			<1	<1		<1
Sayu 01	Sayulita, Nayarit	Gdt	Qd	E, M-g (def)	38	19	15	3	25			1	<1	<1	
Sayu 02	Sayulita, Nayarit	Mzg	Gdt	E, M-g (def)	25	27.5	37.5		10			<1	<1	<1	
Early Miocene															
BC 09-25	Bahía Concepción, Baja California Sur	Mzg		I, M-g	33	22.5	20		7		17.5	<1	<1		1
SC 09-08	Santa Catalina Island	Qzd		E, M-g	58.5	11	7.5	11.5	9		2.5	<1	<1	<1	<1
SC 09-03	Santa Catalina Island	Qzd		I, M-g	55	11	11.5	15	7.5			<1	<1	<1	<1
SC 24	Santa Catalina Island	Qzd		I, M-g	50	25	15	4	6				<1	<1	<1
SC 09-04	Santa Catalina Island	QMz		I, M-g	39	22.5	13.5	10	15			<1	<1	<1	<1
DANA 71D-2	North Pescadero transform	Mzg	QMz	E, M-g	43	23	22	11	1			<1	<1		<1
ROCA 4J-12	North Pescadero transform	Mzg	QMz	I, M-g	33.5	19	30		17.5				<1	<1	<1
ROCA 4J-16	North Pescadero transform	Qzd	Qzd	I, M-g	59	12	12	7	10			<1	<1	<1	<1
ROCA 24J-22	South Pescadero transform	S	S	I, M-g	22	45	31		2				<1		
ROCA 24J-24	South Pescadero transform	Mzg	S	E, C-g	37	31	27		5			<1	<1		<1
ROCA 1J-1	West Nayarit Ridge fault scarp	Mzg	S	E, C-g	27	21	43		9				<1		<1
ROCA 1J-18	West Nayarit Ridge fault scarp	Q-rGD	AG	I, F-g	14	21	60.5		2	2.5			<1		<1
Ros 02	SW of El Rosario, Sinaloa	Qzd	Gdt	E, F-g	51	24	14	11				<1	<1	<1	<1
IXC 01	Santiago Ixcuintla, Nayarit	Qd	QMz	I, M-g	77	0	10	2	8		3	<1	<1		<1
IXC 02	Santiago Ixcuintla, Nayarit	Qd	Qzd	I, M-g	55	5	10	9	3.5		17.5	<1	<1		<1
IXC 03	Santiago Ixcuintla, Nayarit	T	Gdt	I, M-g	43	5	20	19	13			<1	<1		<1
PHC 09	El Cajon dam, Nayarit	Qzd	Qd	I, VF-g (Ph)	60	8	5	5	7		15	<1	<1		5
Oro 1	Santa Maria del Oro, Nayarit	Mzg		E, C-g	25	40	26		9				<1		2
Barr 04	Barrancas, Jalisco	T	Gdt	I, M-g	50	5	25	15	5			<1	<1	<1	<1
Middle Miocene															
BEKL 10D-1	Bank east of Partida Bank	Mzg		I, C-g	37	21	20	2	20		<1	<1	1	<1	<1
BEKL 10D-3	Bank east of Partida Bank	Mzg	Mzg	I, C-g	32.5	22.5	27.5	4	13.5			<1	<1	<1	<1
ROCA 22J-1	Cerralvo Bank	Qzd	Qzd	I, M-g	42.5	20	15	12	10.5				<1		<1
BEKL 6D-1	Cerralvo Bank	Mzg	Qzd	I, M-g	36	23	26	6	9			1	1	<1	<1
BEKL 6D-2	Cerralvo Bank	QMz	QS	I, C-g	32	50	11		7			<1	<1	<1	<1

Note: Mineral modal contents are expressed in vol%. QAP—classification based on the modal content of quartz, alkali feldspar, and plagioclase (QAP diagram for plutonic rocks of Streckeisen, 1976). Q′-ANOR—classification based on the Cross, Iddings, Pirsson and Washington (CIPW) normative composition after Streckeisen and LeMaitre (1979). Grain size after Gillespie and Styles (1999): coarse crystalline (>2 mm), medium crystalline (2–0.25 mm), fine crystalline (<0.25 mm). Geographic coordinates for samples not included in other tables: IXC 01 (21.7827°N, 105.0914°W), IXC 02 (21.9008°N, 105.1759°W), IXC 03 (22.1250°N, 105.1291°W). Abbreviations: Pl—plagioclase; Afs—alkali feldspar; Qz—quartz; Amp—amphibole; Bt—Biotite; Ms—muscovite; Px—pyroxene; Ap—apatite; Zrn—zircon; Ttn—titanite; Op—opaque minerals; Qzd—quartz monzodiorite; Gdt—granodiorite; Qd—quartz diorite; T—tonalite; Mzg—monzogranite; QMz—quartz monzonite; S—syenogranite; Q-rGD—quartz-rich granitoid dike; D—diorite; AG—alkali feldspar granite; QS—quartz syenite; E—equigranular; I—inequigranular; C-g—coarse grained; M-g—medium grained; F-g—fine grained; VF-g—very fine grained; Ph—porphyritic.

TABLE 2. MAJOR AND TRACE ELEMENT ANALYSIS

	Cretaceous												Early Miocene					
Sample:	PB 32	ROCA 2J-4	SC 17	Sayu 01	Conc 01	SCr 27	Tepi 01	Sayu 02	ROCA 2J-8	DANA 47a	BEKL 4D-1	BEKL 8D-6	SC 09-03	PHC 09	SC 09-08	SC 09-04	IXC 02	ROCA 4J-16
Age (Ma):	100.4±1.3	94.5±1.5	96.9±0.9	77.7±0.5	59.4±0.5	98.2±1.5	65.7±0.8	75.2±0.5	98.9±1.4	92.9±0.9	82.4±0.7	96.7±1.1	18.7 ± 0.2	18.2±0.2	22.2±0.4	19.0±0.4		25.1±0.7
Rock type: *	D	QMd	Gdt	QD	Gdt	Gdt	Mg	Gdt	Mg	Mg	Mg	Mg	QMd	QD	QMd	QMd	QMd	QMd
Major elements (wt%)																		
SiO_2	52.79	59.49	63.1	63.63	66.63	67.48	67.87	71.58	72.08	71.96	75.27	75.82	56.51	56.74	58.22	60.29	60.37	62.70
TiO_2	0.922	0.686	0.606	0.441	0.519	0.387	0.429	0.293	0.214	0.177	0.132	0.133	0.811	1.096	1.015	0.622	0.964	0.681
Al_2O_3	18.95	17.2	16.06	18.32	15.46	15.29	15.23	14.89	15.56	15.43	14.07	13.24	17.86	18.07	17.188	17.315	16.24	16.70
Fe_2O_3†	9.45	6.09	6.08	4.44	3.61	4.61	3.86	2.26	1.51	1.38	1.53	1.04	7.06	7.87	6.97	5.53	6.34	5.46
MnO	0.155	0.117	0.089	0.121	0.066	0.055	0.062	0.047	0.027	0.044	0.031	0.029	0.078	0.129	0.109	0.092	0.097	0.102
MgO	3.87	3.20	2.10	0.67	1.6	1.24	1.16	0.65	0.80	0.54	0.13	0.36	4.39	3.06	3.23	3.03	2.69	2.35
CaO	7.56	5.4	4.5	3.87	3.39	3.42	2.55	2.42	1.99	2.17	1.33	1.68	6.37	6.66	5.38	5.64	5.04	3.73
Na_2O	3.76	3.99	3.9	5.51	3.34	3.84	3.35	3.53	4.77	4.71	3.85	3.39	3.93	3.48	4.03	4.28	3.55	4.49
K_2O	1.86	2.2	2.51	1.96	3.85	2.65	3.94	3.52	2.95	3.11	3.66	3.35	2.03	2.10	2.98	2.57	3.42	2.71
P_2O_5	0.276	0.244	0.152	0.141	0.129	0.106	0.100	0.102	0.069	0.062	0.041	0.030	0.168	0.347	0.264	0.186	0.246	0.206
LOI	0.39	1.31	0.56	0.63	0.87	0.7	1.24	0.64	0.72	0.46	0.58	0.6	0.89	0.19	0.51	0.48	0.84	1.13
Total	99.98	99.93	99.66	99.73	99.46	99.78	99.79	99.93	100.69	100.04	100.62	99.67	100.09	99.74	99.90	100.04	99.80	100.26
Trace elements (ppm)																		
Li	17.4		17.9	14.8	26.5	13.5	34.4	24.9			36.2	15.7		13.2			24.4	
Be	1.9		1.6	2.2	2.4	1.2	2	2.1			2.7	2		1.8			2.5	
Sc	4	13	8	4	9	5	7	3	3	3	2	2		17			15	12
V	58	152	93	17	83	61	48	28	25	24	13	20		183			116	101
Cr	429	28	322	3	20	387	6	6	13	5	4	5		13			29	6
Ni	44	8	66	1	9	69	2	2	2	5	1	2		9			18	
Rb	61.7	50.0	53.6	59.2	186.4	25.9	222.5	138.2	69.8	82.8	113.4	114		56.7			169	45.9
Sr	293	800	383	548	337	351	261	425	832	633	173	177		596			422	396
Y	14.4	13.7	15.3	13.9	28.2	6.0	26.1	12.1	4.4	7.5	22	8		29			32.2	23.6
Zr	176	103	180	338	219	126	181	163	89	57	96	114		181			473	292
Nb	12.44	6.92	9.99	9.45	12.86	5.05	9.53	8.17	4.04	3.91	7.05	7.29		8.31			14.69	9.3
Cs	2.21	1.00	2.11	3.89	3.48	1.08	9.37	11.08	3.03	3.57	3.01	2.74		5.02			10.1	0.45
Ba	831	1323	877	937	920	1143	862	1410	1436	1081	1041	395		607			825	974
La	22.03	18.55	20.46	27.66	26.03	26.46	30.09	29.82	12.53	7.87	25.51	17.94		23.34			33.22	26.84
Ce	36.5	36.45	32.71	48.02	55.01	30.68	60.67	53.74	22.89	14.84	47.02	32.71		48.53			67.79	53.19
Pr	4.59	4.59	4.32	5.48	6.94	4.12	7.38	6.14	2.65	1.78	5.51	3.58		7.08			8.9	6.55
Nd	16.52	18.69	16.74	19.14	26.01	13.04	26.41	20.85	9.68	7.24	19.54	11.97		29.03			33.99	25.8
Sm	3.11	4.12	3.38	3.15	5.53	1.98	5.23	3.44	1.85	1.80	4.01	1.75		6.53			6.96	5.43
Eu	0.85	1.38	0.94	1.86	0.89	0.69	0.87	0.87	0.58	0.47	0.57	0.5		1.54			1.32	1.15
Gd	2.68	3.57	2.96	2.64	4.78	1.55	4.55	2.6	1.33	1.56	3.60	1.27		5.86			6.13	4.86
Tb	0.41	0.51	0.46	0.39	0.75	0.22	0.7	0.37	0.16	0.23	0.58	0.18		0.87			0.91	0.76
Dy	2.32	2.83	2.61	2.25	4.48	1.08	4.21	1.99	0.89	1.35	3.60	1.06		5.04			5.24	4.56
Ho	0.46	0.53	0.51	0.48	0.89	0.23	0.84	0.4	0.17	0.27	0.73	0.25		0.97			1.03	0.91
Er	1.35	1.37	1.44	1.39	2.57	0.62	2.38	1.13	0.44	0.70	2.09	0.81		2.62			2.88	2.5
Yb	1.51	1.17	1.51	1.57	2.56	0.65	2.46	1.32	0.40	0.10	2.23	1.26		2.44			2.69	2.36
Lu	0.229	0.18	0.234	0.26	0.371	0.109	0.367	0.215	0.067	0.616	0.329	0.223		0.359			0.404	0.378
Hf	4.28	2.85	4.40	7.10	5.89	3.06	4.94	4.3	2.7	0.09	3.17	4.8		4.34			11.52	7.69
Ta	1.048	0.537	0.742	0.534	1.426	0.373	0.881	0.799	0.283	1.867	0.715	0.955		0.516			0.971	0.671
Pb	9.67	5.30	10.12	11.99	9.15	10.49	23.19	22.91	16.08	20.01	26.82	22.09		9.62			17.21	8.31
Th	8.95	3.03	6.48	7.08	21.33	8.04	21.84	10.69	3.83	3.23	11.88	43.59		6.77			20.56	7.61
U	1.73	1.13	2.19	1.69	7.07	1.12	4.7	3.28	0.85	0.88	3.05	11.4		1.98			9.59	2.34

(*continued*)

TABLE 2. MAJOR AND TRACE ELEMENT ANALYSIS (*continued*)

	Early Miocene													Middle Miocene			
Sample:	IXC 03	DANA 71b	IXC 01	Ros 02	BC 09-25	Barr 04	ROCA 4J-12	SC 24	Oro 01	ROCA 1J-1	ROCA 24J-22	ROCA 24J-24	ROCA 1J-18	ROCA 22J-1	BEKL 6D-1	BEKL 6D-2	BEKL 10D-3
Age (Ma):	20±2[§]	18.7±1.0		21.5±0.2	19.9±0.6	22.7±0.4	21.6±0.4	18.1±0.2	21.3±0.5	18.2±0.2	19.9±0.3	20.1±0.2	18.8±0.07	15.9±0.4	15.4±0.2	14.8±0.1	14.1±0.2
Rock type[*]	Gdt	QM	QM	Gdt	QMd	Gdt	QM	Gdt	AFG	Sg	Sg	Sg	Kfs-G	QMd	QMd	QS	Mg
Major elements (wt%)																	
SiO_2	62.74	63.11	63.55	64.2	64.33	65.53	66.19	67.115	73.421	75.59	75.51	75.44	77.08	62.89	63.84	67.86	71.26
TiO_2	0.586	0.801	1.007	0.582	0.527	0.682	0.668	0.476	0.107	0.125	0.151	0.136	0.063	0.878	0.661	0.434	0.521
Al_2O_3	16.69	16.29	15.85	16.48	16.856	15.93	15.17	16.899	13.37	13.59	13.33	12.98	12.64	15.45	16.4	16.02	15.31
Fe_2O_3[†]	5.27	5.83	5.54	4.46	4.22	4.14	3.96	3.43	1.01	0.81	0.88	1.47	0.62	5.49	4.37	2.25	2.10
MnO	0.095	0.111	0.087	0.121	0.068	0.11	0.083	0.04	0.03	0.106	0.045	0.043	0.048	0.083	0.072	0.024	0.045
MgO	2.651	2.58	1.51	1.58	2.015	1.3	2	1.409	0.052	0.2	0.32	0.25	0.07	2.5	1.98	0.52	0.49
CaO	5.029	3.13	3.09	4.03	4.388	3.14	1.59	3.156	0.549	0.74	0.96	0.93	0.44	4.02	3.82	1.32	2.15
Na_2O	3.003	4.21	3.6	4.63	4.241	4.16	5.41	4.217	3.971	3.96	3.84	3.5	4.04	3.29	3.7	3.92	4
K_2O	2.694	3.63	4.9	2.22	2.686	3.39	3.08	3.254	4.498	5.15	4.6	4.54	4.48	3.89	3.91	5.98	4.13
P_2O_5	0.147	0.204	0.239	0.192	0.156	0.206	0.156	0.101	0.039	0.03	0.038	0.035	0.015	0.214	0.154	0.067	0.08
LOI	0.85	1.36	0.69	0.69	0.34	0.61	2.26	0.14	2.94	0.37	0.51	0.4	0.29	0.74	0.47	0.76	0.65
Total	99.76	101.26	100.06	99.19	99.83	99.20	100.56	100.23	99.98	100.67	100.18	99.72	99.79	99.45	99.38	99.16	100.74
Trace elements (ppm)																	
Li	17.8		15.4	8.5		8.6									20.5	15.2	11.3
Be	1.6		3.6	2		2.3									3.5	2.4	2
Sc	14	15	12	10		8	10			5	3	3	6	16	11	7	3
V	123	109	74	79		70	82			5	7	7		119	86	17	33
Cr	34	15	15	9		8	32			4	4	4	4	41	34	4	9
Ni	15	12	10	4		3	14							14	18	2	4
Rb	137.2	74.7	270.6	55.1		87.9	42.4			185.8	129.8	173.8	253.9	169.4	221.4	226.1	129
Sr	372	365	310	417		308	152			60	105	87	12	337	341	181	292
Y	23.6	36.7	36.4	19		25.5	17			29.7	24.6	33.7	39.1	28.1	25.6	25.7	9.4
Zr	152	332	478	198		241	288			65	105	101	56	236	132	434	106
Nb	8.95	14.44	16.55	10.53		11.81	11.47			18.52	8.8	9.26	20.42	13.89	18.94	23.75	7.7
Cs	7.54	0.64	12.47	1.45		1.56	0.21			4.06	0.84	2.22	10.46	9.82	11.43	7.47	2.97
Ba	688	1297	996	1020		1034	1005			410	915	778	63	917	706	1052	1063
La	24.15	26.12	42.55	19.45		38.38	24.93			23.07	28.13	27.73	16.1	34.73	39.92	32.26	15.82
Ce	48.82	55.66	89.68	39.6		65.3	49.39			44.81	55.43	55.54	40.12	71.39	79.85	62.36	27.93
Pr	6.09	7.15	11.53	5.01		8.4	6.01			5.08	6.32	6.42	5.15	8.78	9.24	7.88	3.02
Nd	22.47	30.44	43.34	19.27		29.92	23.35			17.29	22.36	23.13	18.19	33.52	31.56	29.09	10.57
Sm	4.61	7.22	8.8	3.88		5.54	4.54			3.75	4.49	5.25	5.35	6.73	5.82	5.94	1.97
Eu	0.94	1.23	1.31	1.13		1.36	0.89			0.29	0.46	0.44	0.08	1.41	1.09	1.12	0.67
Gd	4.14	6.45	7.36	3.49		4.86	3.92			3.52	3.85	4.92	5.23	5.88	4.79	5.01	1.76
Tb	0.64	1.07	1.1	0.53		0.72	0.6			0.71	0.66	0.89	1.03	0.94	0.72	0.77	0.26
Dy	3.82	6.6	6.21	3.19		4.2	3.39			4.77	4.04	5.6	6.57	5.43	4.16	4.48	1.52
Ho	0.76	1.35	1.19	0.65		0.84	0.68			0.99	0.87	1.17	1.32	1.09	0.82	0.88	0.32
Er	2.16	3.56	3.31	1.83		2.38	1.77			2.98	2.58	3.38	3.67	2.89	2.33	2.46	0.86
Yb	2.17	3.108	3.17	1.92		2.37	1.83			3.69	2.7	3.52	3.68	2.57	2.39	2.43	0.94
Lu	0.326	0.47	0.466	0.296		0.362	0.295			0.605	0.432	0.545	0.563	0.409	0.35	0.359	0.149
Hf	4.37	8.901	11.34	4.57		5.88	7.92			2.79	3.73	3.86	3.23	6.57	3.43	9.8	2.79
Ta	0.838	0.85	1.071	0.692		0.836	0.67			2.693	0.999	1.168	2.692	1.039	1.518	1.22	0.743
Pb	12.84	8.56	20.72	6.14		13.39	8.25			24.54	12.84	16.22	20.78	18.09	10.45	10	10.6
Th	19.49	9.05	40.05	5.64		9.62	9.04			18.96	18.51	21.29	14.4	18.45	22.21	21.02	19.6
U	6.59	3.05	14.26	1.45		1.98	2.72			4.85	5.28	7.04	4.42	4.9	6.37	6.42	4.78

Note: DANA and ROCA samples were analyzed at GeoAnalytical Laboratory, Washington State University; major elements of all other samples were determined by X-ray fluorescence (XRF) at Instituto de Geología, UNAM, and trace elements by inductively coupled plasma–mass spectrometry at Laboratorio de Estudios Isotópicos, Centro de Geociencias, UNAM. Location of sampling sites are given in Tables 1 and 3. Abbreviations: D—diorite; QMd—quartz monzodiorite; Gdt-granodiorite; QD—Quartz diorite; Mg—Monzogranite; QM—Quartz Monzonite; AFG—Alkali feldspar granites; QS—Quarz syenite; Sg—Syenogranite; Kfs-G—Alkali feldspar granite. LOI—Loss on ignition.

[*]Chemical classification after Streckeisen and LeMaitre (1979).

[†]Values given are total Fe expressed as Fe_2O_3.

[§]Age from Ferrari et al. (2002) for a sample from the same intrusive body (sample ESC 1).

TABLE 3. U/Pb AND $^{40}Ar/^{39}Ar$ AGES OBTAINED FOR INTRUSIVE ROCKS FROM THE SOUTHERN GULF OF CALIFORNIA AND ITS ADJACENT SUBAERIAL MARGINS

Sample	Rock type		Latitude (°N)	Longitude (°W)	Elevation/depth (masl)	Sampling	Age (Ma)	Error (Ma)	Method	Material	Age type	Inherited zircons (Ma)
Cretaceous												
PB 32	Qzd		25.2911	110.9345	0	Field	100.4	1.3	U-Pb	Zrn	wm	110 and 114
							99.86	1.72	$^{40}Ar/^{39}Ar$	Bt	tc	
SCr 09-21	Qd		25.3082	110.6957	0	Field	99.12	1.53	$^{40}Ar/^{39}Ar$	Hbl	tc	
ROCA 2J-8	Gdt		22.8116	107.7310	–1991	ROV	98.93	1.45	$^{40}Ar/^{39}Ar$	Bt	tc	
SCr 27	Mzg		25.3058	110.6997	0	Field	98.2	1.5	U-Pb	Zrn	wm	110 and 115
SC 17	Gdt		25.6832	110.7969	0	Field	96.94	0.86	U-Pb	Zrn	wm	104
							90.97	0.65	$^{40}Ar/^{39}Ar$	Hbl	ofa	
							88.52	0.45	$^{40}Ar/^{39}Ar$	Bt	tp	
BEKL 8D-6	Mzg	(b)	24.7758	110.1308	–1205	Dredge	96.7	1.1	U-Pb	Zrn	wm	108 and 127
		(e)	24.7745	110.1350	–900		96.77	0.35	$^{40}Ar/^{39}Ar$	Bt	tc	
ROCA 2J-4	Gdt		22.8104	107.7336	–2219	ROV	94.53	1.47	$^{40}Ar/^{39}Ar$	Hbl	tc	
BEKL 21D-1	Qzd	(b)	24.9331	110.4116	–1392	Dredge	95.4	2.2	U-Pb	Zrn	wm	119 and 130
		(e)	24.9308	110.4146	–1250							
ROCA 2J-2	Qd		22.8096	107.7347	–2297	ROV	93.18	1.88	$^{40}Ar/^{39}Ar$	Hbl	tc	
DANA 47A	Mzg	(b)	22.5167	106.6992	–1079	Dredge	92.92	0.9	U-Pb	Zrn	wm	130 to 168
		(e)	22.5167	106.6940	–780		19.16	0.06	$^{40}Ar/^{39}Ar$	Bt	wm	
SCr 09-20	T		25.2959	110.7005	0	Field	93.83	0.93	$^{40}Ar/^{39}Ar$	Bt	tc	
BEKL 4D-1	Mzg	(b)	23.8280	109.6020	–1020	Dredge	82.42	0.68	U-Pb	Zrn	wm	95 and 104
		(e)	23.8320	109.6040	–850		75.65	2.39	$^{40}Ar/^{39}Ar$	Bt	tc	
BEKL 4D-2	Mzg	(b)	23.8280	109.6020	–1020	Dredge	81.24	0.7	U-Pb	Zrn	wm	
		(e)	23.8320	109.6040	–850		77.93	0.09	$^{40}Ar/^{39}Ar$	Bt	tp	
LCB 7	Gdt		23.2697	109.4420	0	Field	79.96	0.73	U-Pb	Zrn	wm	160
Sayu 01	Gdt		20.8823	105.4177	114	Field	77.71	0.53	U-Pb	Zrn	wm	
							70.85	0.74	$^{40}Ar/^{39}Ar$	Hbl	wm	
							48.71	0.29	$^{40}Ar/^{39}Ar$	Bt	tp	
Sayu 02	Mzg		20.8685	105.4411	19	Field	75.22	0.53	U-Pb	Zrn	wm	112 to 161
							43.91	0.23	$^{40}Ar/^{39}Ar$	Bt	tp	
Tepi 01	Gdt		21.3161	104.9928	750	Field	65.73	0.83	U-Pb	Zrn	wm	
MDCH 02	Gdt		22.8124	105.2630	377	Field	65.38	0.46	U-Pb	Zrn	wm	
Conc 01	Mzg		23.2725	106.1171	113	Field	59.43	0.51	U-Pb	Zrn	wm	
							55.72	0.47	$^{40}Ar/^{39}Ar$	Hbl	tp	
							56.26	0.34	$^{40}Ar/^{39}Ar$	Bt	tp	
Early Miocene												
ROCA 4J-16	Qzd		24.7899	109.2008	–2455	ROV	25.12	0.67	U-Pb	Zrn	wm	30 - 35
							11.13	0.85	$^{40}Ar/^{39}Ar$	K-fsp	wm	
SC 15	AD		25.6589	110.7649	0	Field	22.8	0.27	$^{40}Ar/^{39}Ar$	Gms	tp	
Barr 04	T		21.0204	104.1917	947	Field	22.67	0.4	U-Pb	Zrn	wm	61
							19.8	0.48	$^{40}Ar/^{39}Ar$	Hbl	wm	
							19.65	0.11	$^{40}Ar/^{39}Ar$	Bt	tp	
SC 09-08	Qzd		25.6387	110.8004	0	Field	22.19	0.42	U-Pb	Zrn	wm	
							18.89	0.47	$^{40}Ar/^{39}Ar$	Hbl	tc	
							18.38	0.08	$^{40}Ar/^{39}Ar$	Bt	tp	

(*continued*)

is bounded toward the gulf by a NNW-trending peninsula, where regional mapping by the Mexican Geological Survey (SGM, 2000) reports several Cretaceous granite to tonalite bodies. However, the highest peaks in Bahía Concepción are formed by an inequigranular medium-grained plutonic rock that intrudes Oligocene ignimbrites. McFall (1968) reported an early Miocene age (ca. 20 Ma, K-Ar) for one sample from this intrusive body, and Godinez et al. (2010) also reported an early Miocene age for an intrusive rock west of Loreto, suggesting the presence of younger magmatism after the Cretaceous in this area. South of Bahía Concepción, intrusive rocks are mainly exposed at Santa Catalina and Santa Cruz islands (Figs. 1 and 4A–4D) and were mapped as Cretaceous in the regional geologic maps of Mexican Geological Survey (SGM, 2000). At Santa Catalina Island, the plutonic rocks intrude a greenish-black metasedimentary sequence with a poorly developed schistose texture overlain by an ~150-m-thick limestone strongly affected by contact metamorphism, which forms marble and an ~1.5-m-thick skarn layer. At Santa Cruz Island, the host rocks are high-grade gneiss, which could have reached migmatitic conditions. These basement rocks could be correlated with the Paleozoic to Late Jurassic basement of the El Fuerte Group, found in northern Sinaloa (Mullan, 1978; Keppie et al., 2006; Vega-Granillo et al., 2008, 2012). Plutonic rocks found on these islands are quite similar and consist of a coarse- to medium-grained granodiorite, which locally passes from quartz-diorite to granite, and in some cases shows ductile deformation at both microscopic and macroscopic scales. Mafic enclaves are common, which are mostly rounded and show a broad range of shapes and sizes (Fig. 4A). At Santa Catalina Island, the main pluton is intruded by younger quartz-monzonite to quartz-monzodiorite rocks with distinctive finer-grained texture (Fig. 4B), which yielded early Miocene U-Pb ages (Dave Kimbrough and Marty Grove [unpublished data], *in* Piñero-Lajas, 2008). A younger set of aplitic dikes and then a series of mafic dikes, which mainly intrude along normal faults, crosscut both plutonic units (Fig. 4C).

Eastern Rifted Margin in Nayarit and Sinaloa (Western Mexico Mainland)

Onshore geology of the Nayarit and Sinaloa margin has been recently described by Ferrari et al. (2013) and is only briefly summarized here. The Sierra Madre Occidental ignimbrite plateau is cut toward the gulf by a series of N-S– and NNW-striking normal faults forming grabens and half grabens. No Cretaceous intrusive rocks have been reported for this margin in northern Nayarit, which is extensively covered by early Miocene ignimbrites of the second Sierra Madre Occidental flare-up (Fig. 1). This area of the Sierra Madre Occidental is affected by several

TABLE 3. U/Pb AND $^{40}Ar/^{39}Ar$ AGES OBTAINED FOR INTRUSIVE ROCKS FROM THE SOUTHERN GULF OF CALIFORNIA AND ITS ADJACENT SUBAERIAL MARGINS (*continued*)

Sample	Rock type		Latitude (°N)	Longitude (°W)	Elevation/depth (masl)	Sampling	Age (Ma)	Error (Ma)	Method	Material	Age type	Inherited zircons (Ma)
Early Miocene (*continued*)												
ROCA 4J-12	Mzg		24.7865	109.2023	–2641	ROV	21.56	0.44	U-Pb	Zrn	wm	
							9.91	0.57	$^{40}Ar/^{39}Ar$	K-fsp	tc	
Ros 02	Qzd		23.0011	105.7498	98	Field	21.46	0.15	U-Pb	Zrn	wm	
Oro 1	Mzg		21.4640	104.5020	381	Field	21.29	0.46	U-Pb	Zrn	wm	
							19.07	0.16	$^{40}Ar/^{39}Ar$	Bt	tp	
							17.65	0.13	$^{40}Ar/^{39}Ar$	K-fsp	tp	
ROCA 24J-24	Mzg		24.0190	109.0390	–1983	ROV	20.13	0.23	U-Pb	Zrn	wm	24
							13.77	0.13	$^{40}Ar/^{39}Ar$	Bt	tp	
ROCA 24J-22	S		24.0200	109.0390	–2009	ROV	19.90	0.27	U-Pb	Zrn	wm	590
							9.84	0.18	$^{40}Ar/^{39}Ar$	K-fsp	wm	
BC 09-25	Mzg		26.7827	111.7911	2	Field	19.89	0.57	U-Pb	Zrn	wm	31, 40, 88 and 89
							19.32	0.35	$^{40}Ar/^{39}Ar$	Bt	tp	
SC 09-04	QMz		25.6275	110.7934	0	Field	18.96	0.35	$^{40}Ar/^{39}Ar$	Hbl	tp	
							19.52	0.2	$^{40}Ar/^{39}Ar$	Bt	tc	
ROCA 1J-18	Q-rGD		22.5541	106.6978	–670	ROV	18.76	0.07	$^{40}Ar/^{39}Ar$	Musc	tp	
DANA 71B	Mzg	(b)	24.7463	109.1667	–3050	Dredge	18.73	1.03	$^{40}Ar/^{39}Ar$	Hbl	tc	
		(e)	24.7487	109.1625	–2780		4.17	0.10	$^{40}Ar/^{39}Ar$	K-fsp		
SC 09-03	Qzd		25.5954	110.1541	1	Field	18.66	0.22	$^{40}Ar/^{39}Ar$	Hbl	tp	
							19.73	0.61	$^{40}Ar/^{39}Ar$	Bt	tc	
ROCA 1J-1	Mzg		22.5564	106.7101	–1486	ROV	18.21	0.22	U-Pb	Zrn	wm	
							18.68	0.1	$^{40}Ar/^{39}Ar$	Bt	tp	
							14.05	0.43	$^{40}Ar/^{39}Ar$	K-fsp	tp	
PHC 09	Qzd		21.5123	104.5179	289	Field	18.16	0.18	U-Pb	Zrn	wm	
SC 24	Qzd		25.6242	110.7931	0	Field	18.10	0.15	$^{40}Ar/^{39}Ar$	Bt	tp	
Middle Miocene												
ROCA 22J-1	Qzd		24.2510	109.6760	–1516	ROV	15.86	0.35	U-Pb	Zrn	wm	
							15.93	0.08	$^{40}Ar/^{39}Ar$	Bt	tp	
BEKL 6D-1	Mzg	(b)	24.1140	109.4586	–1205	Dredge	15.38	0.17	U-Pb	Zrn	wm	
		(e)	24.1148	109.4638	–900		13.71	0.31	$^{40}Ar/^{39}Ar$	Hbl	tp	
							13.45	0.22	$^{40}Ar/^{39}Ar$	Bt	tc	
BEKL 6D-2	QMz	(b)	24.1140	109.4253	–1205	Dredge	14.85	0.14	U-Pb	Zrn	wm	
		(e)	24.1148	109.4638	–900							
BEKL 10D-1	Mzg	(b)	24.8081	109.9233	–1498	Dredge	13.73	0.18	U-Pb	Zrn	wm	
		(e)	24.8050	109.9285	–1200		12.57	0.09	$^{40}Ar/^{39}Ar$	Bt	tp	
BEKL 10D-3	Mzg	(b)	24.8081	109.9233	–1498	Dredge	14.06	0.22	U-Pb	Zrn	wm	
		(e)	24.8050	109.9285	–1200							

Note: U/Pb age errors are expressed in 2σ and $^{40}Ar/^{39}Ar$ errors are in 1σ. Complete data for all the experiments performed are given in supplemental files 4 and 5 (see text footnote 1); (b) begin and (e) end coordinates of dredge track; masl—meters above sea level. Abbreviations: Qzd—quartz monzodiorite; Mzg—monzogranite; Qd—quartz diorite; Gdt—granodiorite; T—tonalite; AD—andesite dike; S—syenogranite; QMz—quartz monzonite; Q-rGD—quartz-rich granitoid dike; Zrn—zircon; Bt—biotite; Hbl—hornblende; K-fsp—K-feldspar; Gms—groundmass; Musc—muscovite; wm—weighted mean; tc—correlation age; ofa—one fraction age; tp—plateau age; ROV—remotely operated vehicle.

NNE to N-S grabens produced by extension between 24 and 18 Ma (Ferrari et al., 2002), which has been related to the onset of rifting of the Gulf of California (Ferrari et al., 2013). The grabens are subsequently cut by NNW extensional fault systems active since ca. 20 Ma that locally expose early Miocene intrusive bodies at very low elevation along the main rivers (Ferrari et al., 2007, 2013; samples Ros 02, Oro 01, and PHC 09; Fig. 1). These plutons are typically inequigranular, with medium- to fine-crystalline and even porphyritic texture (e.g., sample PHC 09). These textural characteristics, and the fact that these plutons intrude the Oligocene ignimbrites, are suggestive of a very shallow depth of emplacement (<5 km). Intrusive rocks were also sampled southwest of Tepic along the NE-striking scarp bounding the mouth of the Gulf of California near Sayulita (samples Sayu 01, Sayu 02, and Tepi 01; Fig. 1). These rocks are equigranular and coarse grained and intrude a metasedimentary or metavolcanic succession of Jurassic to Early Cretaceous age (Valencia et al., 2013), indicating that they are part of the Late Cretaceous Puerto Vallarta Batholith.

Submerged Rifted Margins

Continental Crust on the Flanks of Alarcón Basin

Most of the northwestern boundary of Alarcón Basin has an abrupt contact between oceanic crust with clear magnetic anomalies of the C2An sequence (DeMets, 1995) and a steep continental slope from which silicic lavas and tuffs were dredged. At the northwest end of this continental slope, an orthogonal intersection with a NW-striking fault scarp provides a window into the interior of the slope, and ROCA 24J dive (Figs. 2 and 3) sampled a mainly granitic and andesitic section here (Figs. 4E–4F). The intersecting NW-striking scarp is at the southern end of a major structural lineament, which Lyle and Ness (1991) named the Santa Cruz fault zone and speculated that it was an extinct intracontinental transform fault zone that after ca. 3.7 Ma linked the northeast end of the Alarcón spreading axis to actual or incipient spreading centers in Farallón Basin before opening of the Pescadero Basin. Near the western corner of Alarcón Basin, the rifted continental slope is similarly intersected by the NW-striking Cerralvo Trough, a 10–20-km-wide depression that extends for 75 km to just beyond the northern tip of Cerralvo Island. There is clear geomorphic evidence of an inactive strike-slip fault with at least 30 km of right-lateral offset along the Cerralvo Island (southwest) side of the trough (Lonsdale and Kluesner, 2010; Kluesner, 2011), and we infer that the trough was a transtensional fault zone that, before the Alarcón Basin opened, linked Baja–North America spreading in the mouth of the gulf (i.e., the axes of the Los Frailes and Maria Magdalena Rises, predecessors of the East Pacific Rise; Castillo et al., 2010) to sites of oblique extension within the gulf. The

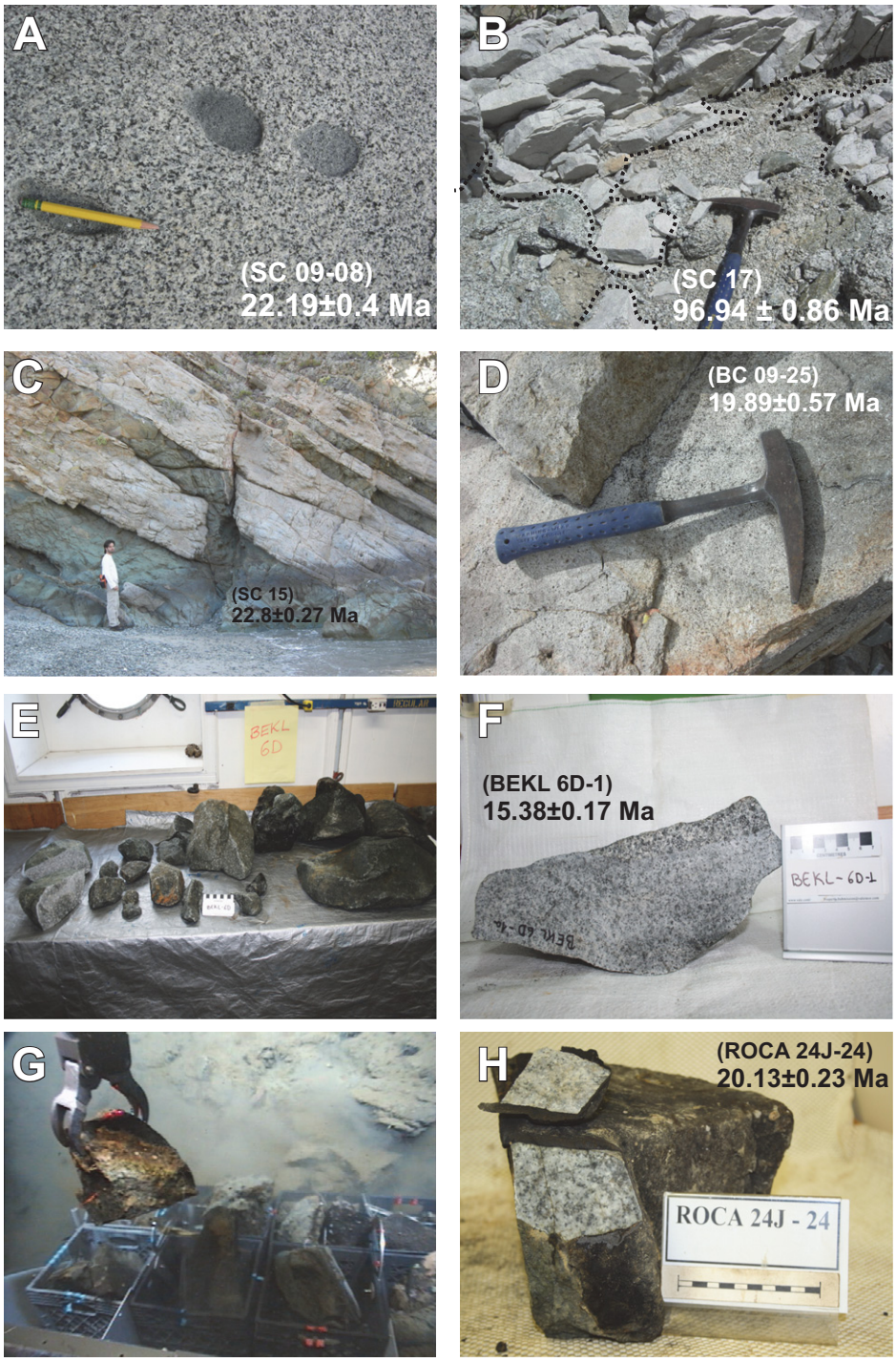

Figure 4. Field and megascopic aspect of studied samples. (A) Detail of early Miocene quartz monzodiorite (SC 09–08) from Santa Catalina Island (25.6387°N, 110.8004°W). (B) Early Miocene quartz monzodiorite (similar to SC 09–08) intruding a Cretaceous tonalite (SC 17) at Santa Catalina Island (25.6832°N, 110.7969°W). (C) Early Miocene mafic dike (SC 15) cutting a Cretaceous tonalite (similar to SC 17), Santa Catalina Island (25.6589°N, 110.7649°W). (D) Early Miocene subvolcanic granite intrusion (BC 09–25) from Bahía Concepción, Baja California (26.7827°N, 111.7911°W). (E) Samples recovered from dredge site BEKL 6D along a fault scarp in the southern part of the East Cerralvo Basin. (F) Megascopic view of the texture of middle Miocene monzogranite sampled at site BEKL 6D-1. (G) Sampling of ROCA 24J-24 sample with the remotely operated vehicle (ROV) *Jason* along the fault scarp bounding the Pescadero Basin to the west (24.0190°N, 109.0390°W, 1983 m below sea level); sample size: 26 × 23 × 13 cm. (H) Megascopic view of the texture of the early Miocene monzogranite recovered at site ROCA 24J-24.

northeast side of Cerralvo Trough is the scarp of a W-dipping, seismically active (Munguía et al., 2006) normal fault; it rises to the rift shoulder named Cerralvo Bank (with a wave-planed summit now at 200–300 m depth), one of the family of large-offset E- and W-dipping faults at the margins of the uplifted Cabo block. ROCA 22J climbed the steep lower part of this scarp, a few kilometers from where a U.S. Geological Survey (USGS) cruise in 1976 had dredged Cretaceous quartz-diorite and an altered middle Miocene hypabyssal rock of andesitic composition (M. Grove, 2007, personal commun.). The dive crossed a young fault scarp in the talus ramp and then climbed a highly altered and fault-brecciated granitic section (Fig. 3). Cerralvo Bank, indeed the whole 35-km-wide block of continental crust between Cerralvo Trough and Santa Cruz fault zone, is cut by extensional faults that strike 005°–015°, 45° oblique to the bounding NW-striking fault zones, and define shallow but steep-walled grabens; BEKL 6D dredged granitic rocks from one of the larger (500-m-high) examples of these N-striking graben-bounding scarps (Figs. 4G–4H). North of ~24.5°N, beyond Cerralvo Trough and the Cerralvo Bank block, most fault scarps maintain a northerly strike, but they tend to define short, isolated horsts rather than well-defined grabens; their lack of parallelism to the main rift-bounding faults (e.g., those of the Main Gulf Escarpment and other faults defining Santa Cruz Basin and Bahía La Paz Basin) may result from rotation of small fault blocks by distributed right-lateral shearing, as demonstrated by fault blocks in similar situations in the northern gulf (Seiler et al., 2011). Dredges BEKL 8D and 10D recovered Cretaceous and Miocene granites from two small N-striking horsts in this distal part of the northwest flank of Alarcón Basin, south of Farallón Basin (Fig. 2). Nearby dredge BEKL 21D collected Cretaceous granite from a very steep, ~650-m-high cliff formed by an E-dipping fault parallel to the Main Gulf Escarpment.

The continental slope at the southeast boundary of the oceanic Alarcón Basin is not quite as steep as the one on the northwest side, and Tamayo Bank (Fig. 2A) is not as shallow as its

conjugate Cerralvo Bank, but it has an equally abrupt contact with the oceanic crust. The sheared-margin scarp at the southwest side of Tamayo Bank, which prior to Alarcón Basin spreading was continuous with the northeast side of Cerralvo Trough (the site of ROCA 22J), was explored by ROCA 2J. Its two upslope profiles (Fig. 3), located 17 km and 20 km southeast of the truncation of the scarp by oceanic crust at the southern corner of Alarcón Basin, climbed a Cretaceous granitic outcrop overlain by sandstone and mudstone. The dredging sites of Niemitz and Bischoff (1981, p. 388–389) are ~10 km southeast of ROCA 2J profile B, near where the sheared-margin scarp intersects the top of the rifted continental margin of Alarcón Basin; they reported a "granodiorite-tonalite suite" plus "a transitional suite of andesitic rocks, recovered from the lowermost part of the slope"; neither suite has been dated. At the ROCA 2J dive sites, the sheared margin of the "proto–Tamayo transform," a largely intracontinental shear zone that extended into Cerralvo Trough, is ~5 km north of the Tamayo fracture zone. The trail of the present Tamayo transform, and the intervening strip, is conjugate to the turbidite-smothered floor of Cerralvo Trough. Fitting the dredging profile shown in figure 9 of Niemitz and Bischoff (1981) to our multibeam bathymetry, it is clear that this strip, sampled at the steep step down to the west flank of the East Pacific Rise, is the source of the reported andesite suite.

Southeast of Tamayo Bank, seismic-refraction profiles (Lizarralde et al., 2007) show dramatic crustal thinning beneath an elongate depression known as Tamayo Trough (Fig. 2). However, seismic-reflection profiles indicate only minor faulting of the discontinuously reflective "basement" layer, which Sutherland et al. (2012) attributed to a volcanic or volcaniclastic section, beneath the trough floor and margins. This could easily be explained if the volcanic section postdated major basin-formation faulting, but if it is part of the lower to middle Miocene Comondú Group, the interpretation favored by Sutherland et al. (2012), this would imply large-scale faulting and basin extension there in the early Miocene. ROCA dive 3J onto Tamayo Dome, a major but mostly sediment-smothered, 40-km-diameter volcanic structure at the northern end of Tamayo Trough, sampled rhyolitic lithic ignimbrite that could have been a source of the structure-obscuring layer in Tamayo Trough. The tuff yielded a ^{40}Ar-^{39}Ar age of 11.70 ± 0.07 Ma (Ferrari et al., 2013), right at the middle-late Miocene boundary, providing a minimum age for this layer.

Further to the southeast, three large (50–70-km-long, up to 1-km-high) fault-bounded ridges, horsts, and half-horsts that strike N-NE (020°), curving to N-NW (340°) near their northern ends, rise above the muddy seafloor. These Nayarit Ridges have wave-planed summits, which step up from 500–600 m deep at the western ridge to 200–300 m deep at the central ridge, and 140–250 m deep at the eastern ridge, and their basement rocks crop out on their sides, especially at the W-dipping fault scarps on their western sides. The fresh granitic samples collected at the DANA 47 site, and the contrast between Cretaceous (U/Pb zircon; M. Grove, 2006, personal commun.) and Neogene ^{40}Ar-^{39}Ar mica cooling ages (published here) observed on some samples prompted us to resample this site during the ROCA cruise (ROCA 1J; Fig. 3).

Continental Crust on the Southeastern Flank of Farallón Basin

Subsided continental crust at the margin of Farallón Basin, which is mostly buried by thick turbidites, is well exposed at a scarp along the North Pescadero Transform (Fig. 2). This transform is a relatively recent link between the spreading center in the broad Farallón Basin and a younger spreading center that has accreted the floor of the much narrower North Farallón Basin. Because of its youth, all of this transform is bounded by continental crust on one or both sides, and because it is significantly oblique to present Baja California–North America relative plate motion (Fig. 2A), a deep transtensional transform valley has opened along these actively shearing continental margins.

The part of the transform valley that extends northwest from the northeastern tip of the North Pescadero spreading axis is relatively protected from terrigenous sediment filling, and it has a valley wall that rises steeply from 3300 m to 1200 m on its northeastern (continental) side. Of course, not all of this 2-km-high wall exposes igneous basement: It has a partly sediment-covered talus ramp that accounts for 600 m of relief at the foot of the scarp, and on the ROCA 4J profile (Fig. 3), we encountered only sedimentary rock at depths shallower that 1700 m. The DANA 71 dredge included Miocene granitic intrusive rocks in its diverse rock collection from the scarp-foot talus, and ROCA 4J was targeted to a nearby site to get more samples of this rock type to define the vertical extent of its outcrop and to attempt to define the stratigraphy of the overlying volcanic sections.

RESULTS

The plutonic rocks of the southern Gulf of California analyzed in this work yielded three separate groups of intrusion (U/Pb) ages: Cretaceous to early Paleocene (ca. 100–60 Ma), early Miocene (ca. 25–18 Ma), and middle Miocene (ca. 15.5–13.5 Ma). Significantly, no Oligocene age of intrusion was found in the study area, supporting the general conclusions of previous studies that the first ignimbrite flare-up of the Sierra Madre Occidental was sourced from areas to the east of the present-day Gulf of California (e.g., Ferrari et al., 2007). These three age groups are used in the description of the petrographic, geochemical, and geochronological results, which are summarized in Tables 1, 2, and 3 and Figures 5, 6, and 7. A brief explanation of each age obtained for the dated sample is given in the supplemental file 4 (see footnote 1).

Petrography and Geochronology

Cretaceous–Paleocene Magmatic Episode

Nineteen samples within and around the Gulf of California yielded Cretaceous to early Paleocene ages (100 and 60 Ma; Fig. 1; Table 3), with younger ages mostly toward the east (Fig. 8). On the western rifted margin, rocks of this group are all older than 80 Ma. They are found to the south of Loreto (Punta Botella; Fig. 1) and along the rifted continental crust offshore southern Baja California at the western border of the Farallón, Pescadero, and Alarcón Basins (Santa Cruz and Santa Catalina Islands, Partida Bank, Los Cabos block). On the eastern rifted margin, dated rocks range between ca. 100 and ca. 60 Ma and were found at the western Nayarit scarp (dredge DANA 47A), along the Tamayo fracture zone (dive ROCA 2J), and in the southern Sinaloa and northern Nayarit coastal area on the mainland (Sayu 01, Sayu 02, MDCH 02, Tepi 1, and Conc 01; Figs. 1 and 2A; Table 3).

Figure 5 (*on following three pages*). U/Pb concordia and ^{40}Ar-^{39}Ar age spectra or ^{36}Ar-^{40}Ar vs. ^{39}Ar-^{40}Ar correlation diagrams for Cretaceous plutons; the obtained age is given for each sample. In the U/Pb concordia diagrams, dashed ellipses indicate data not taken into account for age calculation. In the ^{40}Ar-^{39}Ar ages spectra, t_p and W_m indicate plateau and weighted mean ages, respectively; these ages were calculated using the fractions identified with the horizontal arrow. The value t_c indicates the isochron age, calculated using the fractions identified with the dotted line in the age spectra diagrams. Detailed information on the geochronological analysis is given in supplemental file 4 (see text footnote 1). MSWD—mean square of weighted deviates.

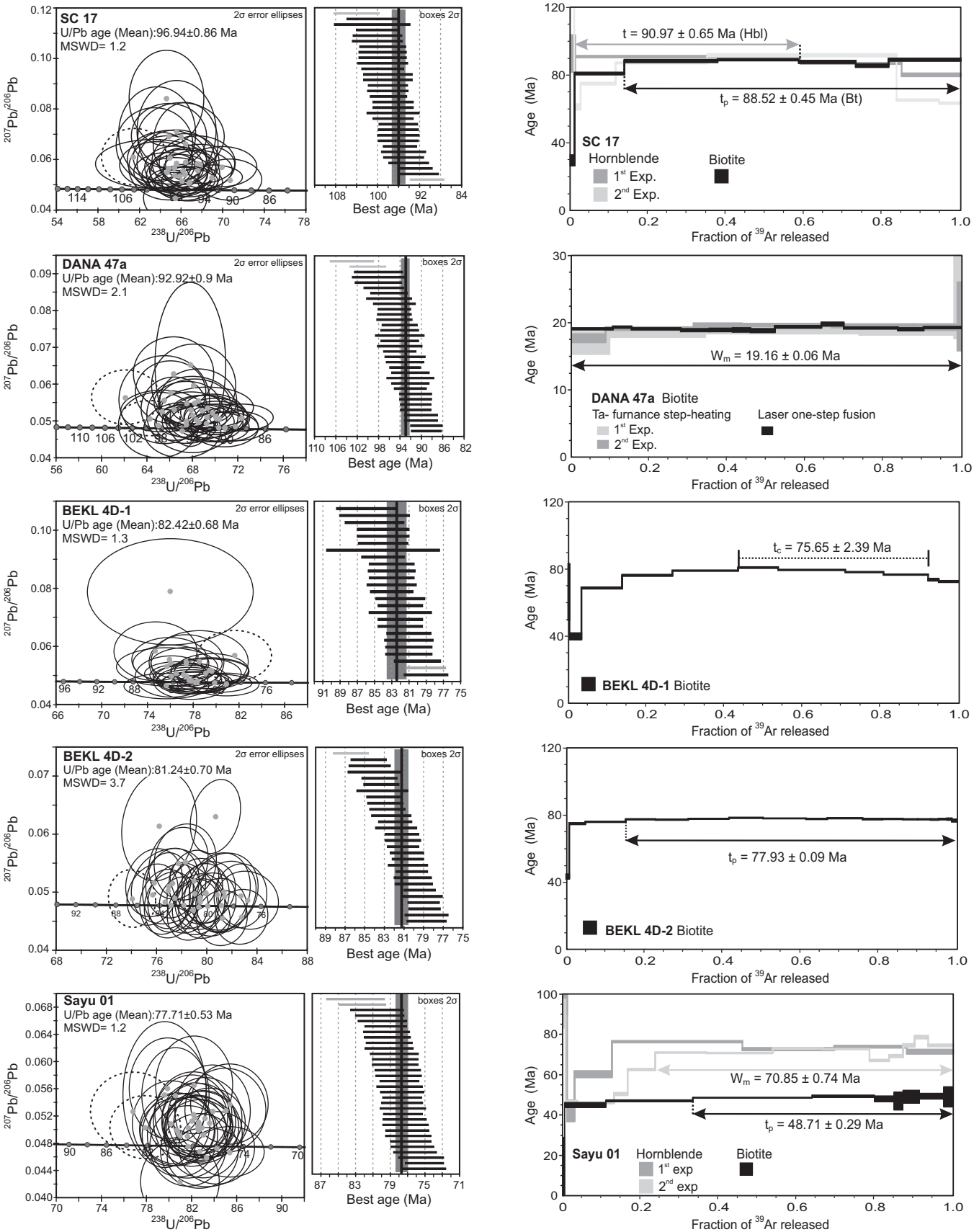

Figure 5.

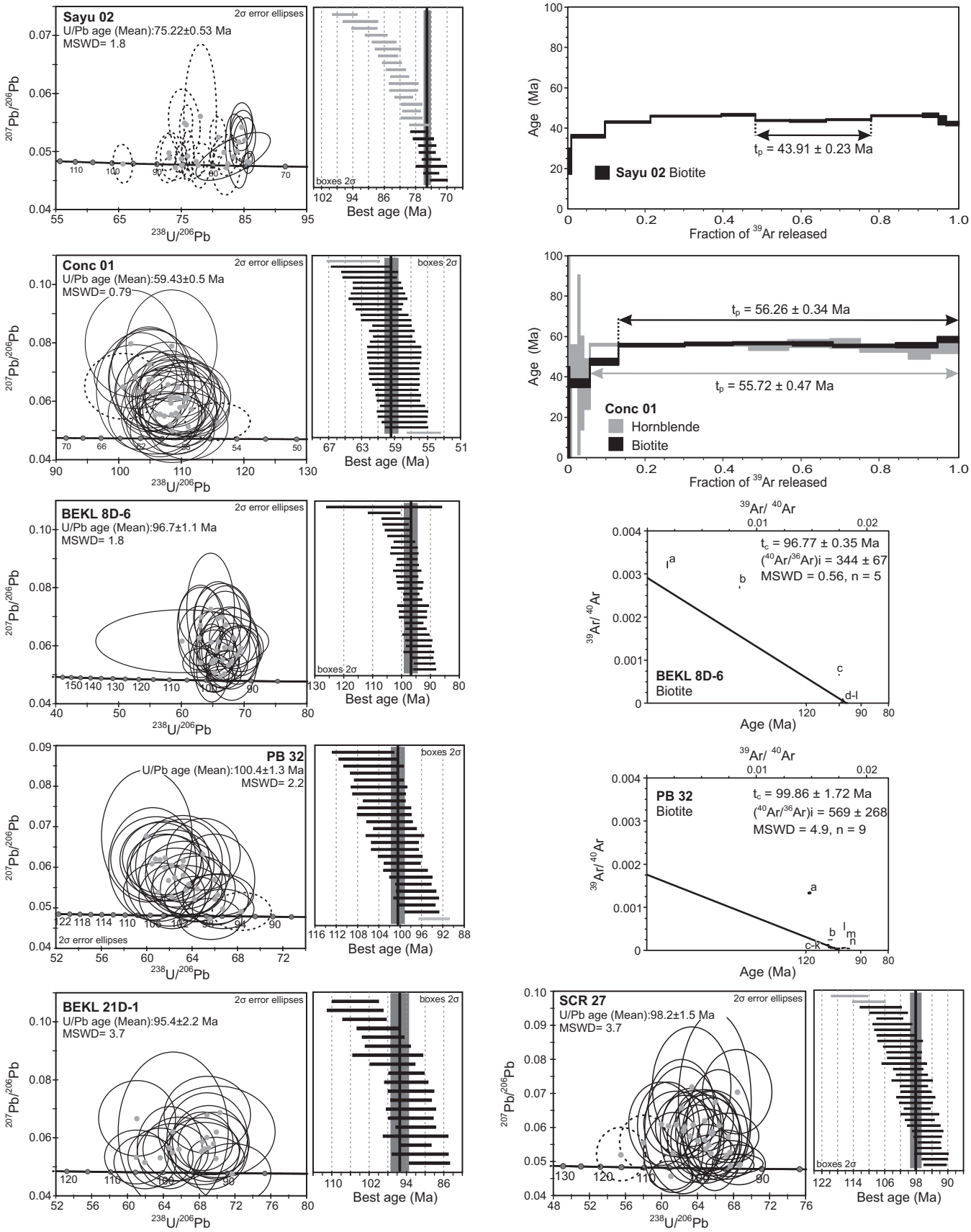

Figure 5 (*continued*).

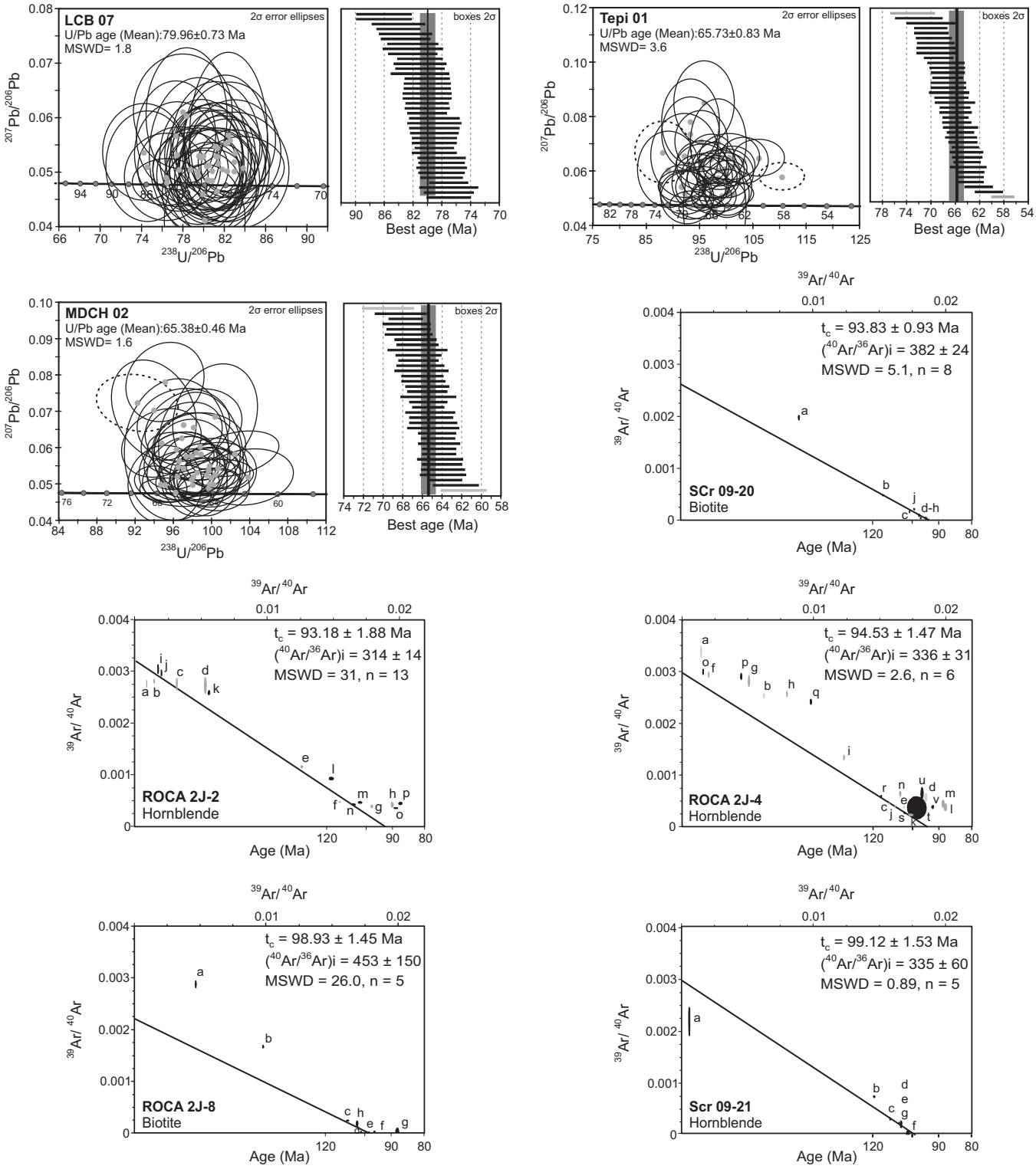

Figure 5 (*continued*).

The studied samples are defined as quartz monzodiorite, granodiorite, quartz diorite, tonalite, and monzogranite in the Streckeisen (1976) classification scheme (Table 1). Samples are mainly equigranular, with hypidiomorphic granular texture and medium to coarse grain size (Table 1). Some samples display an inequigranular texture characterized by an older generation of larger crystals (plagioclase and K-feldspar) and a second generation of medium- to coarse-grained crystals, arranged in a hypidiomorphic granular texture. A factor of note is that all samples from the Mexican mainland are medium grained; coarse-grained samples were found along the lower part of the Tamayo fracture zone at depths

of 2297 and 2219 m below sea level (bsl; ROCA 2J-2 and ROCA 2J-4, respectively; Figs. 2A and 3), and in the western rifted margin (dredges BEKL 4D, 8D, and 21D, depths between 850 and 1392 mbsl; Santa Cruz Island, SCr 09–20, SCr 09–21; Punta Botella, PB 32; Figs. 2 and 3). In the Cretaceous–Paleocene samples, amphibole and biotite are the main ferromagnesian minerals, whereas apatite, zircon, titanite, and Fe-Ti oxides are common accessory minerals. Some Cretaceous samples display mineral lineations, possibly related to the syntectonic older intrusions in southern Baja California and Sinaloa (Henry and Fredrikson, 1987; Henry et al., 2003; Cuéllar-Cárdenas et al., 2012).

Most Cretaceous–Paleocene samples have ^{40}Ar-^{39}Ar ages 5–10 m.y. younger than the corresponding U/Pb age (Figs. 5 and 8). Nevertheless, some samples from western Nayarit and its offshore region (Fig. 1D) yielded a much larger time gap between intrusion and cooling age (Sayu 01, Sayu 02, DANA 47A; Table 3; Fig. 8). Samples Sayu 01 and Sayu 02 represent two different magmatic facies from the same pluton, and they have similar intrusion ages of ca. 76 Ma (Figs. 5 and 8). However, Sayu 01 yielded a ^{40}Ar-^{39}Ar age on hornblende of 70.85 ± 0.74 Ma, and a ^{40}Ar-^{39}Ar biotite age of 48.71 ± 0.29 Ma, similar to the 43.91 ± 0.23 Ma age obtained for a biotite from Sayu 02 (Fig. 5). Sample DANA 47A, dredged on the western Nayarit scarp (Figs. 1D, 2, and 3), has a U/Pb age of 92.92 ± 0.90 Ma, but a ^{40}Ar-^{39}Ar biotite age of 19.16 ± 0.06 Ma. This latter age is similar to the 18.21 ± 0.22 Ma U/Pb age and the 18.68 ± 0.1 Ma ^{40}Ar-^{39}Ar biotite ages of sample ROCA 1J-1 (Figs. 5 and 8), as well as the 18.76 ± 0.07 Ma ^{40}Ar-^{39}Ar muscovite age of sample ROCA 1J-18 (Figs. 5 and 8). These three samples (DANA 47A, ROCA 1J-1, and ROCA 1J-18) were recovered within a few kilometers in the same area of the western Nayarit scarp (Figs. 1D, 2, and 3), which we interpret as formed by a Cretaceous batholith (sampled by DANA 47A) that was subsequently intruded by a series of younger bodies during the early Miocene (ca. 18–19 Ma). The intrusion of these early Miocene rocks likely generated a thermal anomaly, potentially perturbing the ^{40}Ar-^{39}Ar systematics of surrounding rocks. The Cretaceous U/Pb age of sample DANA 47A contrasts with the early Miocene biotite ^{40}Ar-^{39}Ar age obtained on the same sample (19.16 ± 0.06 Ma), which approaches Ar cooling ages for samples ROCA 1J-1 and ROCA 1J-18 (Figs. 5 and 6). These age differences suggest that the DANA 47A biotite was reheated by the intrusion of a plutonic body represented by ROCA 1J-1 and ROCA 1J-18 samples. The age spectra of DANA 47A (Fig. 5) does not show any evidence of perturbation, indicating that the Ar system was completely reset. Furthermore, samples Sayu 01 and Sayu 02, which yield Cretaceous U/Pb ages (ca. 76 Ma), also yielded Eocene (48.71 ± 0.29 Ma and 43.91 ± 0.23 Ma) ^{40}Ar-^{39}Ar biotite ages, which probably are geologically meaningless. In fact, these samples have a so-called "Turner profile" spectra, which is typical of biotites that has undergone incomplete Ar loss (York and López-Martinez, 1986). This is confirmed by the fact that no intrusive or extrusive rocks of Eocene age are found in the surrounding region, which is in turn affected by widespread late Miocene mafic volcanism. We thus interpret the Sayulita pluton to have been only mildly reheated by a younger igneous event causing only partial Ar loss.

Early Miocene Magmatic Episode

Seventeen samples yielded U/Pb zircon ages between 25 and 18 Ma. They span the whole southern gulf from the eastern side of the Baja California peninsula and its neighboring islands, to the submerged rifted blocks, and Mexico mainland in Nayarit and Sinaloa (Table 3; Fig. 6). On the western rifted margin of the gulf, early Miocene plutons were found at Bahía Concepción, on Santa Catalina Island, and in the submerged continental blocks to the east (Figs. 1B–1D and 2). The early Miocene plutons are commonly medium grained, and inequigranular textures predominate over equigranular ones (Table 1), whereas fine-grained and porphyritic rocks were only found in the southeastern part of the gulf. Inequigranular samples are mostly medium grained, with the exception of a fine-grained sample from the western Nayarit scarp collected at 670 mbsl (ROCA 1J-18) and a porphyritic subvolcanic intrusion with very fine-grained matrix from the southwestern foothills of the Sierra Madre Occidental (PHC 09; Fig. 1D). Equigranular samples are hypidiomorphic granular with variable grain size (coarse to fine grained). The only fine-grained equigranular sample (Ros 02) comes from southern Sinaloa, in mainland Mexico. Coarse-grained, equigranular samples were found only at three localities: the southern Pescadero transform fault at depths of 1983 mbsl (ROCA 24J-24), the western Nayarit scarp at depths of 1486 mbsl (ROCA 1J-1), and east of Tepic in the Sierra Madre Occidental foothills (Oro 1) at 381 masl (Figs. 1, 2, and 3).

The least-differentiated early Miocene rocks are quartz diorite, quartz monzodiorite, monzogranite, and tonalite that contain amphibole and biotite as the main ferromagnesian minerals, and titanite, zircon, apatite, and Fe-Ti oxides as accessory minerals. Within the more-evolved rocks, which classify as monzogranite, syenogranite, and granite, the main ferromagnesian mineral is biotite, whereas amphibole and titanite are absent (except for DANA 71B, which has 11% of amphibole). Muscovite, along with biotite, was observed only in a granite sample from the western Nayarit scarp (ROCA 1J-18). In some early Miocene samples, pyroxene constitutes 2%–17.5% of the rock. Usually, pyroxene is found as subhedral crystals exhibiting resorption textures that in some cases obliterate the original crystal structure; the presence of orthopyroxene and clinopyroxene crystals, even in highly differentiated samples (e.g., monzogranite BC 09–25), along with resorption textures, indicates that pyroxene was not in equilibrium with the melt.

Several early Miocene plutonic rocks show little difference between intrusion and cooling ages. A fine-grained monzogranite in the eastern side of Bahía Concepción (sample BC 09–25) yielded almost identical U/Pb and ^{40}Ar-^{39}Ar biotite ages of 19.89 ± 0.57 Ma and 19.32 ± 0.35 Ma, respectively. This indicates that in this area, the pluton cooled very quickly (within ~0.5 m.y.) from emplacement (~900 °C) to below 350–400 °C, the closure temperature of biotite (Reiners et al., 2005; Fig. 6). A rapid cooling at ca. 19–18 Ma can be also inferred at Santa Catalina Island. The quartz-monzonite that crops out in the western part of the island yielded a U/Pb age of 22.19 ± 0.42 Ma (sample SC 09–08; Table 3; Fig. 6), a hornblende age of 18.89 ± 0.47 Ma, and a biotite age of 18.38 ± 0.08 Ma. A dike intruding the Cretaceous pluton in the eastern side of the island (SC 15) yielded a ^{40}Ar-^{39}Ar age of 22.8 ± 0.27 Ma (groundmass), but the rest of early Miocene granitoids sampled at the island (SC 09–03, SC 09–04, and SC 24) all fall in a narrow ^{40}Ar-^{39}Ar age range at ca. 19–18 Ma (Table 3; Fig. 6).

Figure 6 (*on following three pages*). U/Pb concordia and ^{40}Ar-^{39}Ar age spectra or ^{36}Ar-^{40}Ar vs. ^{39}Ar-^{40}Ar correlation diagrams for early Miocene plutons; the obtained age is given for each sample. In the U/Pb concordia diagrams, dashed ellipses indicate data not taken into account for age calculation. In the ^{40}Ar-^{39}Ar age spectra, t_p and W_m indicate plateau and weighted mean ages, respectively; these ages were calculated with the fractions identified with the horizontal arrow. The value t_c indicates the isochron age, calculated using the fractions identified with the dotted line in the age spectra diagrams. Detailed information on the geochronological analysis is given in supplemental file 4 (see text footnote 1). MSWD—mean square of weighted deviates.

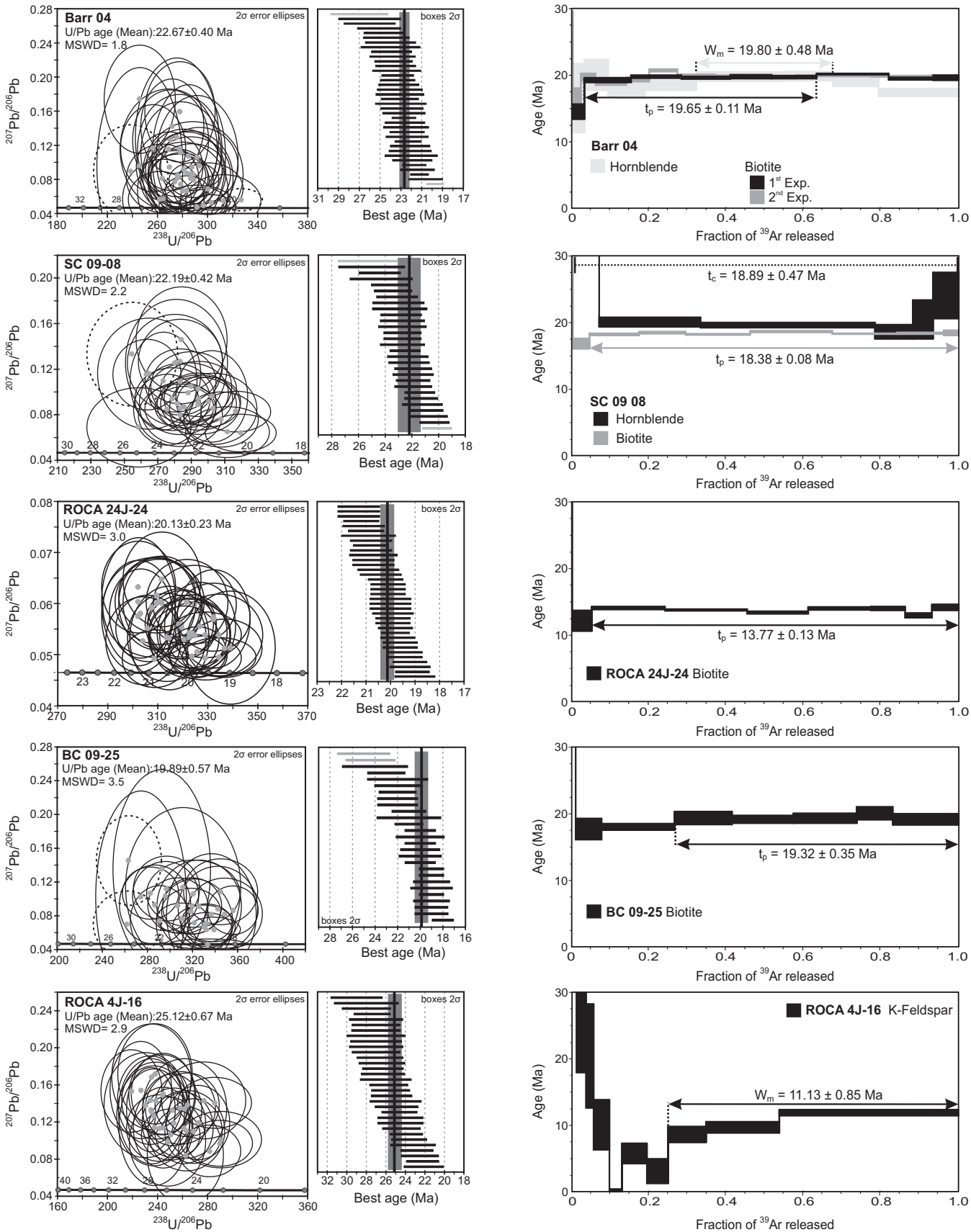

Figure 6.

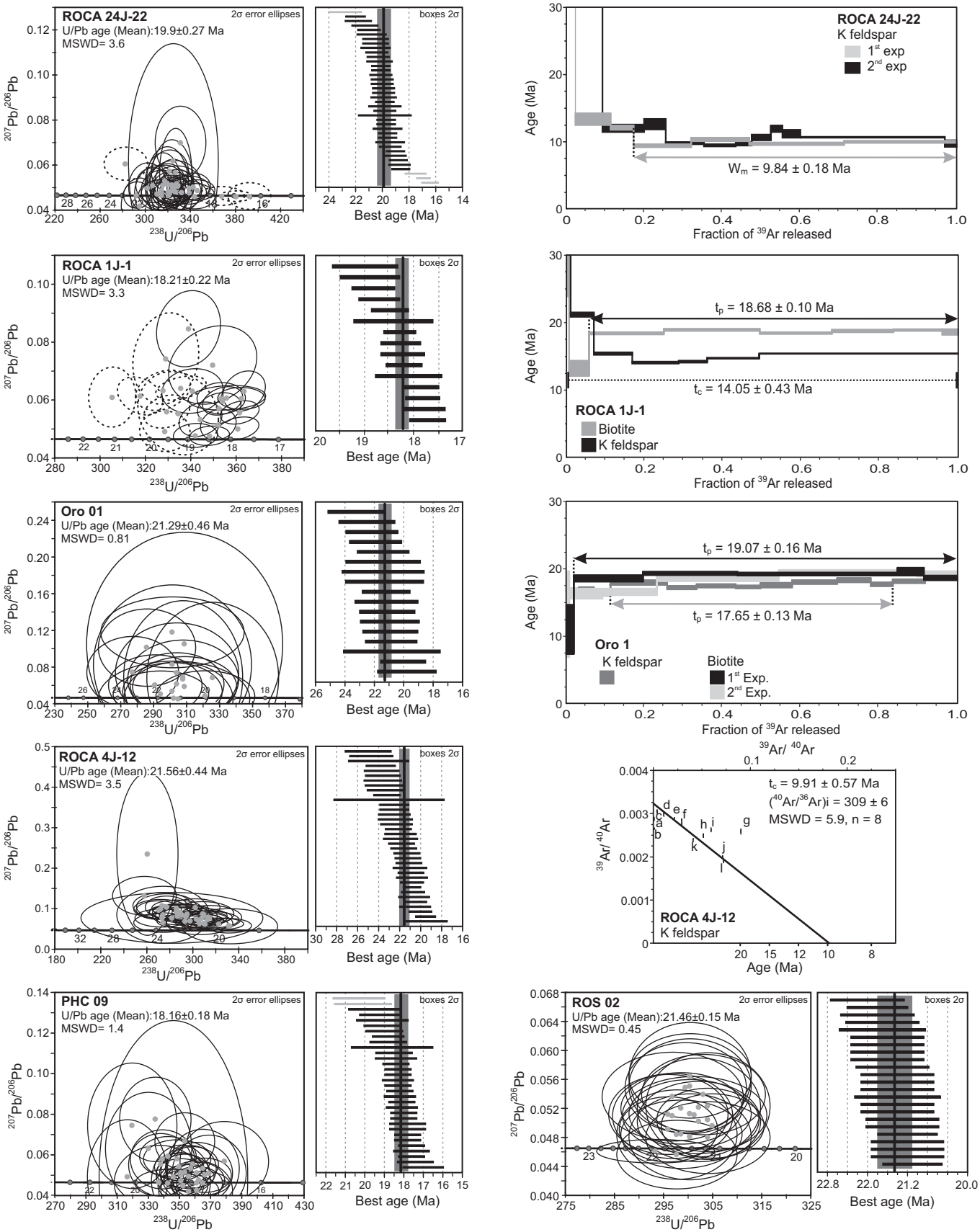

Figure 6 (*continued*).

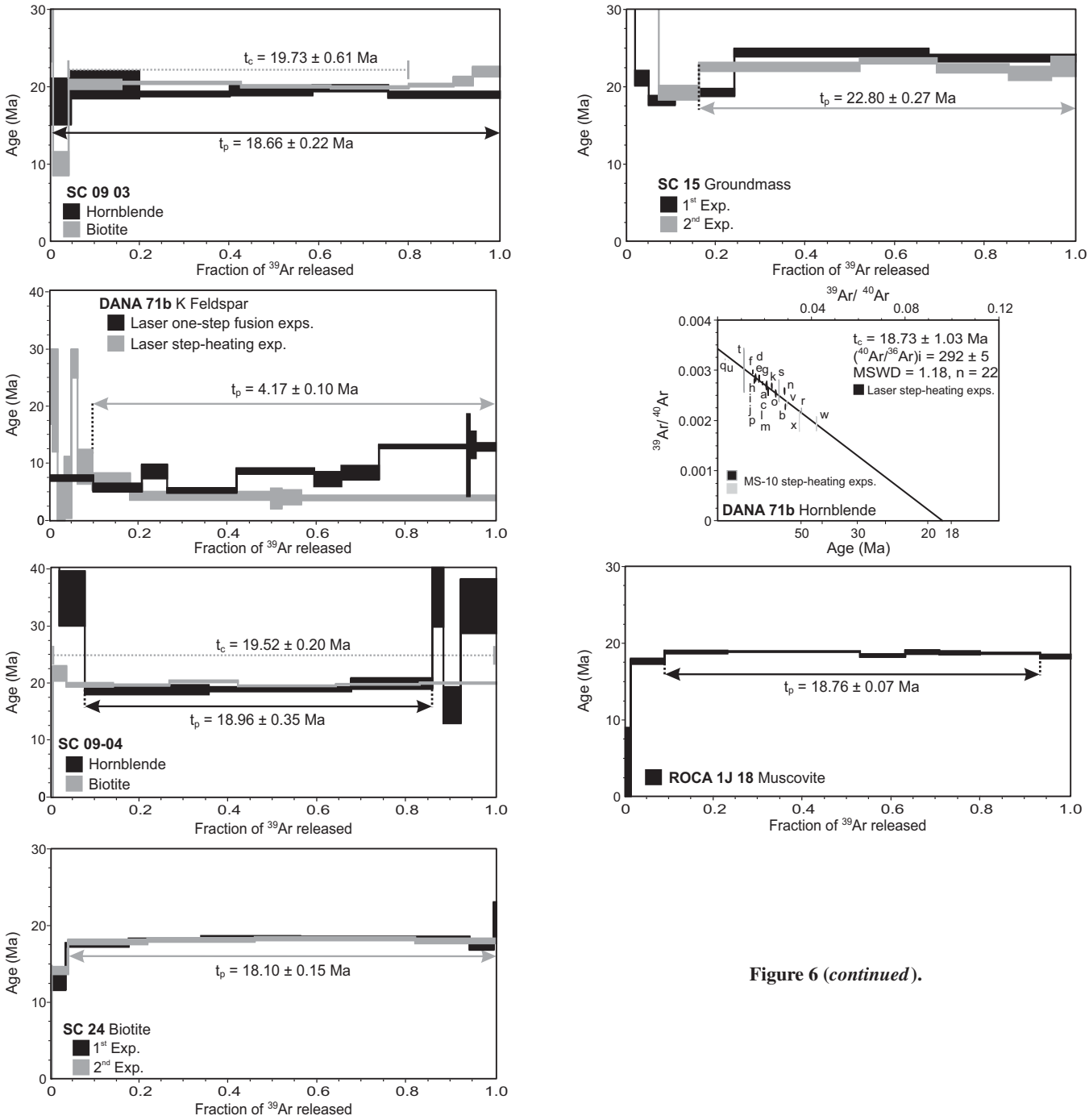

Figure 6 (*continued*).

On mainland Mexico, samples collected in two outcrops 5 km apart from the same pluton along the Río Santiago (northern Nayarit) yielded a U/Pb age of 18.16 ± 0.18 Ma (sample PH 09), a ^{40}Ar-^{39}Ar biotite age of 19.07 ± 0.16 Ma, and a 17.65 ± 0.13 Ma K-feldspar age (sample Oro 01). A sample from an inequigranular, medium-grained granodiorite further to the southeast in the Tepic-Zacoalco rift (Barr 04) yielded a zircon U/Pb age of 22.67 ± 0.4 Ma, with younger and very close ^{40}Ar-^{39}Ar hornblende and biotite ages of 19.8 ± 0.48 Ma and 19.65 ± 0.11 Ma, respectively. Intrusive rocks sampled at the fault scarps bounding the Pescadero Basin (Fig. 2A) show a pervasive alteration that prevented their dating by the ^{40}Ar-^{39}Ar method but yielded consistent early Miocene emplacement ages. Samples ROCA 4J-16 and ROCA 4J-12, recovered north of the Pescadero Basin, yielded U/Pb ages of 25.12 ± 0.67 Ma and 21.56 ± 0.44 Ma, respectively (Fig. 6). Samples from the southwestern scarps of the same basin (ROCA 24J-24 and ROCA 24J-22) yielded slightly younger ages of 20.13 ± 0.23 Ma and 19.90 ± 0.27 Ma.

Samples from sites ROCA 4J and ROCA 24J all have early Miocene U/Pb ages but yielded middle to late Miocene ^{40}Ar-^{39}Ar ages between 13.7 and 9.8 Ma (Table 3; Fig. 6). Sample DANA 71B was dredged very close to ROCA 4J site and yielded a very young ^{40}Ar-^{39}Ar age of 4.17 ± 0.10 Ma on K-feldspar (Table 3; Fig. 6). Experimental results from

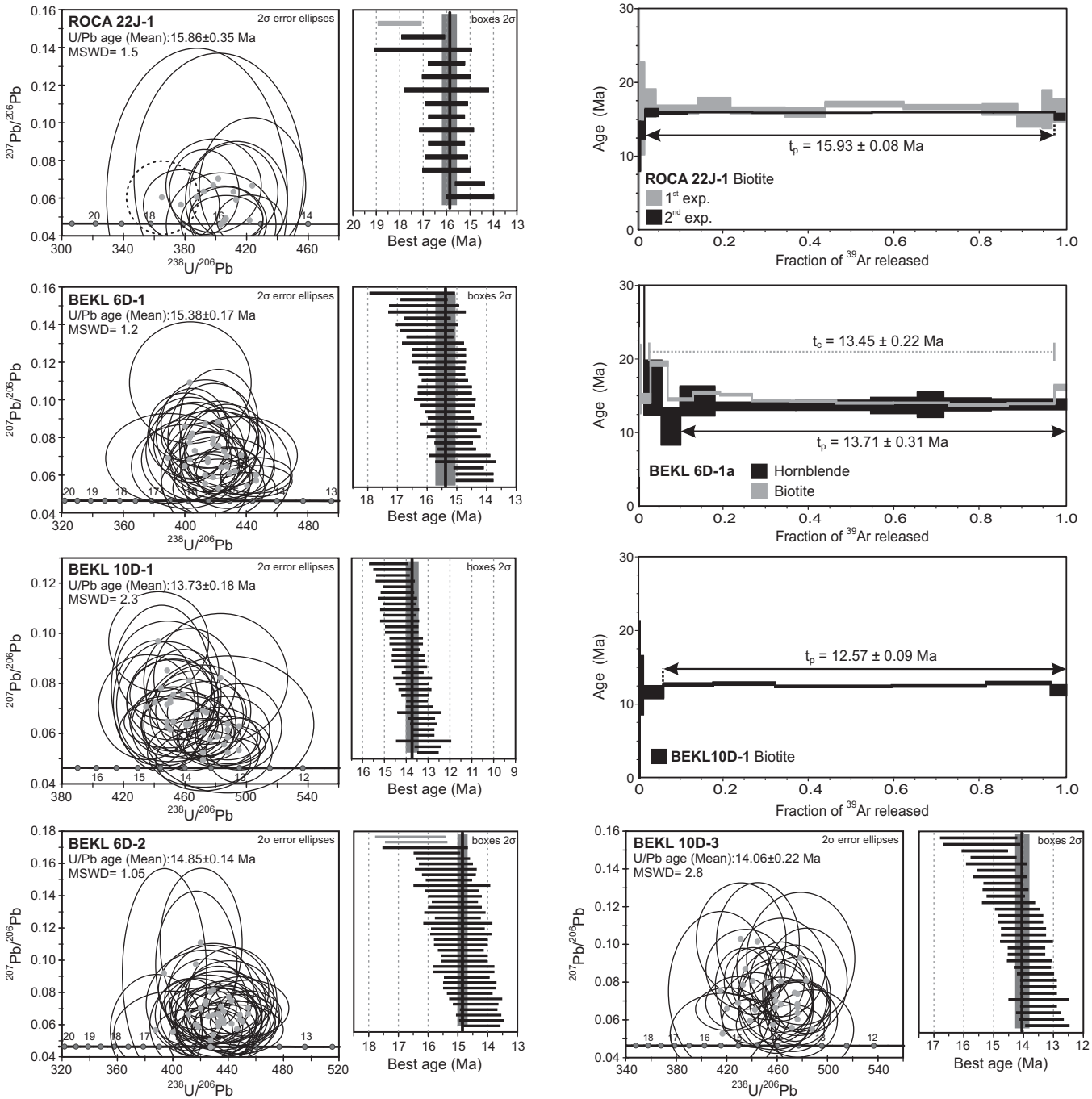

Figure 7. U/Pb concordia and ^{40}Ar-^{39}Ar age spectra or ^{36}Ar-^{40}Ar vs. ^{39}Ar-^{40}Ar correlation diagrams for middle Miocene plutons; the obtained age is given for each sample. In the U/Pb concordia diagrams, dashed ellipses indicate data not taken into account for age calculation. In the ^{40}Ar-^{39}Ar age spectra, t_p indicates plateau ages; these ages were calculated with the fractions identified with the horizontal arrow. Value t_c indicates the isochron age, calculated using the fractions identified with the dotted line in the age spectra diagrams. Detailed information on the geochronological analysis is given in supplemental file 4 (see text footnote 1). MSWD—mean square of weighted deviates.

these samples show evidence of perturbation in the Ar systematics (Fig. 6). All these samples are located around the Pescadero Basin in the central Gulf of California, an area with subsequent middle Miocene magmatism and where late Miocene mafic volcanism (12–10 Ma) has been also reported (Ferrari et al., 2013), suggesting that these early Miocene plutons underwent various degrees of resetting due to later igneous activity.

Middle Miocene Magmatic Episode

Only five samples out of 41 yielded U/Pb zircon ages between 15.8 Ma and 13.4 Ma, providing an indirect indication that middle Miocene plutons are less widespread than early

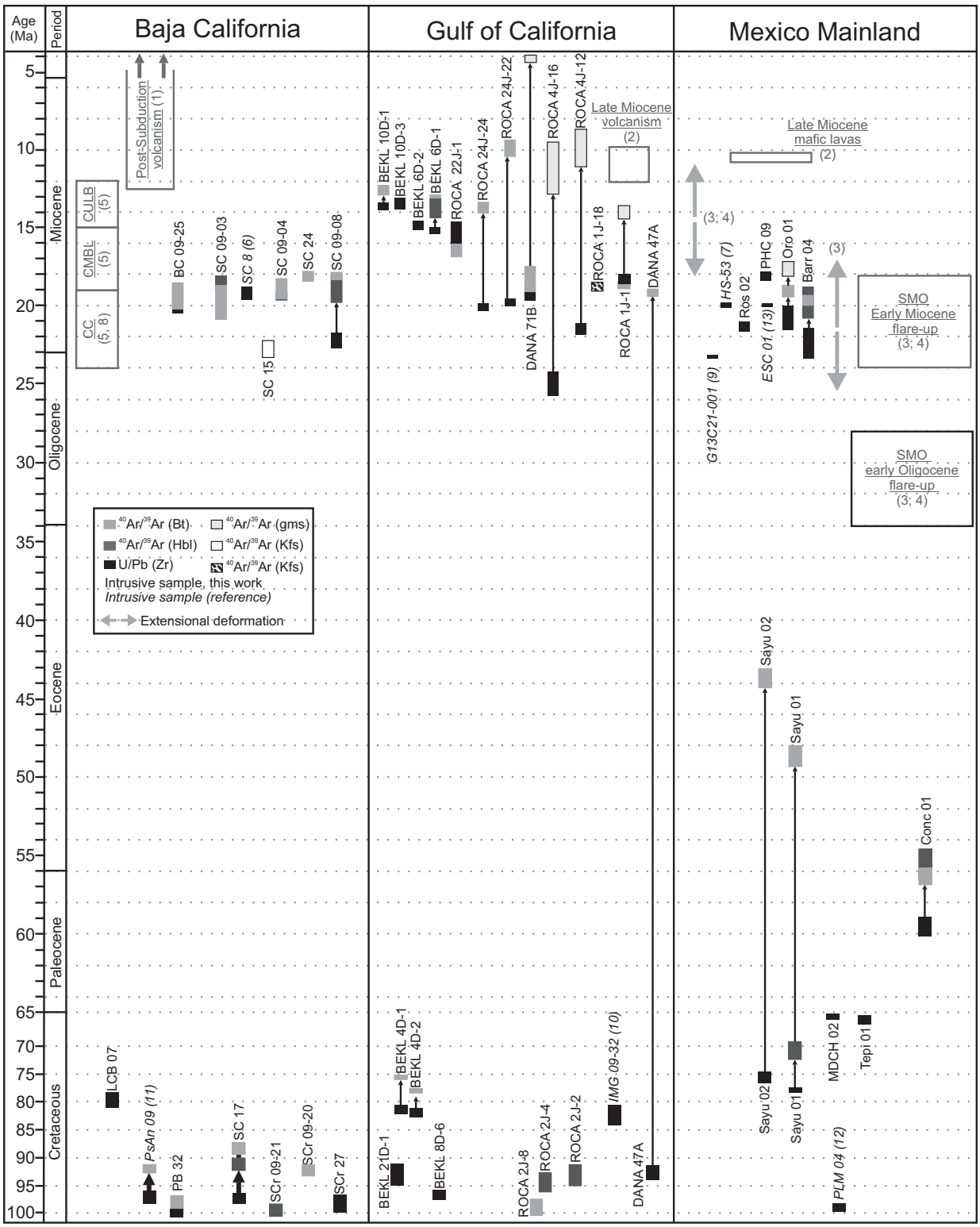

Figure 8. Distribution of U/Pb and ^{40}Ar-^{39}Ar ages obtained in this work for intrusive samples from the southern Gulf of California area and its adjacent margins; ages from the literature for plutons in the area are also included (sample numbers in italics); sample location is given in Figure 1. Main volcanic and tectonic events registered in the area are also shown. (1) Calmus et al. (2011); (2) Ferrari et al. (2013); (3) Ferrari et al. (2002); (4) Ferrari et al. (2007) and references therein; (5) Umhoefer et al. (2001); (6) Piñero-Lajas (2008); (7) Henry et al. (2003); (8) Hausback (1984); (9) Iriondo et al. (2003); (10) Pompa-Mera et al. (2013); (11) Iriondo et al. (2005); (12) Cuéllar-Cárdenas et al. (2012); (13) our unpublished data. CC—Clastic Comondú; CMBL—Comondú middle breccia and lava unit; CULB—Comondú upper lava and breccia unit; SMO—Sierra Madre Occidental; Bt—biotite; Hbl—hornblende; Zr—zircon; Kfs—K-feldspar; gms—groundmass.

Miocene plutons. Middle Miocene intrusive rocks seem to be restricted to the western rifted blocks submerged in the gulf (Fig. 1C), and thus most proximal to the onshore Comondú Group exposures. The dated samples come from three sites along a topographic high, situated halfway between the Pescadero Basin and Baja California margin (Fig. 2A). Sample ROCA 22J-1 was recovered at 1516 mbsl at the southwestern side of the Cerralvo Bank, and four other samples were dredged at sites BEKL 6D (southeast end of Cerralvo Bank at 900–1205 mbsl) and 10D (northernmost part of La Paz Basin at 1200–1498 mbsl; Figs. 1 and 2; Table 1). Studied samples show a peculiar inequigranular texture with phenocrysts of plagioclase and K-feldspar surrounded by finer plagioclase, K-feldspar, quartz, and minor mafic minerals (Table 1), which indicates at least two crystallization stages at different pressure. A group of four samples has similar alkali feldspar content (20%–23%) and classifies as quartz monzodiorite and monzogranite (Table 1); they contain amphibole and biotite as ferromagnesian minerals, as well as apatite, zircon, titanite, and Fe-Ti oxides as accessory minerals. Sample BEKL 6D-2 has a distinctly different composition, with 50% alkali feldspar and a quartz monzonite composition; this sample has biotite as the only ferromagnesian mineral.

Paired U-Pb and Ar-Ar ages could only be obtained for three middle Miocene samples. In these cases, as for the early Miocene samples, the rocks yielded very close U/Pb zircon, hornblende, and/or biotite ages, suggesting very rapid cooling to <375 °C (Table 3; Figs. 7 and 8). Sample ROCA 22J-1 has a U/Pb age of 15.86 ± 0.35 Ma and a ^{40}Ar-^{39}Ar biotite plateau age of 15.86 ± 0.08 Ma (Fig. 6). Sample BEKL 6D-1 yielded a U/Pb zircon age of 15.38 ± 0.17 Ma, a ^{40}Ar-^{39}Ar hornblende plateau age of 13.71 ± 0.31 Ma, and a ^{40}Ar-^{39}Ar biotite plateau age of 13.4 ± 0.22 Ma. Sample BEKL 10D-1 yielded a U/Pb age of 14.06 ± 0.22 Ma and a biotite ^{40}Ar-^{39}Ar plateau age of 12.57 ± 0.09 Ma (Table 3). The middle Miocene samples show no inherited zircons, but they commonly have antecrysts as defined in Ferrari et al. (2013) (Table 3; Fig. 7).

Thermobarometry

To obtain further constraints on magma emplacement depth, thermobarometric calculations were performed on samples representative of each magmatic episode: one Paleocene equigranular, medium-grained monzogranite (Conc 01), one early Miocene inequigranular, medium-grained tonalite (IXC 03), and three middle Miocene inequigranular, medium- to coarse-grained monzogranites (BEKL 6D-1, BEKL 10D-1, BEKL 10D-3). Pressure and temperature of magma crystallization were estimated through iteration of pressure calculated with the Al-in-hornblende barometers of Schmidt (1992) and Anderson and Smith (1995), at temperatures obtained with the Holland and Blundy (1994) hornblende-plagioclase thermometer (reaction edenite + albite = richterite + anorthite), using the spreadsheet published by Anderson et al. (2008). In the analyzed samples, hornblende coexists with the full buffering assemblage required for Al-in-hornblende barometry (quartz + alkali feldspar + plagioclase + biotite + Fe-Ti oxide + titanite; see Table 1). Estimates of pressure and temperature were also obtained with the empirical calibration based on the composition of amphibole recently proposed by Ridolfi and Renzulli (2012). Results obtained with both procedures are plotted in Figure 9 and listed in supplemental file 2 (see footnote 1).

Pressures obtained with the first method (Anderson et al., 2008) for the Paleocene sample range mainly between 231 and 308 MPa, which correspond to 8.8–11.8 km depth for an upper-crustal density of 2.7 g/cm^3, whereas the early Miocene sample yielded lower values between 150 and 196 MPa (5.7–7.5 km depth). Temperatures for these samples plot close to the granite water-saturated solidus and span a broader range for the Paleocene sample (567–720 °C) than for the early Miocene sample (689–722 °C). Middle Miocene samples span over a larger pressure range, with a group plotting close to the granite solidus at 165–309 MPa (6.3–8.8 km depth) and temperatures between 636 °C and 735 °C, and a second group yielding low pressures and temperatures (32–145 MPa, 1.2–5.5 km; 573–665 °C) that plot well below the granite solidus. Amphibole in all samples is classified as magnesiohornblende, but analyses that yield pressure-temperature values below the solidus have lower Al_{tot} (<1.0) and higher Si/Al and Mg/Fe, pointing to subsolidus reequilibration to actinolitic hornblende. Subsolidus reactions have been related to vapor-phase saturation at shallow levels (Hammarstrom and Zen, 1986) or to the infiltration of high-temperature contact aureole fluids (Anderson et al., 2012). These values are therefore not further considered in the discussion.

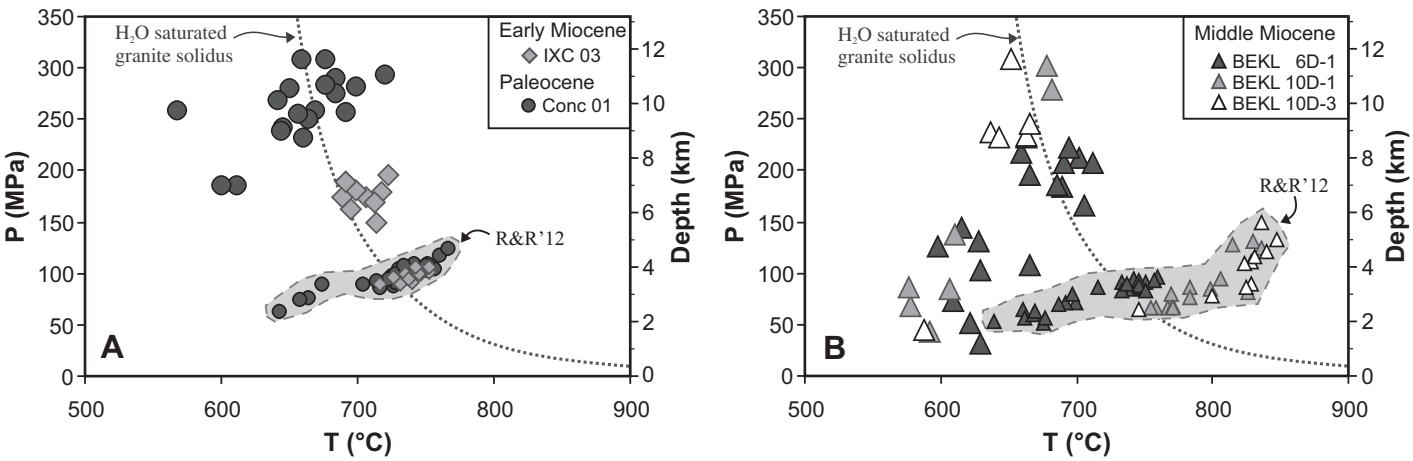

Figure 9. Estimated pressures and temperatures for (A) Paleocene and early Miocene and (B) middle Miocene intrusive rocks from submerged blocks of the Gulf of California. Large symbols correspond to pressure estimates based on the Al-in-hornblende calibration of Schmidt (1992) and Anderson and Smith (1995) and temperatures from the hornblende-plagioclase calibration of Holland and Blundy (1994). Small symbols within the gray fields labeled R&R'12 correspond to pressures and temperature estimates after the Ridolfi and Renzulli (2012) formulation based on amphibole composition.

The empirical thermobarometer of Ridolfi and Renzulli (2012) yielded quite different results for samples plotting close to the solidus, with lower pressures for all samples and higher temperatures for some of the middle Miocene samples (Fig. 9). For the Paleocene sample, pressures between 86 and 125 MPa (3.3–4.8 km depth) and temperatures of 704–767 °C were obtained, whereas the early Miocene sample yielded similar values with slightly lower maxima values at 89–106 MPa (3.4–4.1 km depth) and 716–742 °C. For the middle Miocene, two samples from the same site (BEKL 10D) spanned a large pressure range between 64 and 150 MPa (2.5–5.7 km depth) and had the highest temperatures among the analyzed samples (746– 847 °C). For the third middle Miocene sample (BEKL 6D-1), pressures was between 83 and 97 MPa (3.1–3.7 km depth) and temperatures were between 733 °C and 759 °C. Noteworthy with the Ridolfi and Renzulli (2012) calibration, subsolidus pressure-temperature values were obtained only for some hornblende analyses of a middle Miocene sample (BEKL 6D-1) and of the Paleocene sample.

The discrepancy in the results obtained with the two methods may be ascribed to differences in the calibration approaches. The Al-in-hornblende barometer was experimentally calibrated for pressures between 250 and 1300 MPa (Schmidt, 1992; Anderson and Smith, 1995), corresponding to 9.5–50 km crustal depths, and may thus be inadequate to estimate crystallization pressures of shallow intrusive rocks like those presented here (pressure <308 MPa). On the other hand, the calibration proposed by Ridolfi and Renzulli (2012) is based in a multivariate least-square regression of selected experimental calcic amphibole compositions synthesized in a broader pressure range (130–2200 MPa). A drawback of the barometer formulation is the lack of the required temperature correction; nevertheless, according to Anderson and Smith (1995), such correction would result in even lower pressure values than those obtained with the present formulation. For the pressure range of the studied samples, the calibration of Ridolfi and Renzulli (2012) is probably the most adequate. Variable crystallization pressures down to 64 MPa (2.5 km depth) for the middle Miocene samples also are consistent with the distinct inequigranular textures that characterize these samples (Table 1).

Geochemistry

Cretaceous–Paleocene Magmatic Episode

Cretaceous–Paleocene samples plot in the diorite, quartz monzodiorite, granodiorite, and monzogranite fields in the Q′-ANOR diagram of Streckeisen and Le Maitre (1979), which is based on the parameters Q′ [= 100 × q/(q + or + ab + an)] and ANOR [= 100 × an/(or + an)], derived from the normative proportions of quartz (q), orthoclase (or), albite (ab) and anorthite (an), and belong to the calcic and calc-alkalic series of Frost and Frost (2008) (Figs. 10A and 10B). Most samples have SiO_2 contents in the range of 60–77 wt%, except for one diorite sample, with 53.3 wt% SiO_2, which plots in the field of high-K calc-alkalic series in the SiO_2 versus K_2O diagram (Fig. 10C; Peccerillo and Taylor, 1976).

Trace-element variation is shown in primitive mantle–normalized multi-element diagrams (Fig. 11A; Sun and McDonough, 1989). All studied samples are enriched in large ion lithophile elements (LILEs; e.g., Rb, Ba) and light rare earth elements (LREEs; e.g., La, Ce) with respect to the high field strength elements (HFSEs; e.g., Nb, Ta) and display positive Pb anomalies, features commonly considered characteristic of subduction-related rocks. The enrichment of the middle and heavy rare earth elements (MREEs and HREEs, respectively), as well as Y, is quite variable but cannot be ascribed to the degree of differentiation (expressed as SiO_2 content). In part, the variations result from the stronger HREE depletion found in some of the oldest dated rocks (99.1–92.8 Ma) from Santa Cruz Island and submerged continental blocks offshore southern Baja California and Sinaloa (ROCA 2J-8, SCr 27, BEKL 8D-6, DANA 47A; Fig. 1). The age and composition (e.g., high Sr/Y and La/Yb, low Nb and Ta, absence of negative Eu anomaly) of these rocks resemble those of La Posta–type plutons, which were emplaced in southern California and northern Baja California peninsula between 99 and 92 Ma (Walawender et al., 1990; Kimbrough et al., 2001) and dominate the eastern Peninsular Ranges Batholith. These samples from the southern Gulf of California constitute the southernmost exposures of La Posta–type plutons yet identified.

Early Miocene Magmatic Episode

Intrusive rocks emplaced in the early Miocene show compositional trends distinctive from those of Cretaceous–Paleocene plutons. These rocks can be divided in two groups on the basis of differentiation. A group of samples of intermediate composition, in the range of 61–68 wt% SiO_2, plots in the quartz diorite, quartz-monzodiorite, quartz-monzonite, and granodiorite fields in the Q′-ANOR diagram (Fig. 10A). The narrow range of silica content is reflected in a restricted variation of Q′ at variable ANOR values. A further intermediate-composition sample from a subvolcanic, porphyritic intrusive body (PHC 09) has lower SiO_2 content (57.3 wt%) and lower Q′ value, and it plots in the quartz diorite field (Fig. 10A); this less-evolved sample also yielded the youngest emplacement age (18.1 Ma, U/Pb; Table 3) among the early Miocene rocks. A second group of samples is composed of high-silica granitoids with 75–77 wt% SiO_2, which classify as syenogranite and alkali feldspar granite in the Q′-ANOR diagram (Fig. 10A); this group of samples yielded U/Pb ages in a narrow age range between 20.1 Ma and 18.3 Ma (Table 3; Fig. 10A).

Part of the intermediate and the high-silica intrusive rocks plot in the alkali-calcic field, whereas some of the least-differentiated samples are calc-alkalic (Fig. 10B); also, early Miocene rocks tend to have higher K_2O contents than the Cretaceous ones, and they mostly plot in the field of high-K calc-alkalic rocks (Fig. 10C).

Primitive mantle–normalized trace-element patterns of intermediate early Miocene samples are quite similar (Fig. 11B), despite the fact that they were collected over a broad area both onshore and offshore of Sinaloa and Nayarit States. They are characterized by the enrichment of LILEs and LREEs with respect to HFSEs, positive Pb anomalies, and weakly developed Eu anomalies (Fig. 11B); when compared with the Cretaceous intrusions, they have less prominent negative Nb-Ta and positive Pb anomalies, but REE patterns comparable to those of the less HREE-depleted Cretaceous samples. In the group of high-silica granites, the geochemical features are in part comparable to those of the intermediate magmas, but they are distinguished by stronger Sr, Eu, and Ti depletions, as well as by comparatively higher abundances of MREEs, HREEs and Y, and flat MREE to HREE patterns (Fig. 11B).

Middle Miocene Magmatic Episode

The four analyzed samples belonging to this episode have silica contents between 64 wt% and 71 wt% SiO_2 and classify as quartz monzodiorite, monzogranite, and quartz syenite in the Q′-ANOR diagram (Fig. 10A), where they display a similar trend as the early Miocene rocks. Three samples are high-K calc-alkalic, and one is alkalic with a shoshonitic character, in agreement with the high percentage of alkali feldspar observed in thin section for these rocks.

Among the middle Miocene rocks, the quartz monzodiorite and quartz syenite have trace-element compositions similar to those of the intermediate-composition early Miocene rocks, except for higher Rb, Th, and U abundances (Fig. 11C). A monzogranite sample from submerged crustal blocks offshore southern Baja California (BEKL 10D-3; Fig. 1) displays a different pattern, defined by a strong depletion in REEs, and slightly positive Eu and Sr anomalies (Fig. 11C).

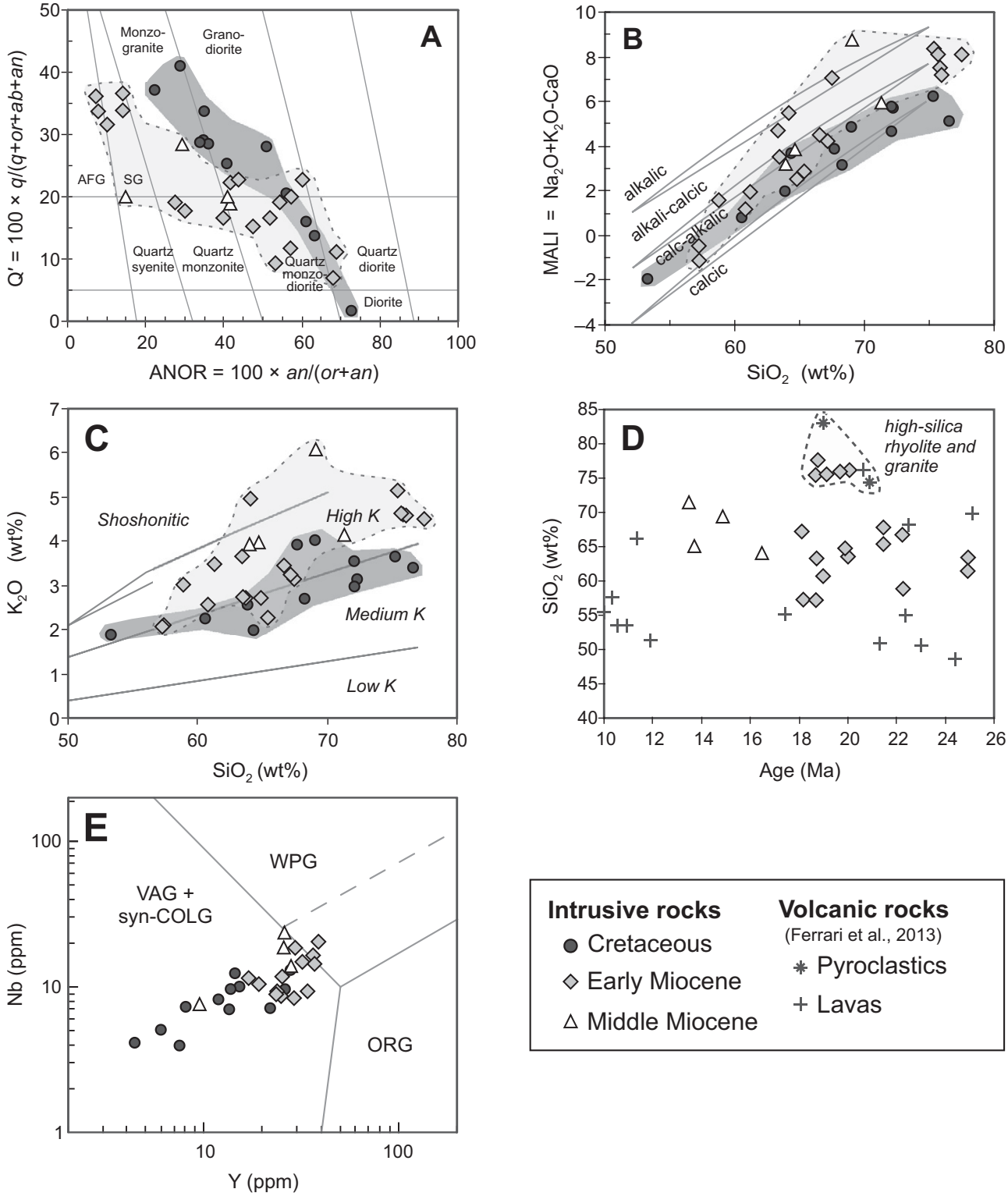

Figure 10. Compositional characterization of analyzed samples. (A) Q′ vs. ANOR diagram (Streckeisen and Le Maitre, 1979) showing rock types according to their normative mineral proportions (q—quartz; or—orthoclase; ab—albite; an—anorthite). SG—syenogranites, AFG—alkali feldspar granites. (B) $Na_2O + K_2O$–CaO vs. SiO_2 diagram showing the approximate ranges for the alkalic, alkali-calcic, calc-alkalic, and calcic rock series (modified after Frost and Frost, 2008). (C) K_2O vs. SiO_2 diagram (Peccerillo and Taylor, 1976). (D) SiO_2 vs. age diagram for Miocene plutons (this work) and Miocene volcanic rocks from Ferrari et al. (2013). (E) Nb vs. Y tectonic discrimination diagram (after Pearce et al., 1984). VAG—volcanic arc granitoids; syn-COLG—syncollisional granitoids; WPG—within-plate granitoids; ORG—ocean-ridge granitoids.

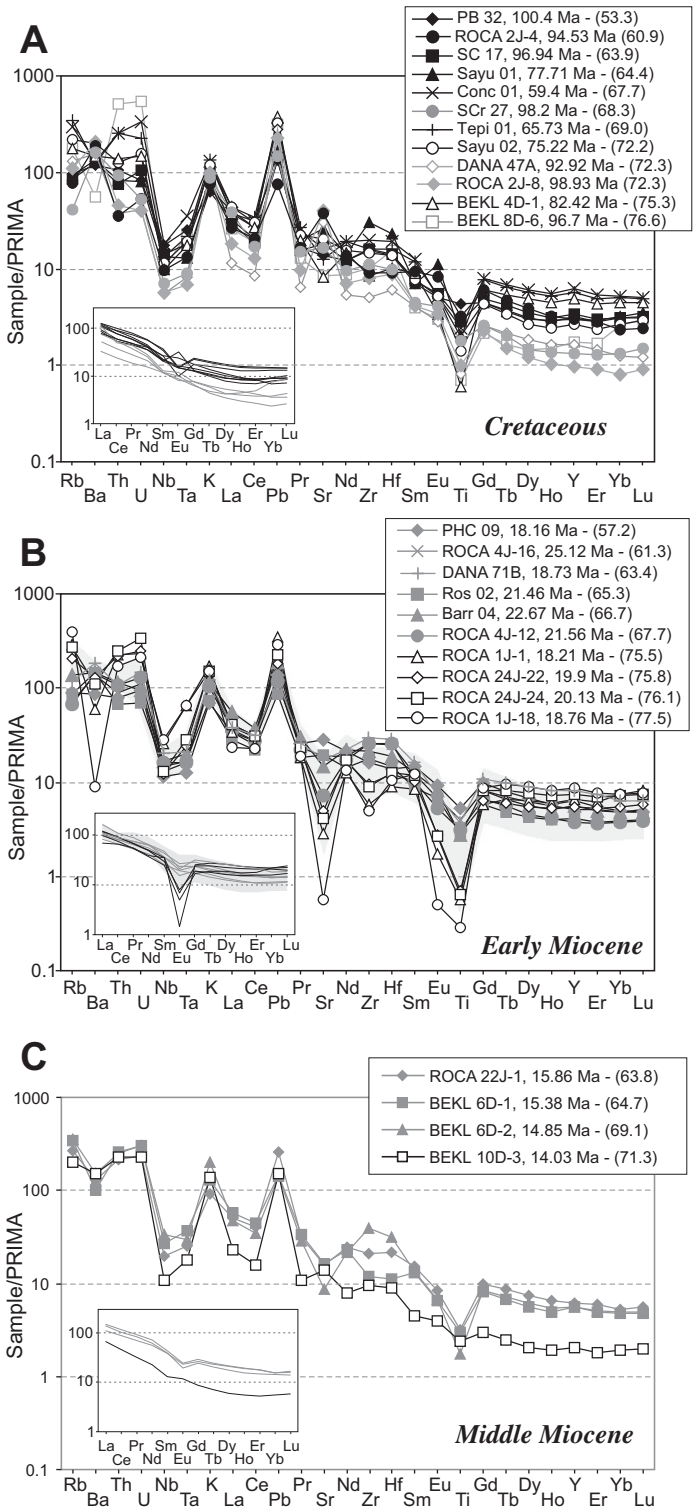

Figure 11. Multi-element diagrams normalized to primitive mantle values of Sun and McDonough (1989) for the intrusive samples. (A) Cretaceous samples. (B) Early Miocene samples; the gray field denotes the compositional range of early Miocene silicic tuffs and lavas reported by Ferrari et al. (2013). (C) Middle Miocene samples. Inserted in each diagram is the chondrite-normalized rare earth element (REE) diagram for the same samples. The legend in each diagram indicates sample name, followed by the U/Pb age (except for sample Roca 1J-18, which is a ^{40}Ar-^{39}Ar age on K-feldspar), and then the SiO_2 content in parenthesis in wt%.

DISCUSSION AND CONCLUSIONS

Geographic Distribution of Miocene Magmatism in the Southern Gulf: Relationships with the Sierra Madre Occidental and the Comondú Group

The geologic, geochemical, and geochronologic results of our study indicate the presence of an extensive silicic plutonic province of early Miocene age across the southern Gulf of California (Figs. 8, 12, and 13) nested within Late Cretaceous to early Paleocene batholiths. Previous studies assumed a progressive westward migration of the locus of Cenozoic magmatism, with the early Miocene silicic pulse of the Sierra Madre Occidental located to the west of the Oligocene pulse, in southern Sinaloa and Nayarit (Ferrari et al., 2002, 2007), and subsequent middle Miocene volcanism of the Comondú Group centered in the gulf just east of Baja California (Hausback, 1984; Umhoefer et al., 2001). However, the occurrence of 24–18 Ma granitic intrusive rocks on both sides of the gulf, as well as in submerged rifted blocks within the gulf, indicates that silicic-dominant early Miocene magmatism of the Sierra Madre Occidental was located not only on the Mexican mainland but spanned a much larger area, elongated in a WNW-ESE direction (Figs. 12 and 13). The composition and age range of these plutons are essentially coincident with those of the ignimbrites exposed in the southern Sierra Madre Occidental and in southern Baja California between La Paz and Loreto (Fig. 12; Hausback, 1984; Umhoefer et al., 2001; Ferrari et al., 2002, 2013; Drake, 2005; Bryan et al., 2008; Ramos-Rosique, 2013). The two compositional groups of the early Miocene plutons also compare well with the silicic volcanic rocks emplaced during the same age span in the southern Sierra Madre Occidental (Fig. 10D; Ferrari et al., 2013). For early Miocene ignimbrites and lavas, two similar compositional groups of high-K rocks are recognized: an older dacite and low-silica rhyolite (SiO_2 < 70 wt%) suite and a younger, high-silica rhyolite (SiO_2 > 74 wt%) suite. Also, trace-element compositions and patterns of volcanic and plutonic rocks are strikingly similar (Fig. 11B) and indicate a limited role for crystal fractionation in the evolution of early Miocene silicic magmas (Ferrari et al., 2013). Zircon inheritance also points to a significant role of crustal melting in the genesis of these rocks, as shown for other onshore Sierra Madre Occidental ignimbrites (e.g., Bryan et al., 2008). Our data add weight to the interpretation that the early Miocene plutonic rocks across the southern gulf region represent intrusive underpinnings to part of the early Miocene Sierra Madre Occidental silicic volcanism.

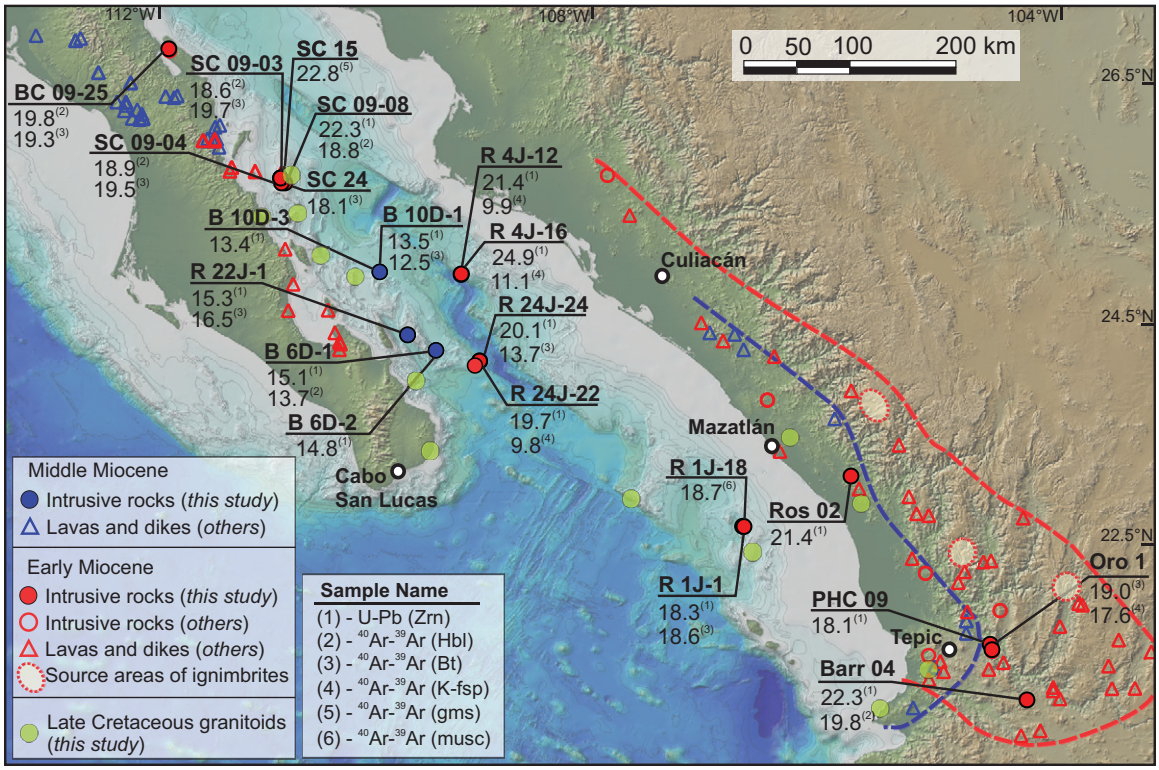

Figure 12. Location and ages of plutonic rocks reported in this work, and distribution of early and middle Miocene intrusive (this work) and volcanic samples compiled from the literature. Sample prefixes of ROCA and BEKL sample names are abbreviated to R and B, respectively. Base map data are from GeoMapApp. Abbreviations: Zrn—zircon; Hbl—hornblende; Bt—biotite; K-fsp—K-feldspar; gms—groundmass; musc—muscovite.

Scarce middle Miocene plutonic rocks were encountered across the southern gulf, and particularly in fault scarps bounding the Cerralvo Bank (Figs. 2 and 12), in the western rifted margin of the southern gulf. These sites lie on the southward prolongation of the few lavas and domes of the same age exposed in Baja California, near Loreto and in Bahía Concepción, which have been assigned to the middle and upper members of the Comondú Group (Figs. 1 and 12; Umhoefer et al., 2001; Drake, 2005). No intrusive rocks of middle Miocene age have been found on the eastern rifted margin, but a few basalts of this age are interlayered with continental sedimentary rocks between Mazatlán and Culiacán (Fig. 1; Ferrari et al., 2013). The distribution of middle Miocene rocks defines a NNW-trending belt in the central and western part of the wider region occupied by the early Miocene intrusive rocks (Fig. 12). As this belt is superimposed on early Miocene magmatism, rather than a westward migration of magmatism, the distribution of middle Miocene igneous rocks suggests the narrowing of the magmatic belt in a position coincident with the future gulf axis.

Two arguments have been that: (1) the Gulf of California opened along a line/zone of hot, thermally weakened crust resulting from igneous activity of the Comondú "arc" (Umhoefer, 2011, and references therein), and (2) thick epiclastic deposits that constitute the bulk of the middle and upper members of the Comondú Group were shed westward from a series of high-standing andesitic stratocones located within the area of the present-day gulf and just east of Baja California peninsula (Hausback, 1984; Umhoefer et al., 2001). We would also expect that rapid subsidence in the gulf region at 12 Ma, allowing a marine incursion by at least 8 Ma, would have enhanced preservation and burial of the arc volcanoes. If this was the case, extensive outcrops of volcanic, resedimented volcaniclastic ± intrusive rocks associated with the core of this volcanic arc should be present in the submerged rifted blocks on both sides of the newly formed oceanic basins within the gulf. However, visual inspection of the submerged blocks during the ROCA dives indicates that the normal fault scarps bounding the Alarcón and Pescadero Basins are dominated by Late Cretaceous or early Miocene intrusive rocks (Figs. 2 and 12). These observations thus require complete removal of any arc volcanic constructs and sedimentary accumulations of the middle Miocene Comondú Group, as well as of thick (at least 1 km) volcanic accumulations of early Miocene age to expose underlying early Miocene and older plutonic rocks; this is despite the requirement for rapid crustal thinning, subsidence, and gulf flooding within a few million years. The scarcity of middle Miocene rocks in the southern gulf casts doubts on the prevailing model of substantial andesitic volcanism occurring along the gulf axis that was sufficiently vigorous to form a significant volume of new arc igneous crust and to thermally weaken the crust (with a prerift thickness of ~40 km, i.e., the present thickness of the unextended part of the Sierra Madre Occidental) prior to the onset of rifting (e.g., Umhoefer, 2011). The geology of the submerged rift flanks in the southern gulf region therefore indicates that Comondú-age magmatism and related sedimentation were not volumetrically significant and not a major tectonomagmatic feature in the middle Miocene. The submarine geology supports recent interpretations of Comondú-age magmatism being synextensional in origin, primarily related to continued lithosphere extension that had affected western Mexico since the late Oligocene and culminated in the opening of the Gulf

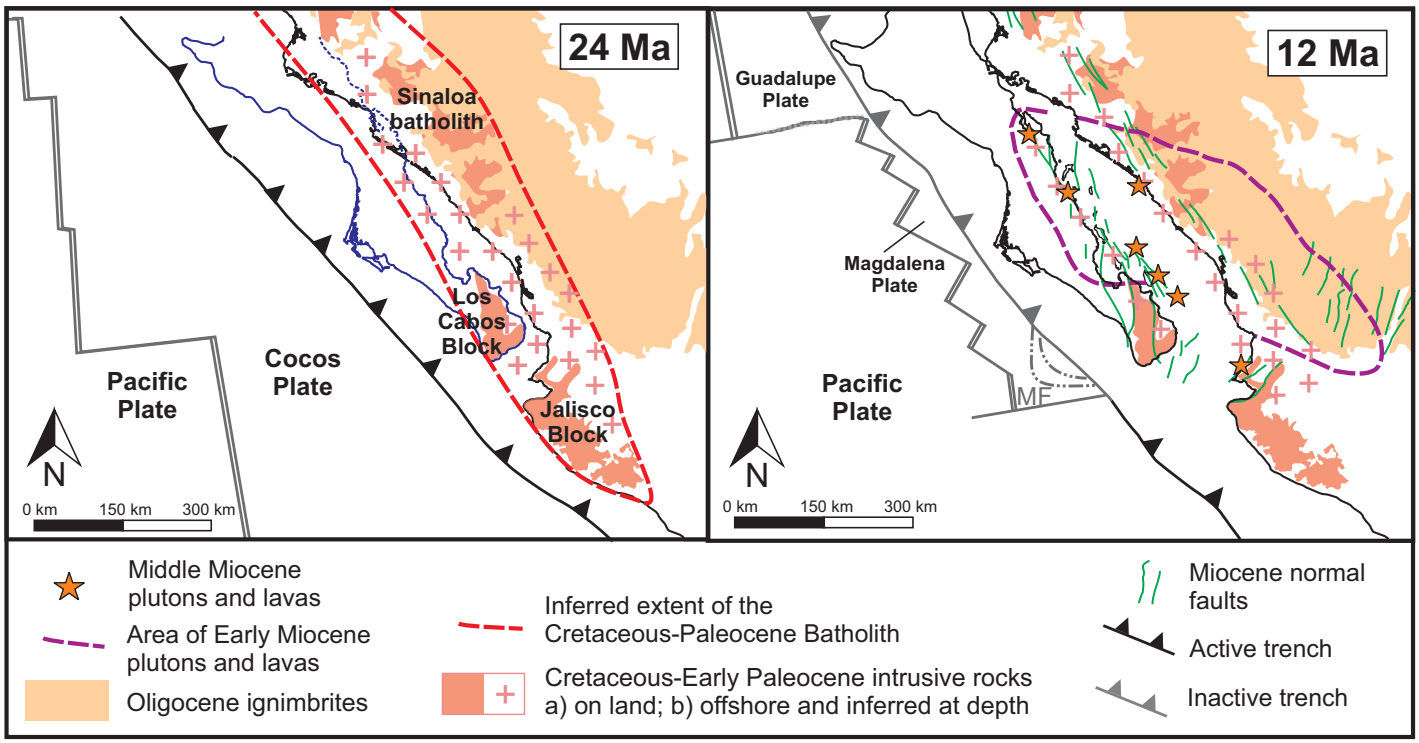

Figure 13. Paleotectonic reconstructions at 24 and 12 Ma showing the distribution of the Late Cretaceous–Paleocene, early Miocene, and middle Miocene magmatic events based on data presented in this work and from the literature. Main extensional faults formed prior to 12 Ma are shown as green lines. Pacific-Cocos plate boundary configuration with respect to North America at 24 Ma is from Atwater and Stock (1998). Magdalena and Guadalupe microplate configuration and location of Magdalena Fan (MF) at 12 Ma are from Fletcher et al. (2007). Geology is modified from Ferrari et al. (2007, 2013). Baja California position is as in Ferrari et al. (2013).

of California in the late Miocene (Bryan et al., 2014; Ferrari et al., 2013).

Previous models also require rapid extension after ca. 12.5 Ma that would produce significant thinning of an almost unextended crust (Stock and Hodges, 1989; Umhoefer et al., 2002; Fletcher et al., 2007; Lizarralde et al., 2007; Sutherland et al., 2012). In such a scenario, one would also expect a significant amount of post–ca. 12 Ma volcanism associated with mantle decompression induced by a high rate of extensional deformation. However, post-Comondú volcanism is scarce in the southern gulf and western Mexico. In fact, after a widespread pulse of basaltic volcanism at ca. 11–10 Ma (Ferrari et al., 2013), an ~7 m.y. gap in volcanism is observed until the late Pliocene and Quaternary on the eastern rifted margin (Ferrari et al., 2013), just when prevailing models predict the main episode of rifting. Alternatively, if a significant part of crustal thinning occurred before the end of subduction, as we propose here and in Ferrari et al. (2013), then the rate of extension after ca. 12 Ma would be much lower and the associated volcanism less abundant, as actually observed (Lizarralde et al., 2007).

Synextensional Nature of Miocene Magmatism

An examination of the thermal evolution of intrusive rocks provides a useful chronometric bracket on the tectonic event responsible for the opening of the Gulf of California. A complete modeling of the thermal history awaits low-temperature geochronologic approaches, such as fission tracks or U-Th/He dating, which are in progress. However, an analysis of the time span between zircon U/Pb and hornblende, biotite, and feldspar ^{40}Ar-^{39}Ar ages obtained in this study consistently indicates that the early and middle Miocene plutons were rapidly cooled after intrusion. All dated early Miocene intrusive rocks emplaced between 25 and 18 Ma (Fig. 8) were cooled below the ^{40}Ar-^{39}Ar biotite closure temperature of 350–400 °C within ~2.5 m.y., with one exception being sample ROCA 24J-24, which, as discussed already, has been likely reset. Significantly, in all cases, ^{40}Ar-^{39}Ar biotite ages are restricted to the 19.7–18.1 Ma interval, and, in the samples where we were able to date both hornblende and biotite, the ^{40}Ar-^{39}Ar ages almost completely overlap in the ca. 19–18 Ma interval (Barr 04, SC 09–08, SC 09–04, SC 09–03; Table 3). Meanwhile, middle Miocene plutons show an even more restricted cooling window of <1.5 m.y. from emplacement defined by the U-Pb zircon age (15.8–13.4 Ma) to the ^{40}Ar-^{39}Ar biotite age (<375 °C), and, as for the early Miocene plutons, almost overlapping hornblende and biotite ages. Middle Miocene intrusive rocks have also distinctive inequigranular textures (Table 1), defined by at least two generations of crystals with grain sizes that change from coarse to fine grained. The presence of crystals formed at different stages and the variable crystallization pressures between 64 and 150 MPa (2.5–5.7 km depth) obtained with the hornblende barometer (Fig. 9; supplemental file 2 [see footnote 1]) support a polybaric crystallization of these intrusive rocks. Consistent with this is the fact that in the three analyzed samples, we consistently obtained higher pressure estimates for core domains (88–150 MPa, 3.4–5.7 km) than for the crystal rims (supplemental file 2 [see footnote 1]). The cooling behavior of the Miocene plutons therefore contrasts with that of spatially related Cretaceous plutons into which they intrude, with the Cretaceous plutons showing a protracted period of intrusion (ca. 100–65 Ma)

and variable cooling time spans to the ^{40}Ar-^{39}Ar biotite age of between 4 and 10 m.y. (Fig. 8).

The time span between U/Pb zircon ages and the ^{40}Ar-^{39}Ar ages indicates cooling rates of 52–130 °C/m.y. for the Late Cretaceous–Paleocene rocks, ~210 °C/m.y. for the early Miocene plutons, and ~350 °C/m.y. or more for the middle Miocene rocks. Such a rapid cooling can be explained by a shallow level of intrusion (comparable to those observed in porphyry copper intrusions; Ballard et al., 2001), by ongoing extensional tectonics at the time of emplacement (as observed in synextensional granitoids in core complexes; Ring and Collins, 2005), or both. Geobarometric data from the four Miocene samples that we analyzed are not conclusive in this respect. The Al-in-hornblende barometer of Anderson and Smith (1995) yielded pressure estimates corresponding to a 6.3–11.8 km depth range, but this barometer was calibrated for a range of pressures corresponding to greater depths (>9.5 km). With the empirical thermobarometer of Ridolfi and Renzulli (2012), we obtained pressure estimates corresponding to a 2.5–5.7 km depth range for a subset of data that plot close to the granite subsolidus. If the depth range obtained using the Anderson and Smith (1995) geobarometer is used, then rapid unroofing by extension is required to explain the fast cooling of the plutonic rocks. However, a shallow level of emplacement is suggested by the textural characteristics of most Miocene samples and is confirmed by field evidence both in Baja California (Bahia Concepción) and in Nayarit, where fine-grained granitoids are found intruding <2.5-km-thick volcanic successions only 2–8 m.y. older. Ferrari et al. (2013) estimated significant crustal thinning (up to ~100%) along the southeastern margin of the gulf between ca. 18 and 11 Ma, which importantly corresponds to the period of intrusion and rapid cooling of our studied plutonic samples. A critical factor here is that the remarkably uniform ca. 19–18 Ma ^{40}Ar-^{39}Ar biotite ages obtained for early Miocene granitoids point to regional extension across the southern gulf region to explain widely spaced plutonic samples simultaneously crossing the 375 °C isotherm. Although more data are required, we consider that extension in the southern gulf was ongoing in the middle Miocene, even though thermochronological data from the now subaerial part of the Baja California margin indicated that cooling through the apatite annealing zone (<110 °C) occurred principally in the late Miocene (e.g., Fletcher et al., 2000; Seiler et al., 2011).

Some early Miocene plutons (sites ROCA 24J, 4J, and DANA 71B) show a wider time span between U-Pb zircon crystallization and ^{40}Ar-^{39}Ar cooling ages (7–13 m.y.; Fig. 8). These samples are all located in the central part of the Gulf of California along the scarps of the Pescadero Basin. At these sites, the ^{40}Ar-^{39}Ar cooling ages are interpreted as being thermally perturbed by the younger magmatism and high heat flow that were focused along the pull-apart basins of the central part of the Gulf of California rift since the late Miocene (e.g., Wang et al., 2009). Thermal perturbation of some ^{40}Ar-^{39}Ar age spectra is also observed for some Cretaceous plutons located near the axis of the gulf. In other samples away from the rift axis (Sayu 01 and Sayu 02), we only observed an incomplete resetting, possibly due to the distance from local heat sources (plutons). A similar resetting of the ^{40}Ar-^{39}Ar system is reported for Paleozoic and Jurassic basement gneisses and granites found near the northern Sinaloa coast (El Fuerte area), for which Keppie et al. (2006) reported muscovite and biotite ages of 16.5 ± 1 Ma and 13 ± 1 Ma, respectively.

Evolution of Miocene Magmatism: A Drying Mantle?

On the basis of limited whole-rock chemical and isotope signatures, early to middle Miocene volcanism in the southern Gulf of California area has traditionally been related to suprasubduction arc volcanism during the final stages of subduction beneath this part of the North America plate (e.g., Hausback, 1984; Sawlan and Smith, 1984; Wark et al., 1990; Umhoefer et al., 2001). Recent studies have shown that the silicic rocks of the Sierra Madre Occidental are largely the product of crustal melting (Bryan et al., 2008, and reference therein; see also Ruiz et al., 1988, 1990). Bryan et al. (2014) further showed that the intermediate-composition Comondú-age igneous rocks can be explained by mixing and hybridization of crustal silicic melts and mantle magmas. The geochemical signature of the early and middle Miocene rocks may have been inherited from the crust or by the past ~100 m.y. of subduction and provide no unambiguous constraint on early and middle Miocene tectonic setting and mantle source.

The onset of extensional faulting in the western part of the Sierra Madre Occidental (southwestern Chihuahua, Sinaloa, and Nayarit States) has been recently documented to have initiated at the end of the Oligocene (Ferrari et al., 2013; Bryan et al., 2014), concurrent with the well-documented extension that took place in central and western Sonora (McDowell et al., 1997; Gans, 1997; González-León et al., 2000; Vega-Granillo and Calmus, 2003; Wong et al., 2010; Bryan et al., 2014). In this study, we have further shown evidence for an important extensional event also taking place in the gulf area in the early to middle Miocene. In this context, the Sierra Madre Occidental and Comondú magmatic episodes can be seen as the manifestation of the initial and continuing stages, respectively, of lithosphere stretching that led to the formation of the Gulf of California. We propose that during this long period of rifting (>25 m.y.), extension-induced decompression melting prevailed, overwhelming any partial melting of the mantle in response to the fluxing of fluids derived from the subducting plates (Fig. 10E). Since the late Oligocene, the age of the subducting plate at the trench off Baja California was less than 15 m.y. old, and progressively decreased to 1–5 m.y. old at ca. 12.5 Ma. This is because the age of the oceanic lithosphere entering the subduction zone was extremely young as the East Pacific Rise approached the trench, being only 4.5–1 m.y. old for the Magdalena microplate and 5–4 m.y. old for the Guadalupe microplate at 12.5 Ma (Lonsdale, 1991; Stock and Lee, 1994). It has been long recognized that when a young plate is thin and warm, slab dehydration reactions occur at shallow depth (Stern, 2002). Numerical modeling and experimental petrology show that for a plate younger than ca. 15 Ma entering the subduction zone, dehydration will occur mostly before the slab reaches 100 km depth, strongly limiting the volatile flux to the mantle wedge (e.g., Peacock and Wang, 1999; Green and Harry, 1999). Consequently, fluid fluxing of the mantle beneath western Mexico due to slab dehydration became increasingly limited, and instead, decompression of previously hydrated mantle, induced by lithosphere thinning, was the dominant melting mechanism. At the same time, infiltration of dry and hot asthenosphere from the slab window that was forming to the north (Atwater and Stock, 1998) and the widespread melting associated with the Sierra Madre Occidental may have resulted in a dry and hotter mantle.

CONCLUDING REMARKS

The results of our study are consistent with an early Miocene broad extensional region developing across the area of the future Gulf of California between the relatively undeformed belt of the Peninsular Range Batholith of Baja California and the Sierra Madre Occidental core. The widespread occurrence of middle Miocene (ca. 19–13 Ma) ^{40}Ar-^{39}Ar cooling ages for both early and middle Miocene intrusions across the southern gulf region is incompatible with all gulf extension and thus with crustal cooling and exhumation only occurring after ca. 12.3 Ma (e.g., Stock and Hodges, 1989; Fletcher et al., 2007; Lizarralde et al., 2007; Umhoefer, 2011). Rather, our study indicates that early and middle

Miocene plutons intruded into a belt of extending crust, thinning up to ~100% at ca. 18–12 Ma (Ferrari et al., 2013; Bryan et al., 2014), which was subsequently exploited by transtensional deformation in the central part of the gulf since the late Miocene.

A significant volume of intermediate-composition and high-silica granitic plutons intruded this area in the early Miocene, forming plutonic equivalents to the ignimbrite flare-up recorded in the southern Sierra Madre Occidental. Volumetrically subordinate intrusions were emplaced during the middle Miocene, and these temporally correlate with the onshore middle and upper member of the Comondú Group.

The rifting process envisaged here for the pre–late Miocene deformation in the southern gulf agrees with models and observations in other rifts that pass from a wide to a narrow rift and where extension controls the locus of volcanism (e.g., Parsons et al., 1998; Corti et al., 2003). A rapid opening of the gulf had been inferred by considering that extension in the Gulf Extensional Province only began at the end of the middle Miocene and was guided by the presence of an active Comondú "arc." Our results suggest not only that rifting began much earlier, but also that crustal extension guided the location of volcanism and not the other way round.

ACKNOWLEDGMENTS

This research was supported by grant CONACYT (Consejo Nacional de Ciencia y Tecnología) 82378 (to Ferrari), UC-MEXUS CN-09-312 (to Ferrari and Lonsdale), CONACYT P46600-F (to López-Martinez), and National Science Foundation (NSF) grant OCE-11-44558 to Lonsdale. S. Bryan was in part supported by a Vice Chancellor's fellowship at Queensland University of Technology. We thank M. Grove and D. Kimborough for providing unpublished U-Pb ages that helped us in selecting samples sites at Santa Catalina Island and several dive sites. We thank J. Aranda for providing a sample from Los Cabos block. We also acknowledge the help of many individuals in field and laboratory work: C. Ortega for assistance in U/Pb dating, O. Pérez Arvizu for inductively coupled plasma–mass spectrometry trace-element analysis, R. Lozano-Santacruz for X-ray fluorescence analysis, M.A. García for help with Ar-Ar mass spectrometry, A.S. Rosas Montoya, V.M. Pérez Arroyo, G. Rendón, and L. Gradilla for Ar-Ar sample preparation, J.T. Vázquez for thin section preparation, and G. Norini, G. Antillón Mata, Y. González Romo, J. González Romo, J.C. Castro Climaco, Iisel Calderón Durán, and M. Michell for field assistance and mineral separation. We also thank S. Poli for providing access to the microprobe laboratory at Università di Milano and A. Risplendente for assistance with the electron microprobe analysis. DANA and ROCA samples were collected during research cruises by R/V *Revelle* and R/V *Atlantis* (funded by NSF grants 0203348 and 0646563 to Lonsdale); BEKL samples were collected during a R/V *New Horizon* cruise funded by an award from the State of California to Kluesner. We thank the government of Mexico for operating permission, and the ships' officers and crews for their expert help. Cathy Busby, Lawford Anderson, and Associate Editor Calvin Miller provided critical reviews that helped to improve the final version of the manuscript. We also appreciate the editorial support of Nancy Riggs.

REFERENCES CITED

Abbate, E.P., Balestrieri, M.L., and Bigazzi, G., 2001, Uplifted rift-shoulder of the Gulf of Aden in northwestern Somalia: Palinspastic reconstructions supported by apatite fission-track data, *in* Ziegler, P.A., et al., eds., Peri-Tethys Memoir 6: Peri-Tethyan Rift/Wrench Basins and Passive Margins. Memoires du Museum National d'Histoire Naturelle 186, p. 629–640.

Anderson, J.L., and Smith, D.R., 1995, The effects of temperature and fO_2 on the Al-in-hornblende barometer. The American Mineralogist, v. 80, p. 549–559.

Anderson, J.L., Barth, A.P., Wooden, J.L., and Mazdab, F., 2008, Thermometers and thermobarometers in granitic systems. Reviews in Minerology and Geochemistry, v. 69, p. 121–142.

Anderson, J.L., Morrison, J., and Paterson, S.R., 2012, Post-emplacement fluids and pluton thermobarometry: Mount Stuart batholith, Washington Cascades. International Geology Review, v. 54, no. 5, p. 491–508.

Aranda-Gómez, J.J., and McDowell, F.W., 1998, Paleogene extension in the southern Basin and Range Province of Mexico: Syndepositional tilting of Eocene red beds and Oligocene volcanic rocks in the Guanajuato Mining District. International Geology Review, v. 40, no. 2, p. 116–134, doi:10.1080/00206819809465201.

Atwater, T., and Stock, J., 1998, Pacific–North America plate tectonics of the Neogene southwestern United States: An update. International Geology Review, v. 40, no. 5, p. 375–402, doi:10.1080/00206819809465216.

Ballard, J.R., Palin, J.M., Williams, I.S., Campbell, I.H., and Faunes, A., 2001, Two ages of porphyry intrusion resolved for the super-giant Chuquicamata copper deposit of northern Chile by ELA-ICPMS and SHRIMP. Geology, v. 29, n. 5, p. 383–386.

Bendick, R., McClusky, S., Bilham, R., Asfaw, L., and Klemperer, S., 2006, Distributed Nubia–Somalia relative motion and dike intrusion in the Main Ethiopian Rift. Geophysical Journal International, v. 165, no. 1, p. 303–310, doi:10.1111/j.1365-246X.2006.02904.x.

Bernal, J.P., and Lozano-Santacruz, R., 2005, Characterization of a new set of eight geochemical reference materials for XRF major and trace element analysis. Revista Mexicana de Ciencias Geológicas, v. 22, no. 3, p. 329–344.

Bohannon, R.G., Naeser, C.W., Schmidt, D.L., and Zimmermann, R.A., 1989, The timing of uplift, volcanism, and rifting peripheral to the Red Sea: A case for passive rifting? Journal of Geophysical Research–Solid Earth, v. 94, no. B2, p. 1683–1701, doi:10.1029/JB094iB02p01683.

Bryan, S., 2007, Silicic large igneous provinces. Episodes, v. 30, no. 1, p. 20.

Bryan, S.E., and Ferrari, L., 2013, Large igneous provinces and silicic large igneous provinces: Progress in our understanding over the last 25 years. Geological Society of America Bulletin, v. 125, p. 1053–1078, doi:10.1130/B30820.1.

Bryan, S.E., Ferrari, L., Reiners, P.W., Allen, C.M., Petrone, C.M., Ramos-Rosique, A., and Campbell, I.H., 2008, New insights into crustal contributions to large volume rhyolite generation at the mid-Tertiary Sierra Madre Occidental Province, Mexico, revealed by U/Pb geochronology. Journal of Petrology, v. 49, no. 1, p. 47–77, doi:10.1093/petrology/egm070.

Bryan, S.E., Orozco-Esquivel, T., Ferrari, L., and López-Martínez, M., 2014, Pulling apart the mid to late Cenozoic magmatic record of the Gulf of California: Is there a Comondú arc?, *in* Gómez-Tuena, A., Straub, S.M., and Zellmer, G.F., eds., Orogenic Andesites and Crustal Growth. Geological Society of London Special Publication 385, p. 389–407.

Busby, C., 2004, Continental growth at convergent margins facing large ocean basins: A case study from Mesozoic convergent-margin basins of Baja California, Mexico. Tectonophysics, v. 392, no. 1, p. 241–277, doi:10.1016/j.tecto.2004.04.017.

Busby, C., Smith, D., Morris, W., and Fackler-Adams, B., 1998, Evolutionary model for convergent margins facing large ocean basins: Mesozoic Baja California, Mexico. Geology, v. 26, no. 3, p. 227–230, doi:10.1130/0091-7613(1998)026<0227:EMFCMF>2.3.CO;2.

Calais, E., Lesne, O., Déverchère, J., San'kov, V., Lukhnev, A., Miroshnitchenko, A., Buddo, V., Levi, K., Zalutzky, V., Bashkuev, Y., and Bashkuev, Y., 1998, Crustal deformation in the Baikal rift from GPS measurements. Geophysical Research Letters, v. 25, no. 21, p. 4003–4006.

Calmus, T., Pallares, C., Maury, R.C., Aguillón-Robles, A., Bellon, H., Benoit, M., and Michaud, F., 2011, Volcanic markers of the post-subduction evolution of Baja California and Sonora, Mexico: Slab tearing versus lithospheric rupture of the Gulf of California. Pure and Applied Geophysics, v. 168, no. 8–9, p. 1303–1330.

Cameron, K.L., Nimz, G.J., Kuentz, D., Niemeyer, S., and Gunn, S., 1989, Southern Cordilleran basaltic andesite suite, southern Chihuahua, Mexico: A link between Tertiary continental arc and flood basalt magmatism in North America. Journal of Geophysical Research, v. 94, no. B6, p. 7817–7840, doi:10.1029/JB094iB06p07817.

Carreño, A.L., 1992, Neogene microfossils from the Santiago Diatomite, Baja California Sur, Mexico. Paleontología Mexicana, v. 59, p. 1–37.

Castillo, P.R., Clague, D.A., Davis, A.S., and Lonsdale, P.F., 2010, Petrogenesis of Davidson Seamount lavas and its implications for fossil spreading center and intraplate magmatism in the eastern Pacific. Geochemistry Geophysics Geosystems, v. 11, no. 2, p. 1297, doi:10.1029/2009GC002992.

Cherniak, D.J., and Watson, E.B., 2001, Pb diffusion in zircon. Chemical Geology, v. 172, no. 1, p. 5–24, doi:10.1016/S0009-2541(00)00233-3.

Corti, G., 2009, Continental rift evolution: From rift initiation to incipient break-up in the Main Ethiopian Rift, East Africa. Earth-Science Reviews, v. 96, no. 1, p. 1–53.

Corti, G., Van Wijk, J., Bonini, M., Sokoutis, D., Cloetingh, S., Innocenti, F., and Manetti, P., 2003, Transition from continental break-up to punctiform seafloor spreading: How fast, symmetric and magmatic. Geophysical Research Letters, v. 30, no. 12, p. 1604, doi:10.1029/2003GL017374.

Cuéllar-Cárdenas, M.A., Nieto-Samaniego, Á.F., Levresse, G., Alaniz-Álvarez, S.A., Solari, L., Ortega-Obregón, C., and López-Martínez, M., 2012, Límites temporales de la deformación por acortamiento Laramide en el centro de México. Revista Mexicana de Ciencias Geológicas, v. 29, no. 1, p. 179–203.

DeMets, C., 1995, A reappraisal of seafloor spreading lineations in the Gulf of California: Implications for the transfer of Baja California to the Pacific plate and estimates of Pacific–North America motion. Geophysical Research Letters, v. 22, no. 24, p. 3545–3548, doi:10.1029/95GL03323.

Drake, W.R., 2005, Structural Analysis, Stratigraphy, and Geochronology of the San José Island Accommodation Zone, Baja California Sur, Mexico [M.S. thesis]. Flagstaff, Arizona, Northern Arizona University, 271 p.

Fernandes, R.M.S., Ambrosius, B.A.C., Noomen, R., Bastos, L., Combrinck, L., Miranda, J.M., and Spakman, W., 2004, Angular velocities of Nubia and Somalia from continuous GPS data: Implications on present-day relative kinematics. Earth and Planetary Science Letters, v. 222, no. 1, p. 197–208.

Ferrari, L., López-Martínez, M., and Rosas-Elguera, J., 2002, Ignimbrite flare-up and deformation in the southern Sierra Madre Occidental, western Mexico—Implications for the late subduction history of the Farallon plate. Tectonics, v. 21, no. 4, doi:10.1029/2001TC001302.

Ferrari, L., Valencia-Moreno, M., and Bryan, S.E., 2007, Magmatism and tectonics of the Sierra Madre Occidental and its relation with the evolution of the western margin of North America, *in* Alaniz-Álvarez, S.A., and Nieto-Samaniego, A.F., eds., Geology of México:

Celebrating the Centenary of the Geological Society of México. Geological Society of America Special Paper 422, p. 1–39, doi:10.1130/2007.2422(01).

Ferrari, L., López-Martínez, M., Orozco-Esquivel, T., Bryan, S.E., Duque-Trujillo, J., Lonsdale, P., and Solari, L., 2013, Late Oligocene to middle Miocene rifting and syn-extensional magmatism in the southwestern Sierra Madre Occidental, Mexico: The beginning of the Gulf of California rift. Geosphere, v. 9, p. 1161–1200, doi:10.1130/GES00925.1.

Fletcher, J.M., and Munguía, L., 2000, Active continental rifting in southern Baja California, Mexico: Implications for plate motion partitioning and the transition to seafloor spreading in the Gulf of California. Tectonics, v. 19, no. 6, p. 1107–1123, doi:10.1029/1999TC001131.

Fletcher, J.M., Kohn, B.P., Foster, D.A., and Gleadow, A.J.W., 2000, Heterogeneous Neogene cooling and exhumation of the Los Cabos block, southern Baja California: Evidence from fission-track thermochronology. Geology, v. 28, no. 2, p. 107–110, doi:10.1130/0091-7613(2000)28<107:HNCAEO>2.0.CO;2.

Fletcher, J.M., Grove, M., Kimbrough, D., Lovera, O., and Gehrels, G.E., 2007, Ridge-trench interactions and the Neogene tectonic evolution of the Magdalena Shelf and southern Gulf of California; insights from detrital zircon U/Pb ages from the Magdalena Fan and adjacent areas. Geological Society of America Bulletin, v. 119, no. 11–12, p. 1313–1336, doi:10.1130/B26067.1.

Frost, B.R., and Frost, C.D., 2008, Geochemical classification for feldspathic igneous rocks. Journal of Petrology, v. 49, no. 11, p. 1955–1969, doi:10.1093/petrology/egn054.

Gans, P.B., 1997, Large-magnitude Oligo-Miocene extension in southern Sonora: Implications for the tectonic evolution of northwest Mexico. Tectonics, v. 16, no. 3, p. 388–408, doi:10.1029/97TC00496.

Gastil, R.G., 1975, Plutonic zones in the Peninsular Ranges of southern California and northern Baja California. Geology, v. 3, no. 7, p. 361–363, doi:10.1130/0091-7613(1975)3<361:PZITPR>2.0.CO;2.

Gastil, R.G., 1993, Prebatholithic history of peninsular California, *in* Gastil, R.G., and Miller, R.H., eds., The Prebatholithic Stratigraphy of Peninsular California. Geological Society of America Special Paper 279, p. 145–156, doi:10.1130/SPE279-p145.

Gastil, R.G., Krummenacher, D., and Jensky, W.A., 1979, Reconnaissance geology of west-central Nayarit, Mexico: Summary. Geological Society of America Bulletin, v. 90, no. 1, p. 15–18, doi:10.1130/0016-7606(1979)90<15:RGOWNM>2.0.CO;2.

Gastil, R.G., Diamond, J., Knaack, C., Walawender, M., Marshall, M., Boyles, C., Chadwick, B., and Erskine, B., 1990, The problem of the magnetite/ilmenite boundary in southern and Baja California, *in* Anderson, J., ed., The Nature and Origin of Cordilleran Magmatism. Geological Society of America Memoir 174, p. 19–32.

Gillespie, M.R., and Styles, M.T., 1999, Classification of Igneous Rocks: Keyworth, Nottingham, U.K., British Geological Survey, Research Report RR 99-06, 2nd edition, 52 p.

Godinez, N.S., Kimbrough, D.L., and Kohel, C., 2010, Stratigraphy and petrologic evolution of the Oligocene–Miocene Comondú Group near Bahia Concepcion and Loreto, Baja California Sur, Mexico. Geological Society of America Abstracts with Programs, v. 42, no. 4, p. 66.

González-León, C.M., McIntosh, W.C., Lozano-Santacruz, R., Valencia-Moreno, M., Amaya-Martínez, R., and Rodríguez-Castañeda, J.L., 2000, Cretaceous and Tertiary sedimentary, magmatic, and tectonic evolution of north-central Sonora (Arizpe and Bacanuchi quadrangles), northwest Mexico. Geological Society of America Bulletin, v. 112, no. 4, p. 600–610, doi:10.1130/0016-7606(2000)112<600:CATSMA>2.0.CO;2.

Green, N.L., and Harry, D.L., 1999, On the relationship between subducted slab age and arc basalt petrogenesis, Cascadia subduction system, North America. Earth and Planetary Science Letters, v. 171, no. 3, p. 367–381, doi:10.1016/S0012-821X(99)00159-4.

Hammarstrom, J.M., and Zen, E., 1986, Aluminum in hornblende: An empirical igneous geobarometer. American Mineralogist, v. 71, p. 1297–1313.

Hausback, B.P., 1984, Cenozoic volcanic and tectonic evolution of Baja California Sur, Mexico, *in* Frizzell, V.A., ed., Geology of the Baja California Peninsula. Pacific Section, Society of Economic Paleontologists and Mineralogists Book 39, p. 219–236.

Henry, C.D., 1989, Late Cenozoic Basin and Range structure in western México adjacent to the Gulf of California. Geological Society of America Bulletin, v. 101, p. 1147–1156, doi:10.1130/0016-7606(1989)101<1147:LCBARS>2.3.CO;2.

Henry, C.D., and Aranda-Gomez, J.J., 1992, The real southern Basin and Range: Mid- to late Cenozoic extension in Mexico. Geology, v. 20, no. 8, p. 701–704, doi:10.1130/0091-7613(1992)020<0701:TRSBAR>2.3.CO;2.

Henry, C.D., and Aranda-Gomez, J.J., 2000, Plate interactions control middle-late Miocene, proto–Gulf and Basin and Range extension in the southern Basin and Range. Tectonophysics, v. 318, no. 1, p. 1–26, doi:10.1016/S0040-1951(99)00304-2.

Henry, C.D., and Fredrikson, G., 1987, Geology of Part of Southern Sinaloa, Mexico, Adjacent to the Gulf of California. Geological Society of America Maps and Chart MCH063, 1 sheet, 14 p. text.

Henry, C.D., McDowell, F.W., and Silver, L.T., 2003, Geology and geochronology of the granitic batholithic complex, Sinaloa, México: Implications for Cordilleran magmatism and tectonics, *in* Johnson, S.E., Paterson, S.R., Fletcher, J.M., Girty, G.H., Kimbrough, D.L., and Martín-Barajas, A., eds., Tectonic Evolution of Northwestern México and the Southwestern USA. Geological Society of America Special Paper 374, p. 237–273.

Holland, T., and Blundy, J., 1994, Non-ideal interactions in calcic amphiboles and their bearing on amphibole-plagioclase thermometry. Contributions to Mineralogy and Petrology, v. 116, p. 433–447, doi:10.1007/BF00310910.

Iriondo, A., Kunk, M.J., Winick, J.A., and Consejo de Recursos Minerales (CRM), 2003, $^{40}Ar/^{39}Ar$ Dating Studies of Minerals and Rocks in Various Areas in Mexico: USGS/CRM scientific collaboration (Part I). U.S. Geological Survey Open-File Report 03–020, 79 p.

Iriondo, A., Nieto-Samaniego, A.F., Alaniz-Alvarez, S.A., and Tolson-Jones, G., 2005, Time constraints for a pseudotachylyte event hosted by the Late Cretaceous Las Cruces granite near La Paz, B.C.S., Mexico. Actas INAGEQ, v.11, p. 101–102.

Keppie, J.D., Dostal, J., Miller, B.V., Ortega-Rivera, A., Roldán-Quintana, J., and Lee, J.W., 2006, Geochronology and geochemistry of the Francisco Gneiss: Triassic continental rift tholeiites on the Mexican margin of Pangea metamorphosed and exhumed in a Tertiary core complex. International Geology Review, v. 48, no. 1, p. 1–16, doi:10.2747/0020-6814.48.1.1.

Kimbrough, D.L., Smith, D.P., Mahoney, J.B., Moore, T.E., Grove, M., Gastil, R.G., Ortega-Rivera, A., and Fanning, C.M., 2001, Forearc-basin sedimentary response to rapid Late Cretaceous batholith emplacement in the Peninsular Ranges of southern and Baja California. Geology, v. 29, no. 6, p. 491–494, doi:10.1130/0091-7613(2001)029<0491:FBSRTR>2.0.CO;2.

Kluesner, J., 2011, Marine Geophysical Study of Cyclic Sedimentation and Shallow Sill Intrusion in the Floor of the Central Gulf of California [Ph.D. dissertation]. San Diego, California, University of California, 232 p.

Köhler, H., Schaaf, P., Müller-Sohnius, D., Emermann, R., Negendank, J.F.W., and Tobschall, H.J., 1988, Geochronological and geochemical investigations on plutonic rocks from the complex of Puerto Vallarta, Sierra Madre del Sur. Geofísica Internacional, v. 27, p. 579–592.

Langenheim, V.E., Jachens, R.C., and Aiken, C., 2014, Geophysical framework of the Peninsular Ranges batholith—Implications for tectonic evolution and neotectonics, *in* Morton, D.M., and Miller, F.K., eds., Peninsular Ranges Batholith, Baja California and Southern California. Geological Society of America Memoir 211, p. 1–20.

Lizarralde, D., Axen, G.J., Brown, H.E., Fletcher, J.M., González-Fernández, A., Harding, A.J., Holbrook, W.S., Kent, G.M., Paramo, P., Sutherland, F., and Umhoefer, P.J., 2007, Variation in styles of rifting in the Gulf of California. Nature, v. 448, p. 466–469, doi:10.1038/nature06035.

Lonsdale, P.F., 1989, Geology and tectonic history of the Gulf of California, *in* Winterer, E.L., Hussong, D.M., and Decker, R.W., eds., The Eastern Pacific Ocean and Hawaii. Boulder, Colorado, Geological Society of America, Decade of North American Geology, v. N, p. 499–521.

Lonsdale, P.F., 1991, Structural patterns of the Pacific floor offshore of peninsular California, *in* Dauphin, J.P., and Simoneit, B.R.T., The Gulf and Peninsular Province of the Californias. American Association of Petroleum Geologists Memoir 47, p. 87–125.

Lonsdale, P.F., 1995, Segmentation and disruption of the East Pacific Rise in the mouth of the Gulf of California. Marine Geophysical Researches, v. 17, no. 4, p. 323–359, doi:10.1007/BF01227039.

Lonsdale, P.F., and Kluesner, J., 2010, Routing of terrigenous clastics to oceanic basins in the Southern Gulf of California, inherited from features of the pre-spreading protogulf. San Francisco, California, American Geophysical Union, fall meeting supplement, abstract T33C-2265.

Luhr, J.F., Henry, C.D., Housh, T.B., Aranda-Gómez, J.J., and McIntosch, W.C., 2001, Early extension and associated mafic alkalic volcanism from the southern Basin and Range Province: Geology and petrology of the Rodeo and Nazas volcanic fields, Durango, México. Geological Society of America Bulletin, v. 113, no. 6, p. 760–773, doi:10.1130/0016-7606(2001)113<0760:EEAAMA>2.0.CO;2.

Lyle, M., and Ness, G.E., 1991, The opening of the southern Gulf of California, *in* Dauphin, J.P., and Simoneit, B.R.T., eds., The Gulf and Peninsular Province of the Californias. American Association of Petroleum Geologists Memoir 47, p. 403–423.

Mark, C., Gupta, S., Carter, A., Mark, D.F., Gautheron, C., and Martín, A., 2014, Rift flank uplift at the Gulf of California: No requirement for asthenospheric upwelling. Geology, v. 42, p. 259–262.

Martín-Barajas, A., Stock, J.M., Layer, P., Hausback, B., Renne, P., and López-Martínez, M., 1995, Arc-rift transition volcanism in the Puertecitos volcanic province, northeastern Baja California, Mexico. Geological Society of America Bulletin, v. 107, no. 4, p. 407–424.

McCloy, C., Ingle, J.C., and Barron, J.A., 1988, Neogene stratigraphy, foraminifera, diatoms, and depositional history of Maria Madre Island, Mexico: Evidence of early Neogene marine conditions in the southern Gulf of California. Marine Micropaleontology, v. 13, no. 3, p. 193–212, doi:10.1016/0377-8398(88)90003-5.

McDowell, F.W., and Clabaugh, S.E., 1979, Ignimbrites of the Sierra Madre Occidental and their relation to the tectonic history of western Mexico, *in* Chapin, C.E., and Elston, W.E., eds., Ash-Flow Tuffs. Geological Society of America Special Paper 180, p. 113–124, doi:10.1130/SPE180-p113.

McDowell, F.W., and Keizer, R.P., 1977, Timing of mid-Tertiary volcanism in the Sierra Madre Occidental between Durango City and Mazatlán, Mexico. Geological Society of America Bulletin, v. 88, no. 10, p. 1479–1487, doi:10.1130/0016-7606(1977)88<1479:TOMVIT>2.0.CO;2.

McDowell, F.W., Roldán-Quintana, J., and Amaya-Martínez, R., 1997, Interrelationship of sedimentary and volcanic deposits associated with Tertiary extension in Sonora, Mexico. Geological Society of America Bulletin, v. 109, no. 10, p. 1349–1360, doi:10.1130/0016-7606(1997)109<1349:IOSAVD>2.3.CO;2.

McFall, C.C., 1968, Reconnaissance Geology of the Concepcion Bay Area, Baja California, Mexico. Stanford University Publications in Geological Sciences 10, no. 5, 25 p.

McLean, H., 1988, Reconnaissance Geologic Map of the Loreto and Part of the San Javier Quadrangles, Baja California Sur, Mexico. U.S. Geological Survey Miscellaneous Field Studies Map MF-2000, scale 1:50,000, 10 p. text.

McTeague, M.S., 2006, Marginal Strata of the East Central San Jose del Cabo Basin, Baja California Sur, Mexico [Ph.D. thesis]. Flagstaff, Arizona, Northern Arizona University, 152 p.

Menzies, M., Gallagher, K., Yelland, A., and Hurford, A.J., 1997, Volcanic and nonvolcanic rifted margins of the Red Sea and Gulf of Aden: Crustal cooling and margin evolution in Yemen. Geochimica et Cosmochimica Acta, v. 61, no. 12, p. 2511–2527, doi:10.1016/S0016-7037(97)00108-7.

Mori, L., Gómez-Tuena, A., Cai, Y., and Goldstein, S.L., 2007, Effects of prolonged flat subduction on the Miocene magmatic record of the central Trans-Mexican volcanic belt. Chemical Geology, v. 244, no. 3, p. 452–473, doi:10.1016/j.chemgeo.2007.07.002.

Mullan, H.S., 1978, Evolution of part of the Nevadan orogen in northwestern Mexico. Geological Society of America Bulletin, v. 89, no. 8, p. 1175–1188, doi:10.1130/0016-7606(1978)89<1175:EOPOTN>2.0.CO;2.

Munguía, L., González, M., Mayer, S., and Aguirre, A., 2006, Seismicity and state of stress in the La Paz–Los Cabos region, Baja California Sur, Mexico. Bulletin of the Seismological Society of America, v. 96, no. 2, p. 624–636, doi:10.1785/0120050114.

Murray, B.P., Busby, C.J., Ferrari, L., and Solari, L.A., 2013, Synvolcanic crustal extension during the mid-Cenozoic ignimbrite flare-up in the northern Sierra Madre Occidental, Mexico: Evidence from the Guazapares Mining District region, western Chihuahua. Geosphere, v 9, p. 1201–1235, doi:10.1130/GES00862.1.

Nagel, T.J., and Buck, W.R., 2007, Control of rheological stratification on rifting geometry: A symmetric model resolving the upper plate paradox. International Journal of Earth Sciences, v. 96, no. 6, p. 1047–1057.

Niemitz, J.W., and Bischoff, J.L., 1981, Tectonic elements of the southern part of the Gulf of California. Geological Society of America Bulletin, Part II, v. 92, no. 3, p. 360–407.

Normark, W.R., and Curray, J.R., 1968, Geology and structure of the tip of Baja California, Mexico. Geological Society of America Bulletin, v. 79, no. 11, p. 1589–1600, doi:10.1130/0016-7606(1968)79[1589:GASOTT]2.0.CO;2.

Omar, G.I., and Steckler, M.S., 1995, Fission track evidence on the initial rifting of the Red Sea: Two pulses, no propagation. Science, v. 270, no. 5240, p. 1341–1344, doi:10.1126/science.270.5240.1341.

Ortega-Rivera, A., 2003, Geochronological constraints on the tectonic history of the Peninsular Ranges Batholith of Alta and Baja California: Tectonic implications for western Mexico, *in* Johnson, S.E., Paterson, S.R., Fletcher, J.M., Girty, G.H., Kimbrough, D.L., and Martín-Barajas, A., eds., Tectonic Evolution of Northwestern Mexico and the Southwestern USA. Geological Society of America Special Paper 374, p. 297–336.

Oskin, M., and Stock, J., 2003, Pacific–North America plate motion and opening of the upper Delfin basin, northern Gulf of California, Mexico. Geological Society of America Bulletin, v. 115, no. 10, p. 1173–1190, doi:10.1130/B25154.1.

Oskin, M., Stock, J., and Martín-Barajas, A., 2001, Rapid localization of Pacific–North America plate motion in the Gulf of California. Geology, v. 29, no. 5, p. 459–462, doi:10.1130/0091-7613(2001)029<0459:RLOPNA>2.0.CO;2.

Páramo, P., Holbrook, W.S., Brown, H.E., Lizarralde, D., Fletcher, J.M., Umhoefer, P., Kent, G., Harding, A., Gonzalez, A., and Axen, G., 2008, Seismic structure of the southern Gulf of California from Los Cabos block to the East Pacific Rise. Journal of Geophysical Research, v. 113, no. B3, p. B03307, doi:10.1029/2007JB005113.

Parsons, T., Thompson, G.A., and Smith, R.P., 1998, More than one way to stretch: A tectonic model for extension along the plume track of the Yellowstone hotspot and adjacent Basin and Range Province. Tectonics, v. 17, no. 2, p. 221–234, doi:10.1029/98TC00463.

Peacock, S.M., and Wang, K., 1999, Seismic consequences of warm versus cool subduction metamorphism: Examples from southwest and northeast Japan. Science, v. 286, no. 5441, p. 937–939, doi:10.1126/science.286.5441.937.

Pearce, J.A., Harris, N.B., and Tindle, A.G., 1984, Trace element discrimination diagrams for the tectonic interpretation of granitic rocks. Journal of Petrology, v. 25, no. 4, p. 956–983.

Peccerillo, A., and Taylor, S.R., 1976, Geochemistry of Eocene calc-alkaline volcanic rocks from the Kastamonu area, northern Turkey. Contributions to Mineralogy and Petrology, v. 58, p. 63–81, doi:10.1007/BF00384745.

Pik, R., Marty, B., Carignan, J., Yirgu, G., and Ayalew, T., 2008, Timing of East African Rift development in southern Ethiopia: Implication for mantle plume activity and evolution of topography. Geology, v. 36, p. 167–170, doi:10.1130/G24233A.1.

Piñero-Lajas, D., 2008, Sísmica de Reflexión y Fechamiento 40Ar-39Ar del Basamento Continental en el Margen Oeste de la Cuenca Farallón (Sur del Golfo de California, México) [Ms.C. thesis]. Ensenada, Baja California, Mexico, Centro de Investigación Científica y de Educación Superior de Ensenada (CICESE), 183 p.

Plattner, C.R., Malservisi, R., Dixon, T.H., LaFemina, P., Sella, G.F., Fletcher, J.M., and Suarez-Vidal, F., 2007, New constraints on relative motion between the Pacific plate and Baja California microplate (Mexico) from GPS measurements. Geophysical Journal International, v. 170, no. 3, p. 1373–1380, doi:10.1111/j.1365-246X.2007.03494.x.

Pompa-Mera, V., Schaaf, P., Hernández-Treviño, T., Weber, B., Solís-Pichardo, G., Villanueva-Lascurain, D., and Layer, P., 2013, Geology, geochronology, and geochemistry of Isla María Madre, Nayarit, Mexico. Revista Mexicana de Ciencias Geológicas, v. 30, p. 1–23.

Ramos-Rosique, A., 2013, Timing and evolution of Late Oligocene to early Miocene magmatism and epithermal mineralization in the central Bolaños Graben, southern Sierra Madre Occidental, México [Ph.D. thesis]. London, UK, Kingston University, 215 p.

Reiners, P.W., Ehlers, T.A., and Zeitler, P.K., 2005, Past, present, and future of thermochronology. Reviews in Mineralogy and Geochemistry, v. 58, no. 1, p. 1–18, doi:10.2138/rmg.2005.58.1.

Ridolfi, F., and Renzulli, A., 2012, Calcic amphiboles in calc-alkaline and alkaline magmas: Thermobarometric and chemometric empirical equations valid up to 1,130 °C and 2.2 GPa. Contributions to Mineralogy and Petrology, v. 163, p. 877–895.

Ring, U., and Collins, A.S., 2005, U-Pb SIMS dating of synkinematic granites: Timing of core-complex formation in the northern Anatolide belt of western Turkey. Journal of the Geological Society of London, v. 162, p. 289–298, doi:10.1144/0016-764904-016.

Ruiz, J., Patchett, P., and Arculus, R.J., 1988, Nd-Sr isotope composition of lower crustal xenoliths—Evidence for the origin of mid-Tertiary felsic volcanics in Mexico. Contributions to Mineralogy and Petrology, v. 99, p. 36–43, doi:10.1007/BF00399363.

Ruiz, J., Patchett, P.J., and Arculus, R.J., 1990, Reply to "Comments on Nd-Sr isotopic compositions of lower crustal xenoliths—Evidence for the origin of mid-Tertiary felsic volcanics in Mexico" by K.L. Cameron and J.V. Robinson. Contributions to Mineralogy and Petrology, v. 104, no. 5, p. 615–618, doi:10.1007/BF00306669.

Sawlan, M.G., 1991, Magmatic evolution of the Gulf of California rift, *in* Dauphin, J.P., and Simoneit, B.R., eds., The Gulf and Peninsular Province of the Californias. American Association of Petroleum Geologists Memoir 47, p. 301–369.

Sawlan, M.G., and Smith, J.G., 1984, Petrologic characteristics, age and tectonic setting of Neogene volcanic rocks in northern Baja California Sur, Mexico, *in* Frizzell, V.A., ed., Geology of the Baja California Peninsula. Pacific Section, Society of Economic Paleontologists and Mineralogists Book 39, p. 237–251.

Schaaf, P., Morán-Zenteno, D., Hernández-Bernal, M.D.S., Solís-Pichardo, G., Tolson, G., and Köhler, H., 1995, Paleogene continental margin truncation in southwestern Mexico: Geochronological evidence. Tectonics, v. 14, no. 6, p. 1339–1350.

Schaaf, P., Böhnel, H., and Pérez-Venzor, J.A., 2000, Pre-Miocene palaeogeography of the Los Cabos block, Baja California Sur: Geochronological and palaeomagnetic constraints. Tectonophysics, v. 318, no. 1, p. 53–69, doi:10.1016/S0040-1951(99)00306-6.

Schmidt, M.W., 1992, Amphibole composition in tonalite as a function of pressure: An experimental calibration of the Al-in-hornblende barometer. Contributions to Mineralogy and Petrology, v. 110, p. 304–310, doi:10.1007/BF00310745.

Seiler, C., Fletcher, J.M., Kohn, B.P., Gleadow, A.J., and Raza, A., 2011, Low temperature thermochronology of northern Baja California, Mexico: Decoupled slip exhumation gradients and delayed onset of oblique rifting across the Gulf of California. Tectonics, v. 30, no. 3, TC3004, doi:10.1029/2009TC002649.

Servicio Geológico Mexicano (SGM), 2000, Carta Geológico-Minera Villa Constitución. Servicio Geológico Mexicano Map G12–7-8, scale 1:250,000, 1 sheet.

Shepard, F.P., 1964, Sea-floor valleys of Gulf of California, *in* van Andel, T.H., and Shor, G.G., eds., Marine Geology of the Gulf of California. American Association of Petroleum Geologists Memoir 3, p. 1157–1192.

Silver, L.T., and Chappell, B.W., 1988, The Peninsular Ranges Batholith: An insight into the evolution of the Cordilleran batholiths of southwestern North America. Transactions of the Royal Society of Edinburgh–Earth Sciences, v. 79, p. 105–121, doi:10.1017/S0263593300014152.

Stern, R.J., 2002, Subduction zones. Reviews of Geophysics, v. 40, no. 4, p. 3-1–3-38, doi:10.1029/2001RG000108.

Stock, J.M., and Hodges, K.V., 1989, Pre-Pliocene extension around the Gulf of California and the transfer of Baja California to the Pacific plate. Tectonics, v. 8, no. 1, p. 99–115, doi:10.1029/TC008i001p00099.

Stock, J.M., and Lee, J., 1994, Do microplates in subduction zones leave a geological record? Tectonics, v. 13, no. 6, p. 1472–1487, doi:10.1029/94TC01808.

Streckeisen, A.L., 1976, To each plutonic rock its proper name. Earth-Science Reviews, v. 12, p. 1–33.

Streckeisen, A.L., and LeMaitre, R.W., 1979, Chemical approximation to modal QAPF classification of the igneous rocks. Neues Jahrbuch für Mineralogie, Abhandlungen, v. 136, p. 169–206.

Sun, S.S., and McDonough, W.F., 1989, Chemical and isotopic systematics of oceanic basalts: Implications for mantle composition and processes, *in* Saunders, A.D., and Norry, M.J., eds., Magmatism in the Ocean Basins. Geological Society of London Special Publication 42, p. 313–345, doi:10.1144/GSL.SP.1989.042.01.19.

Sutherland, F.H., Kent, G.M., Harding, A.J., Umhoefer, P.J., Driscoll, N.W., Lizarralde, D., Fletcher, J.M., Axen, G.J., Holbrook, W.S., González-Fernández, A., and Lonsdale, P.F., 2012, Middle Miocene to early Pliocene oblique extension in the southern Gulf of California. Geosphere, v. 8, no. 4, p. 752–770, doi:10.1130/GES00770.1.

Todd, V.R., Erskine, B.G., and Morton, D.M., 1988, Metamorphic and tectonic evolution of the northern Peninsular Ranges Batholith, southern California, *in* Ernst, W.G., ed., Metamorphism and Crustal Evolution of the Western United States (Rubey Volume VII). Englewood Cliffs, New Jersey, Prentice-Hall, p. 894–937.

Umhoefer, P.J., 2011, Why did the southern Gulf of California rupture so rapidly?—Oblique divergence across hot, weak lithosphere along a tectonically active margin. GSA Today, v. 21, no. 11, p. 1–10.

Umhoefer, P., Dorsey, R., Willsey, S., Mayer, L., and Renne, P., 2001, Stratigraphy and geochronology of the Comundú Group near Loreto, Baja California Sur, Mexico. Sedimentary Geology, v. 144, no. 1, p. 125–147, doi:10.1016/S0037-0738(01)00138-5.

Umhoefer, P.J., Mayer, L., and Dorsey, R.J., 2002, Evolution of the margin of the Gulf of California near Loreto, Baja California Peninsula, Mexico. Geological Society of America Bulletin, v. 114, p. 849–868, doi:10.1130/0016-7606(2002)114<0849:EOTMOT>2.0.CO;2.

Valencia, V.A., Righter, K., Rosas-Elguera, J., López-Martínez, M., and Grove, M., 2013, The age and composition of the pre-Cenozoic basement of the Jalisco block: Implications for and relation to the Guerrero composite terrane. Contributions to Mineralogy and Petrology, v. 166, p. 1–24, doi:10.1007/s00410-013-0908-z.

Vega-Granillo, R.V., and Calmus, T., 2003, Mazatan metamorphic core complex (Sonora, Mexico): Structures

along the detachment fault and its exhumation evolution. Journal of South American Earth Sciences, v. 16, no. 4, p. 193–204, doi:10.1016/S0895-9811(03)00066-X.

Vega-Granillo, R., Salgado-Souto, S., Herrera-Urbina, S., Valencia, V., Ruiz, J., Meza-Figueroa, D., and Talavera-Mendoza, O., 2008, U-Pb detrital zircon data of the Río Fuerte Formation (NW Mexico): Its peri-Gondwanan provenance and exotic nature in relation to southwestern North America. Journal of South American Earth Sciences, v. 26, no. 4, p. 343–354, doi:10.1016/j.jsames.2008.08.011.

Vega-Granillo, R., Vidal-Solano, J., and Herrera-Urbina, S., 2012, Island arc tholeiites of Early Silurian, Late Jurassic and Late Cretaceous ages in the El Fuerte region, northwestern Mexico. Revista Mexicana de Ciencias Geológicas, v. 29, no. 2, p. 492–513.

Walawender, M.J., Gastil, R.G., Clinkenbeard, J.P., McCormick, W.V., Eastman, B.G., Wernicke, R.S., Wardlaw, M.S., Gunn, S.H., and Smith, B.M., 1990, Origin and evolution of the zoned La Posta–type plutons, eastern Peninsular Ranges Batholith, southern and Baja California, *in* Anderson, J., ed., The Nature and Origin of Cordilleran Magmatism. Geological Society of America Memoir 174, p. 1–18.

Wang, Y., Forsyth, D.W., and Savage, B., 2009, Convective upwelling in the mantle beneath the Gulf of California. Nature, v. 462, no. 7272, p. 499–501, doi:10.1038/nature08552.

Wark, D.A., Kempter, K.A., and McDowell, F.W., 1990, Evolution of waning subduction-related magmatism, northern Sierra Madre Occidental, Mexico. Geological Society of America Bulletin, v. 102, no. 11, p. 1555–1564, doi:10.1130/0016-7606(1990)102<1555:EOWSRM>2.3.CO;2.

Wong, M.S., Gans, P.B., and Scheier, J., 2010, The $^{40}Ar/^{39}Ar$ thermochronology of core complexes and other basement rocks in Sonora, Mexico: Implications for Cenozoic tectonic evolution of northwestern Mexico. Journal of Geophysical Research, v. 115, no. B7, B07414, doi:10.1029/2009JB007032.

York, D., and López-Martinez, M., 1986, The two-faced mica. Geophysical Research Letters, v. 13, no. 9, p. 973–975, doi:10.1029/GL013i009p00973.

Ziegler, P.A. and Cloetingh, S., 2004, Dynamic processes controlling evolution of rifted basins. Earth-Sciences Reviews, v. 64, p. 1–50.

Zimmermann, J.L., Stussi, J.M., Gonzalez Partida, E., and Arnold, M., 1988, K-Ar evidence for age and compositional zoning in the Puerto Vallarta–Río Santiago Batholith (Jalisco, Mexico). Journal of South American Earth Sciences, v. 1, no. 3, p. 267–274, doi:10.1016/0895-9811(88)90005-3.

Science Editor: Nancy Riggs
Associate Editor: Calvin F. Miller

Manuscript Received 8 October 2013
Revised Manuscript Received 2 September 2014
Manuscript Accepted 29 October 2014

Printed in the USA